UNIVERSIDADE FEDERAL DO PARANÁ

BIANCA HAZT

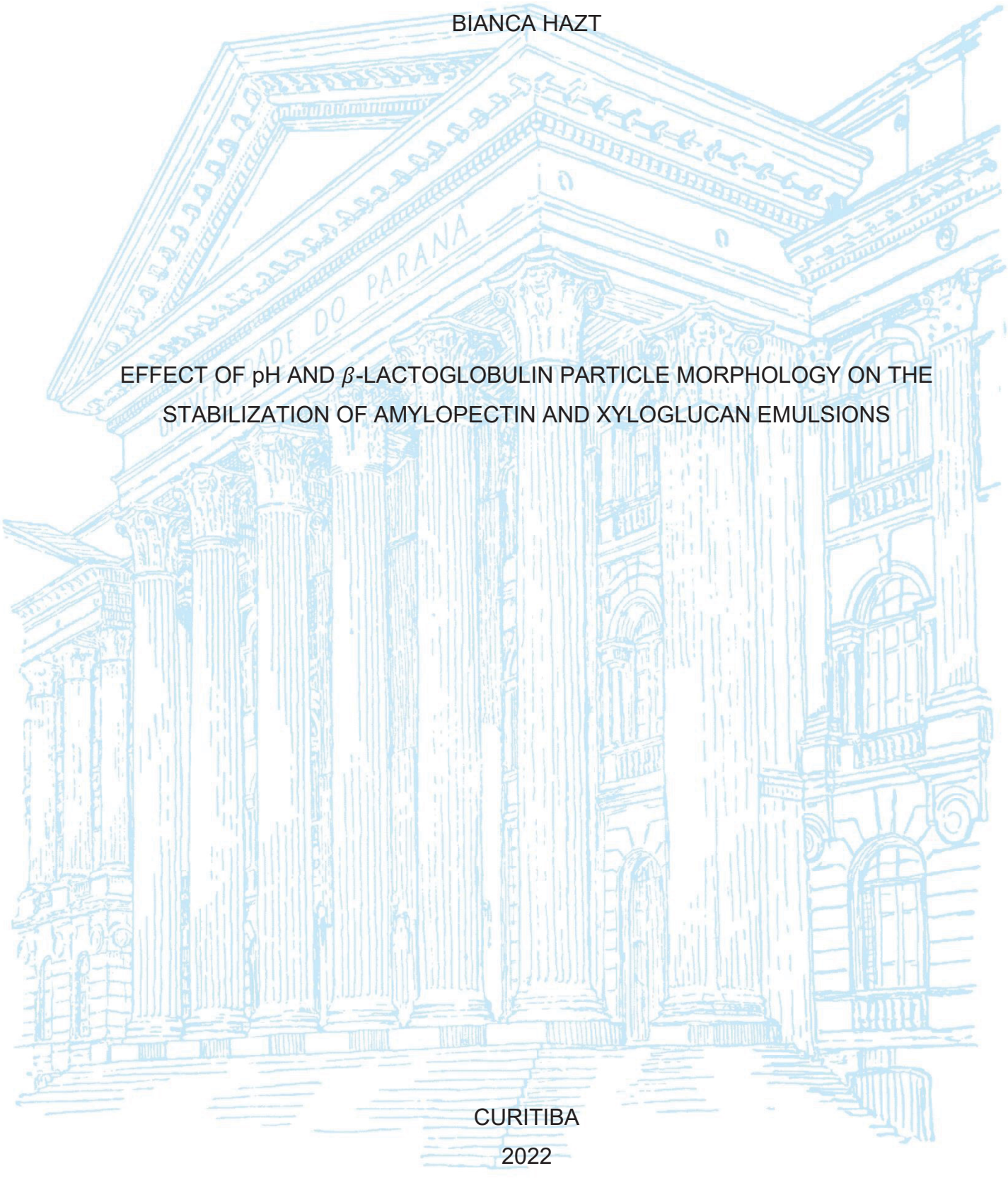

EFFECT OF pH AND β-LACTOGLOBULIN PARTICLE MORPHOLOGY ON THE STABILIZATION OF AMYLOPECTIN AND XYLOGLUCAN EMULSIONS

CURITIBA

2022

BIANCA HAZT

EFFECT OF pH AND β-LACTOGLOBULIN PARTICLE MORPHOLOGY ON THE STABILIZATION OF AMYLOPECTIN AND XYLOGLUCAN EMULSIONS

Dissertação apresentada ao Programa de Pós-Graduação em Química, Setor de Ciências Exatas, Universidade Federal do Paraná, como requisito parcial à obtenção do título de Mestre em Química.

Orientador: Prof. Dr. Rilton Alves de Freitas

CURITIBA

2022

DADOS INTERNACIONAIS DE CATALOGAÇÃO NA PUBLICAÇÃO (CIP)
UNIVERSIDADE FEDERAL DO PARANÁ
SISTEMA DE BIBLIOTECAS – BIBLIOTECA CIÊNCIA E TECNOLOGIA

Hazt,Bianca
Effect of pH and β-lactoglobulin particle morphology on the stabilization of amylopectin and xyloglucan emulsions / Bianca Hazt . – Curitiba, 2022.
1 recurso on-line : PDF.

Dissertação (Mestrado) – Universidade Federal do Paraná, Setor de Ciências Exatas, Programa de Pós-Graduação em Química.
Orientador: Prof. Dr. Rilton Alves de Freitas

1. Emulsões. I. Freitas, Rilton Alves de. II. Universidade Federal do Paraná. Programa de Pós-Graduação em Química. III. Título.

Bibliotecária: Roseny Rivelini Morciani CRB-9/1585

MINISTÉRIO DA EDUCAÇÃO
SETOR DE CIÊNCIAS EXATAS
UNIVERSIDADE FEDERAL DO PARANÁ
PRÓ-REITORIA DE PESQUISA E PÓS-GRADUAÇÃO
PROGRAMA DE PÓS-GRADUAÇÃO QUÍMICA - 40001016026P2

APPROVAL MINUTE

The Examining board designated by the Faculty of the Graduate Program of the Federal University of Paraná in QUÍMICA were invited to argue the THESIS of MASTER OF SCIENCES by BIANCA HAZT, entitled: EFFECT OF pH AND β-LACTOGLOBULIN PARTICLE MORPHOLOGY ON THE STABILIZATION OF AMYLOPECTIN AND XYLOGLUCAN EMULSIONS, under the supervision of Dr. RILTON ALVES DE FREITAS, which and after assessment of the candidate and the work, the Examining Board decided for the __approval__ in the present rite. The granting of the title of master of sciences is contingent upon the fulfillment of all the requirements indicated by the Examining Board and terms determined in the regulation of the Graduate Program.

CURITIBA, January 27th, 2022.

RILTON ALVES DE FREITAS
President of the Examining Board

DENISE FREITAS SIQUEIRA PETRI
External Member (UNIVERSIDADE DE SÃO PAULO)

EDUARDO LEMOS DE SÁ
Internal Member(UNIVERSIDADE FEDERAL DO PARANÁ)

ANWESHA SARKAR
External Member (UNIVERSITY OF LEEDS)

To my beloved mamma and papà,

Adriana and Adir

ACKNOWLEDGMENTS

I would like to thank my supervisor Dr. Rilton Alves de Freitas for accepting me as an undergrad student, and also as a graduate student at BioPol. Working with you during my graduation sparked a light in my heart for scientific research and I cannot express in words my gratitude for that – but I can surely tell you that without your precious guidance I would not have developed so many abilities and evolved as a student. Thanks for all the help, support, patience, and teaching during my scientific initiation and master's degree.

I would like to thank professors Dr. Denise Freitas Siqueira Petri, Dr. Eduardo Lemos de Sá, and Dr. Thiago Cervantes who evaluated me in my qualification exam – your suggestions were of the utmost importance for guiding this research to the final thesis. I would like to thank professors Dr. Anwesha Sarkar, Dr. Denise Freitas Siqueira Petri, and Dr. Eduardo Lemos de Sá who willingly accepted the invitation to evaluate my master's thesis defense.

My gratitude also goes to all the teachers who are dedicated to guiding students through the graduate disciplines. Learning with you was an immeasurable great experience, professors Rilton, Eduardo, Diego, and Izabel.

I would like to thank my mother Adriana and my father Adir who always have encouraged me to go further, even if it means staying miles away. I am sure that your love, educational and emotional support were the main pillars of my personal, professional, and academic development. Thanks also for taking care of my dog while I was away – I am sure that Rodolfo loves all the petting and snacking that he gets from you. To my sister Beatriz, for all the love, support, and for being my partner in crime since we were young. I am also thankful to Pedro Henrique who keeps reminding me about my own capabilities. Thanks for making me laugh, for your songs, for sharing petit gateaus, also for supporting me no matter what.

I could not leave behind in this acknowledgments page everyone who helped me during my period at the BioPol research group. Special thanks go to Franciely, Gabriela, Joslaine, Fernanda, Larissa, and Ana – you girls will always have a special place in my heart. Thanks to the scientific initiation students who taught me a little about teaching - Andres, Bernardo, Pedro, and Larissa. Also, to the entire BioPol

group: thanks for the scientific and non-scientific discussions, the shared coffees, cakes and teas, and many other things that make the daily work easier.

To my graduation friends Ana, Caroline, Letícia, and Viktor – thanks for celebrating our conquers together. To my hometown friends, who at some point guaranteed good laughs and special moments.

Special thanks go to João Luiz, who helped a lot with the restricted access to the confocal laser scanning microscope, caused by the Covid-19 pandemic.

I am also grateful for the financial support provided by CAPES and CNPq.

To the Chemistry Department.

To the Chemistry Post-graduation Program.

To Universidade Federal do Paraná.

Each day has a story that deserves to be told, because we are made of stories. I mean, scientists say that human beings are made of atoms, but a little bird told me that we are also made of stories.

Eduardo Galeano

RESUMO

As emulsões são sistemas coloidais compostos por uma fase contínua e outra dispersa que estão presentes em alimentos do cotidiano - exemplos dessas emulsões incluem a manteiga, sorvetes e maioneses. Embora a separação de fases em sistemas poliméricos seja um problema encontrado industrialmente, um tipo de emulsão que ainda não está presente na indústria alimentícia são as de água em água (a/a), que são compostas por dois polímeros hidrofílicos, mas termodinamicamente incompatíveis entre si. Esses sistemas se manifestam de maneira particularmente promissora para a indústria alimentícia por abrirem a possibilidade do desenvolvimento de emulsões livres de uma fase oleosa. Alguns materiais se apresentam como alternativas para estabilizar tais sistemas a/a que separam fase, como é o caso das partículas proteicas que se adsorvem na interface pelo efeito Pickering. Aqui, são mostradas emulsões de amilopectina em xiloglucana estabilizadas por microgéis e nanofibrilas de β-lactoglobulina (β-lg). A amilopectina (AMP) é o principal componente do amido, um homopolissacarídeo que possui grande relevância industrial e nutricional. O outro polissacarídeo utilizado, a xiloglucana (XG), é obtido a partir do endosperma de sementes de tamarindo, material comercializado em países como a Índia e o Japão. A β-lactoglobulina (β-lg) é uma das proteínas presentes na fração solúvel do soro do leite bovino (WPI). No presente trabalho, diferentes fontes de xiloglucana foram utilizadas e foi possível comparar o efeito que a massa molar desses materiais tem na estabilidade das emulsões. As emulsões de AMP e XG foram avaliadas em diferentes valores de pH (4,0, 5,0, 6,0 e 7,0) a fim de comparar o efeito da morfologia de partículas esféricas e no formato de bastões em cada condição de pH. Baseando-se nos três diagramas de fase construídos, foi possível identificar que a separação de fases leva mais tempo para ocorrer ao aumentar a massa molar da xiloglucana utilizada. Ao comparar o efeito da morfologia da partícula utilizada, percebeu-se que as nanofibrilas apresentaram maior capacidade de se adsorver na interface, tanto por maiores períodos de tempo quanto em uma maior faixa de pH, visto que ao utilizar nanofibrilas se observou efeito Pickering quando o pH era maior do que 5,0, efeito não observado para os microgéis. Tal vantagem apresentada pelas fibrilas se deve ao seu maior ponto isoelétrico, além da sua morfologia de bastão que pode apresentar um maior número de pontos de contato na interface. Por meio da adição de diferentes concentrações salinas foi avaliado o efeito da blindagem dos potenciais repulsivos presentes na interface das partículas sobre a estabilidade das emulsões. Os resultados obtidos indicam que um dos parâmetros relevantes na estabilização das emulsões aqui avaliadas é a partícula proteica estar em um pH abaixo de seu ponto isoelétrico e ter a sua carga positiva mantida. Embora ainda exista muito a ser estudado e discutido, o presente trabalho se apresenta como um passo a mais rumo ao desenvolvimento de produtos alimentícios que sejam nutritivos, agradáveis sensoriamente, dietéticos e estáveis.

Palavras-chave: Emulsões água em água. Amilopectina. Xiloglucana. β-lactoglobulina. Emulsões de Pickering.

ABSTRACT

Emulsions are colloidal systems composed of continuous and dispersed phases. They are present in daily foods - examples of these emulsions include butter, ice cream, and mayonnaise. Although the phase separation in polymeric systems is an industrial problem, a type of emulsion that is not yet present in the food industry is the water-in-water (w/w), which is composed of two hydrophilic polymers that are thermodynamically incompatible with each other. These systems are particularly promising for the food industry as they open up the possibility of developing oily-free emulsions. Some materials present themselves as good alternatives to stabilize such phase-separated w/w systems, and that is the case of protein particles that adsorb at the interface by the so-called Pickering effect. Here, amylopectin (AMP) in xyloglucan (XG) emulsions were stabilized by β-lactoglobulin (β-lg) microgels and nanofibrils. Amylopectin is the main component of starch, a homopolysaccharide with industrial and nutritional relevance. The other polysaccharide used, xyloglucan, is obtained from the endosperm of tamarind seeds, a commercial material used and exported by countries such as India and Japan. β-lactoglobulin is one of the proteins in the soluble fraction of bovine whey protein (WPI). In the present work, different sources of xyloglucan were used and it was possible to compare the effect that the molar mass of these materials had on the stability of the emulsions. The AMP and XG emulsions were evaluated at different pH values (4.0, 5.0, 6.0, and 7.0) in order to compare the effect of spherical and rod particle shapes in each condition of pH. Based on the three phase diagrams constructed, it was possible to identify that the phase separation takes longer to occur when increasing the molar mass of the xyloglucan used. When comparing the effect of the particle morphology, it was noticed that the nanofibrils showed a greater ability to adsorb at the interface, both for longer periods of time and in a greater pH range, since they stabilized the emulsions by the Pickering effect when the pH was higher than 5.0, while microgels did not. This advantage presented by fibrils is due to their higher isoelectric point, in addition to their rod morphology, which can present a greater number of contact points at the interface. Through the addition of different saline concentrations, the effect of screening the repulsive potentials present at the particle interface on the stability of the emulsions was evaluated. The results obtained indicate that one important parameter in the stabilization of the AMP and XG emulsions is that the protein particle is below its isoelectric point and has its positive surface potential preserved. Although there is still much to be studied and discussed, the present work presents itself as a step towards the development of food products that are nutritious, dietetic, and stable.

Keywords: Water-in-water emulsions. Amylopectin. Xyloglucan. β-lactoglobulin. Pickering emulsions.

LIST OF FIGURES

Figure 1 - REPRESENTATION OF AN (a) HYDROPHOBIC SPHERICAL PARTICLE AND (b) AN HYDROPHILIC ROD-LIKE PARTICLE OF RADIUS r ADSORBED TO AN INTERFACE BETWEEN OIL AND WATER. 24
Figure 2 - SCHEMATIC REPRESENTATION OF INSTABILITY MECHANISMS THAT LEAD TO PHASE SEPARATION IN AN EMULSIFIED SYSTEM. 26
Figure 3 – a) TERNARY AND b) BINARY SCHEME REPRESENTATION FOR TWO POLYMERS (A AND B) IN THE SAME SOLVENT, WHICH UNDERGO A SEGREGATIVE PHASE SEPARATION. IN THE DIAGRAM, THERE IS THE BINODAL LINE THAT SEPARATES THE MACROSCOPICALLY SINGLE-PHASE REGION FROM THE TWO-PHASE REGION WITH THE CRITICAL POINT. THE DOTTED LINES ARE THE TIE LINES, WHICH CONNECT ONE COMPOSITION TO THE OTHER, PASSING THROUGH THE 50: 50 LINE (V/V). 29
Figure 4 – TENSION VECTORS AND THE THREE-PHASE CONTACT ANGLE θ FOR A SOLID PARTICLE ADSORBED AT AN INTERFACE BETWEEN TWO IMMISCIBLE PHASES A AND B.....30
Figure 5 - SCHEMATIC REPRESENTATIONS OF THE CHEMICAL STRUCTURES OF (a) AMYLOPECTIN WITH α-D-GLUCOSE UNITS LINKED AT (1→4) AND (1→6) (IN BLACK) AND (b) XYLOGLUCAN, IN WHICH THE MAIN CHAIN IS COMPOSED OF β-D-GLUCOSES LINKED AT (1 → 4) (IN BLACK), α-D-XYLOSE BRANCHES LINKED AT (1→6) (IN BLUE), AND TWO β-D-GALACTOSE UNITS AS XYLOSE SUBSTITUENTS LINKED AT O-2 (IN RED).....36
Figure 6 - SCHEME OF THE XYLOGLUCAN EXTRACTION AND PURIFICATION. AS DESCRIBED IN THE SCHEME, XG1 AND XG3 WERE PURIFIED AND XG2 WAS BOTH EXTRACTED AND PURIFIED. 38
Figure 7 - SCHEME OF THE PROCESS USED IN AMYLOPECTIN PURIFICATION 39
Figure 8 - a) TAMARIND FRUITS (TAMARINDUS INDICA) PURCHASED IN THE CURITIBA CITY MARKET. b) TAMARIND SEEDS. c) TKP PRODUCED AFTER MILLING THE COTYLEDONS IN A BLENDER AND PERFORMING

SOXHLET EXTRACTION. d) FINAL APPEARANCE OF EXTRACTED XYLOGLUCAN XG2. e) XG3, DONATED BY DSP GOKYO FOOD & CHEMICALS. 45
Figure 9 - SIZE EXLUSION CHROMATOGRAPHY (SEC) ELUTION PROFILES FOR XYLOGLUCAN a) XG1; b) XG2; AND c) XG3, USING AS MOBILE PHASE $NaNO_3$ 0.1 MOL L^{-1} AND NaN_3 AT 200 PPM AT A FLOW RATE OF 0.4 mL MIN^{-1}. 47
Figure 10 - CONFOCAL LASER SCANNING MICROSCOPY IMAGE OF A STARCH SAMPLE STAINED WITH 5 PPM RHODAMINE. 49
Figure 11 – SIZE EXCLUSION CHROMATOGRAPHY ELUTION PROFILES FOR SAMPLES (a) AMYLOPECTIN – SIGMA AND (b) PURIFIED AMYLOPECTIN, USING AS MOBILE PHASE $NaNO_3$ 0.1 MOL L^{-1} IN NaN_3 AT 200 PPM AT A FLOW RATE OF 0.4 mL MIN^{-1}. 50
Figure 12 – SIZE EXLUSION CHROMATOGRAPHY (SEC) ELUTION PROFILE OF THE PURIFIED WPI SAMPLE, NAMED FROM NOW ON β-LACTOGLOBULIN, USING AS MOBILE PHASE NaNO3 0.1 MOL L^{-1} IN NaN_3 AT 200 PPM AT A FLOW OF 0.4 ML MIN^{-1}.....51
Figure 13 - SCHEMATIC MODEL FOR THE MECHANISM OF FIBRIL FORMATION WHILE STIRRING DURING THE HEATING PROCESS AT pH 2.0. THE GREEN CIRCLES REPRESENT THE PROTEIN MONOMERS, WHICH ARE FOLLOWED BY THE ACTIVATED MONOMERS. LIGHTER BLUE OVALS REPRESENT REVERSIBLE AGGREGATES WHILE DARKER BLUE REPRESENTS THE IRREVERSIBLE ONES. THE RED CIRCLES WITH AN “H” ARE HYDROLYZED MONOMERS. 54
Figure 14 - ATOMIC FORCE MICROSCOPY IMAGES FOR β-LACTOGLOBULIN NANOFIBRILS AT pH 2.0 OF a) 4 μm^2 b) 0.6 μm^2 c) 1.14 μm^2 d) HEIGHT VERSUS DISTANCE FOR THE LINES 1 AND 2 REPRESENTED IN c). β-LACTOGLOBULIN MICROGELS AT pH 6.9 OF d) 2 μm^2 e) 0.78 μm^2.....55
Figure 15 - TITRATION CURVES OF ζ POTENTIAL IN RELATION TO pH FOR β-LACTOGLOBULIN MICROGELS ($\beta\text{-lg}_{MG}$) AND NANOFIBRILS ($\beta\text{-lg}_{NF}$), CALCULATED FROM a) STREAMING POTENTIAL ON A STABINO PARTICLE CHARGE MAPPING AND b) ELECTROPHORETIC MOBILITY ON A ZETASIZER NANO SERIES ZS. 56

Figure 16 – a) TITRATION CURVES OF ζ-POTENTIAL IN RELATION TO pH FOR β-LACTOGLOBULIN MICROGELS (B-LG_{MG}) AND NANOFIBRILS (β-LG_{NF}) IN WATER, NaCl 0.01 MOL L^{-1} OR NaCl 0.1 MOL L^{-1} AND b) REPRESENTATION OF THE POTENTIAL WINDOW ACCESSED AT EACH SOLVENT. 57
Figure 17 – MACROSCOPIC EVALUATION OF THE MIXTURES PREPARED FOR THE PHASE DIAGRAM CONSTRUCTION FOR XG2 MATERIAL.....58
Figure 18 - PHASE DIAGRAMS FOR AMP AND a) XG1, b) XG2 OR c) XG3, AFTER 162 H (COMPLETE PHASE SEPARATION). THE EMULSIONS WERE PREPARED AT THE CONCENTRATIONS DESCRIBED IN TABLE 1. THE RED AND BLUE TRIANGLES CORRESPONDS TO THE EMULSIONS STUDIED IN THIS REPORT: 1.023: 1.300 AND 5.200: 0.302 AMP: XG wt.%, RESPECTIVELY. 59
Figure 19 - MACROSCOPIC EVALUATION OF AMP EMULSIONS IN XG1 (1.023: 1.300 wt.%) IN THE (1) ABSENCE OF FLUOROPHORE, AND IN THE PRESENCE OF (2) AMYLOPECTIN LABELED WITH FLUORESCEIN ISOTHIOCYANATE (AMP-FITC) (3) AMYLOPECTIN LABELED WITH ISOTHIOCYANATE AND 5 PPM OF RHODAMINE 4) 5 PPM OF RHODAMINE. 61
Figure 20 - MACROSCOPIC EVALUATION OF AMP IN XG1 EMULSIONS (1.023: 1.300 wt.%) IN THE PRESENCE OF β-LG MICROGELS AND NANOFIBRILS AT DIFFERENT pH VALUES (4.0; 5.0; 6.0 AND 7.0). 62
Figure 21 - MACRO AND MICROSCOPIC EVALUATION (CLSM) OF AMP EMULSIONS IN XG1 (1.023: 1.300 wt.%) IN THE PRESENCE OF 1.0 wt.% β-LG MICROGELS AT DIFFERENT pH VALUES (4, 5, 6 AND 7) AFTER 24 H OF REST. 64
Figure 22 – CONFOCAL LASER SCANNING MICROSCOPY (CLSM) 3D PROJECTION OF AN AMP IN XG1 (1.023: 1.300 WT.%) EMULSION AT pH 4 AFTER 24 H OF RESTING, IN THE PRESENCE OF 1.0 wt.% β-lg MICROGELS.....65
Figure 23 - MICROSCOPIC EVALUATION (CLSM) OF AMP EMULSIONS IN XG1 (1.023: 1.300 wt.%) WITH 1.0 wt.% β-LG a) MICROGELS (ABOVE) OR b)

NANOFIBRILS (BELOW) AT DIFFERENT pH VALUES AFTER 1 H OF REST. EACH IMAGE IS ACCOMPANIED BY A DROPLET ZOOM-IN.....66
Figure 24 – CLSM EVALUATION OF PARTICLE AGGREGATION (MICROGELS – β-lg_{MG} OR NANOFIBRILS – β-lg_{NF} at 1.0 wt.%) ONLY IN AMP OR IN XG1 FROM pH 4.0 TO 7.0, AFTER 24 H OF REST. 67
Figure 25 - MACRO AND MICROSCOPIC (CLSM) EVALUATION OF AMP IN XG2 EMULSIONS (1.023: 1.300 wt.%) IN THE PRESENCE OF 1.0 wt.% β-LG MICROGELS. ALL OF THE CLSM IMAGES ARE IN THE PRESENCE OF 1.0 wt.% β-LG_{MG}. 68
Figure 26 - MACRO AND MICROSCOPIC (CLSM) EVALUATION OF XG2 IN AMP EMULSIONS (0.302: 5.200 wt.%) IN THE PRESENCE OF 1.0 wt.% β-LG MICROGELS, AT pH 4.0; 5.0; 6.0 AND 7.0. 70
Figure 27 - EMULSIONS IN THE PRESENCE OF 1.0 wt.% OF MICROGELS (β-lg_{MG}) OR NANOFIBRILS (β-lg_{NF}) AT CONCENTRATIONS OF 1.300: 1.023 XG3: AMP wt.%.....72
Figure 28 - CONFOCAL LASER SCANNING MICROSCOPY (CLSM) IMAGES OF AMP-IN-XG3 EMULSIONS AT 1.023:1.300 wt.% AT 1H AND 24 H AT DIFFERENT pH VALUES. 73
Figure 29 – COMPARISON BETWEEN THE BEHAVIOUR OF β-LG_{MG} AND β-LG_{NF} AT THE INTERFACE OF AMP IN XG3 (1.023:1.300) EMULSIONS AT DIFFERENT pH VALUES.THE NANOFIBRILS ADSORB AT THE INTERFACE WITHIN A HIGHER RANGE OF pH.....74
Figure 30 – MACROSCOPIC AND MICROSCOPIC (CLSM) EVALUATION OF AMP-IN-XG3 EMULSIONS (1.023: 1.300 wt.%) IN THE PRESENCE OF AN EQUAL MIXTURE OF NANOFIBRILS AND MICROGELS, EACH ONE AT 1.0 wt.%. 76
Figure 31 – MACROSCOPIC EVALUATION OF AMP IN XG3 EMULSIONS (1.023: 1.300 wt.%) WITH β-LG MICROGELS OR FIBRILS AT a) 0.01 MOL L^{-1} NaCl AND b) 0.1 MOL L^{-1} NaCl.....77
Figure 32 - MICROSCOPIC EVALUATION OF AMP IN XG3 EMULSIONS (1.023: 1.300 wt.%) WITH β-LG MICROGELS OR FIBRILS AT BOTH 0.01 MOL L^{-1} NaCl OR 0.1 MOL L^{-1} NaCl. 78

LIST OF TABLES

Table 1 - POLYSACCHARIDE CONCENTRATION VALUES USED IN PHASE DIAGRAM CONSTRUCTION.....43
Table 2 - MACROMOLECULAR INFORMATIONS OF THE EXTRACTED AND PURIFIED XYLOGLUCANS.....48
Table 3 - MACROMOLECULAR INFORMATION OF PURIFIED AND NON-PURIFIED AMYLOPECTIN 50

CONTENTS

1 INTRODUCTION 18
1.1 OBJECTIVES 20
1.1.1 General objective 20
1.1.2 Specific objectives 20
2 LITERATURE REVIEW 21
2.1 GENERAL FEATURES OF EMULSIONS 21
2.2 WATER IN WATER EMULSIONS 27
2.2.1 Biopolymers used on the formation of emulsions 31
2.2.1.1 Milk protein particles 31
2.2.1.2 Amylopectin and xyloglucan polysaccharides 33
3 MATERIAL AND METHODS 37
3.1 POLYSACCHARIDE PURIFICATION 37
3.1.1 Xyloglucan purification 37
3.1.2 Amylopectin purification 38
3.2 WPI PURIFICATION AND NANOPARTICLE PREPARATION 39
3.3 CHARACTERIZATION OF THE PURIFIED POLYSACCHARIDES AND PROTEIN. 40
3.3.1 Size Exclusion Chromatography (SEC) of the protein and polysaccharides, ^{1}H Nuclear Magnetic Ressonance (NMR) and protein content 40
3.3.2 Size, Particle morphology and Zeta potential 41
3.4 PHASE DIAGRAM CONSTRUCTION 42
3.5 EMULSION PREPARATION AND EMULSION STABILITY EVALUATION 43
4 RESULTS PRESENTATION 45
4.1 CHARACTERIZATION OF THE PURIFIED PROTEIN AND POLYSACCHARIDES. 45
4.1.1 Xyloglucan characterization 45
4.1.2 Characterization of amylopectin 48
4.1.3 Whey Protein Isolate (WPI) 50
4.1.4 CHARACTERIZATION OF THE PRODUCED PARTICLES 52
4.1.4.1 Particle morphology 52
4.1.4.2 Particle charge 55

4.2 PHASE DIAGRAM CONSTRUCTION.....57
4.3 MACRO AND MICROSCOPIC EMULSION STABILITY 60
4.3.1 Emulsions of XG1 and AMP 60
4.3.2 Emulsions with XG2 and AMP.....68
4.3.3 Emulsions with XG3 and AMP.....71
5 FINAL CONSIDERATIONS 80
REFERENCES 82
APPENDIX 1 – ^{1}H NMR SPECTRA OF XG1, 2 AND 3 89
ANNEX 1 – ACADEMIC INFORMATION 90

1 INTRODUCTION

Emulsions are colloidal systems in which liquid droplets and/or liquid crystals are dispersed in a liquid, formed by mixing two immiscible (or low miscibility) liquids. One particular type of emulsion is the water-in-water (w/w). They are composed of thermodynamically incompatible macromolecules in solution, and separate into two distinct phases, enriched with one or another polymer.

Stable emulsions present themselves in several industrial sectors such as food, cosmetics, pharmaceuticals, agrochemical, and paints. In the food industry, there are plenty of food emulsions composed of mixtures between oils and water. Changing the oily phase from emulsion food products to an aqueous one, producing w/w emulsions, is an interesting approach to reduce fat content, which would extend the possibilities for food-grade products that contain polymers and polysaccharides which phase separate when mixed.

Amphiphilic molecules are not able to stabilize w/w emulsions due to the interface thickness, which is larger than the one between oil and water with bigger interfacial tension values. The width of the w/w interface is larger than the correlation length of the polymer segment chains, which means a few nanometers (Tromp et al., 2014).

An alternative for obtaining stable water-in-water emulsions is the addition of solid particles that adsorb at the interface by the so-called Ramsden-Pickering effect. The stabilization of these w/w emulsions depends on the interaction between the solid particles and the aqueous polymers phases. Although calling particles that arise from macromolecules simply as solid Pickering particles might ignore important changes in biopolymer conformation at interfaces, this should not stop food researchers from finding materials that deliver the properties of true Pickering emulsions (Murray, 2019). Studying these complex interactions is of utmost importance for figuring out which is the next step of research in this field - until w/w emulsions are found at the supermarket shelves.

Up until now, some aqueous biphasic systems have been reported in the literature. Dickinson (2019) published a review that presents examples of particle-based stabilized w/w emulsions. Although many studies are on non-edible model systems like poly(ethylene oxide) (PEO) and dextran, some reports of biocompatible polymers are found - a good example is the aqueous mixtures of amylopectin (AMP)

and xyloglucan (XG), firstly evaluated by Freitas et al. (2016). These authors investigated the stabilization of AMP and XG emulsions by the addition of β-lactoglobulin microgels (β-lg$_{MG}$), which occurred for pH ≤ 5.0, a condition in which the interaction of the protein particles with the XG lead the particles to enter the interface of the droplets. The interaction between β-lg$_{MG}$ and XG was further discussed by Gtari et al. (2016), who investigated the spontaneous binding of XG into microgels.

Using a model system, Gonzalez-Jordan et al. (2016) compared the influence of the β-lactoglobulin particle morphology on the stabilization of w/w emulsions of PEO and dextran. They found that the partition of the protein particles to each phase depended on the pH, on which phase is the continuous one, and on the particle morphology.

Another important aspect is associated with the comparison between particles with different morphologies but the same volume. Faraudo and Bresme (2003) obtained analytical results for the particles detachment energy with different aspect ratios and orientations at the interface. In general, it is expected for the spherical-shape ones to have higher desorption energy than particles with high aspect ratios (rod-shaped ones) (Faraudo; Bresme, 2003). However, the rod particles could cover a large interfacial area, compared to spherical particles, and when considering different volumes of particles, factors other than desorption energy govern the emulsion stabilization phenomenon - such as the formation of multilayered particles in the shape of fibrils that cover the interface, as reported by Song et al. (2016) for nanofibrils stabilizing poly(ethylene glycol) (PEG) and dextran emulsions.

The amylopectin and xyloglucan emulsions have been, so far, stabilized when the pH is set below 5.0. Since many food formulations are in higher pH values than this, this work seeks to expand the knowledge on the stabilization of w/w emulsions composed of amylopectin and xyloglucan. The stability will be explored through the addition of isolated protein nanoparticles or in mixtures of them, with spherical and cylindrical morphologies. The purpose is to compare the effect on the stabilization of the emulsions as a function of time, particle shape and pH.

1.1 OBJECTIVES

1.1.1 General objective

The general objective of this project is to develop w/w emulsions based on polysaccharides and evaluate their stabilization against the addition of particles with different morphologies.

1.1.2 Specific objectives

To purify and characterize the polysaccharides and the protein that will be used in w/w emulsions – amylopectin, xyloglucan, and β-lactoglobulin;

To construct the phase diagram for the purified polysaccharide mixtures;

To produce protein particles with different morphologies (microgels and nanofibrils);

To characterize the protein particles produced through atomic force and confocal laser scanning microscopies, through dynamic light scattering and zeta potential analysis;

To analyse the stability of emulsions formed by amylopectin and xyloglucan through the addition of protein particles with the same compositions but with different morphologies in water and in NaCl solutions.

2 LITERATURE REVIEW

2.1 GENERAL FEATURES OF EMULSIONS

According to the definition given in the Gold Book of IUPAC (2014), an emulsion consists of a fluid colloidal system in which liquid droplets and/or liquid crystals are dispersed in another liquid. Even though the limits for the dispersed phase of colloidal systems defined by IUPAC are in the size regime from 1 to 1000 nanometers, the emulsion droplets often may exceed these limits (McNaught; Wilkinson, 1997). Generally, emulsions are firstly classified by means of their **type** or **size**. When considering the **types**, there are water/oil (o/w or w/o), oil/oil (o/o), water/water (w/w) or multiple emulsions such as oil/water/oil (o/w/o), water/oil/water (w/o/w) or water/water/water (w/w/w) emulsions. In the absence of emulsion stabilizers, the type of emulsion formed depends on some factors, such as the volumetric ratio of the liquids in the emulsion and the viscosity of the two pure liquids. When the emulsions are classified by their **size**, it should be highlighted that the classification is not rigorous, serving only as a guide depending on the emulsion, as shown: the dispersed phase droplets are, in the case of macroemulsions, larger than 0.1 μm and lesser than 5 μm; for nanoemulsions between 20 and 100 nm and for microemulsions between 5 and 50 nm, which are also called micellar systems (Schramm, 2014; Goodarzi, Zendehboudi, 2019).

Stable emulsified products can be found in the form of mayonnaise, drinks, ice cream (food industry); creams, lotions, and sunscreens (cosmetics/pharmaceuticals); anaesthetics; herbicides, insecticides (agrochemical industry); in addition to resin emulsions (paints) (Murray, 2019).

When in the presence of surfactants and cosurfactants the microemulsions are systems considered thermodynamically stable, as their spontaneous formation takes place through the strong adsorption of surfactants at the interface between the two phases. The stability of these microemulsions is something atypical in ordinary emulsions (Shaw, 1992), as will be discussed. Such thermodynamic behaviour of emulsions is explained by the associated change in the free energy, which is proportional to the sum of the free energy needed to create a new area of interface ($\Delta A\gamma_{AB}$) and to the configurational entropy (ΔS_{conf}), according to equation (1).

$$\Delta G_{form} = \Delta A \gamma_{AB} - T\Delta S_{conf} \quad (1)$$

In the emulsions formation, the generated systems have interfacial area change equal to $4\pi r^2$ (for each droplet of radius r) and interfacial tension γ_{AB} between phases A and B at a temperature T (Cosgrove, 2009). With a significant number of droplets, the value of ΔS_{conf} is positive, and the interfacial adsorption of amphiphilic molecules causes a decrease in the tension γ_{AB}. In this way, the enthalpic term represented by $\Delta A \gamma_{AB}$ has a positive and small value, leading to a negative free energy change (ΔG_{form}), which reflects on the spontaneous formation of a microemulsified system.

It is noticed that the value for interfacial tension commonly found for classic emulsions formed by oil and water ($\gamma_{o/w}$), which phase separate, are in the order of 30 mN m^{-1} as described by Esquena (2016), although values between 13 and 51 mN m^{-1} are found elsewhere (Li et al., 2021), depending on the type of oil used.

The term referring to the interfacial area variation ΔA is associated with values in the order of 10^4 to 10^5 m^2. This means that in the absence of a surfactant, in order to fulfill the requirement $\Delta A \gamma_{AB} \leq T\Delta S_{conf}$ the term $T\Delta S_{conf}$ should be associated with $1000 k_B T$ (where k_B is the Boltzmann constant), and the value of $\gamma_{o/w}$ must be small enough to satisfy this condition. Low interfacial tensions values (in the order of magnitude of 10^{-4} to 10^{-2} mN m^{-1}) lead to a greater ΔS_{conf} term than $\Delta A \gamma_{AB}$ and to a negative value of ΔG_{form}. The condition described above can be attained by adding surfactants or co-surfactants to the system. When the emulsion stabilization occurs with the presence of plenty of small droplets that do not collide, the system is said to be kinetically stabilized since the tendency to coalescence is reduced (Cosgrove, 2009; McClements, 2016).

When emulsions are stabilized by solid particles that adsorb at the interface between the two liquids, stabilization occurs by the so-called Pickering effect (Aveyard et al., 2003). Even though the usual term is “Pickering”, who gave an explanation to the phenomenon of emulsification using solid particles, Ramsden had described the presence of solid particles in oil drops in water four years early (Ramsden, 1904; Pickering, 1907).

For Pickering emulsions stabilized with a monolayer of nanoparticles adsorbed at the interface, the contact angle measured between the tangent of the solid particle

surface (θ) with one of the liquids (commonly taken through the more polar one) is a key parameter. Following the empirical rule described by Finkle et al. (1923), the type of emulsion formed depends on the particle wettability in water and oil, as follows: when the θ angle locates between $0° \leq \theta \leq 90°$, the particle is wetted by the aqueous phase, which interferes on the curvature of the interface that will be formed, leading to the formation of an oil-in-water (o/w) emulsion. If the value of θ is between $90° \leq \theta \leq 180°$, the particle is wetted by the oil phase and there is a tendency to form a water-in-oil (w/o) emulsion (Finkle et al., 1923; Binks; Horozov, 2006). In situations where $\theta = 0°$ or $\theta = 180°$, the particle is completely wetted in the aqueous or oil phases, respectively, so that the emulsion is not stabilized by the Pickering effect.

By adding spherical particles that attach to the surface of the dispersed phase droplets, a reduction in the interfacial free energy occurs. Because of the interface deformation when the particle is moved, the angle formed between the particle and the interface changes. Considering a fixed angle as the initial state and the final state as the particle entirely submerged, it is easier to determine the change of the surface free energy (ΔG) considering the detachment of the particle from the interface.

The minimum energy needed to desorb a particle from the interface and move into a bulk phase is represented by ΔG_d. ΔG_d is related to the squared radius R of the droplets, to the interfacial tension between the phases γ as well as to the value of θ, which is the angle that the particle makes with the aqueous interface, that is, for systems formed by oil and water, the angle θ is always measured towards the most polar phase, according to eq. (2) and (3) (Binks; Horozov, 2006).

According to this equation, one can observe that the value for the desorption of a hydrophilic particle from the interface to the oily phase (ΔG_{do}) requires more energy than to aqueous one ($\Delta G_{do} > \Delta G_{dw}$). The sign inside the parentheses is negative when considering the removal of the particle in direction to the aqueous phase (eq. (3)), opposite to the situation when the sign is positive, when the detachment occurs towards the oil phase, see eq. (2). If the particle is hydrophilic, one can deduce that the sign is negative when considering that the removal of the particle is in relation to the phase by which the particle is preferably wetted; and with a positive sign a thermodynamically unfavorable situation occurs.

$$\Delta G_{do} = \pi R^2 \gamma \, (1 + \cos\theta)^2 \tag{2}$$

$$\Delta G_{dw} = \pi R^2 \gamma \ (1 \ - \cos\theta)^2 \tag{3}$$

For particles that have a higher aspect ratio in relation to spheres, that is, in the form of rods, equation (4) is considered for particle with contact angles between $0° \leq \theta \leq 90°$ and equation (5) for angles between $90° \leq \theta \leq 180°$ to the interface of an emulsion. Parameters a and b that appear in equations (4) and (5) are positive constants related to the particle geometry, representing a correction of equation (2) and (3), where a is the value of the largest and b the smallest value of the half-axis length of the particle, as FIGURE 1 shows (Binks; Horozov, 2006; Machado et al., 2019).

$$\Delta G_{dw} = \gamma \pi b^2 (1 - cos\ \theta)^2 \left[1 + \frac{\left(\frac{a}{b} - 1\right)^2}{(1 - \cos\theta)} + \frac{2\left(\frac{a}{b} - 1\right)(\sin\theta - \theta\cos\theta)}{(1 - \cos\theta)^2}\right] \tag{4}$$

$$\Delta G_{do} = \Delta G_{dw} + 2\gamma \pi b^2 \cos\theta \left[\left(\frac{a}{b} - 1\right)^2 + \pi\left(\frac{a}{b} - 1\right) + 2\right] \tag{5}$$

Figure 1 - REPRESENTATION OF AN (a) HYDROPHOBIC SPHERICAL PARTICLE AND (b) AN HYDROPHILIC ROD-LIKE PARTICLE OF RADIUS r ADSORBED TO AN INTERFACE BETWEEN OIL AND WATER.

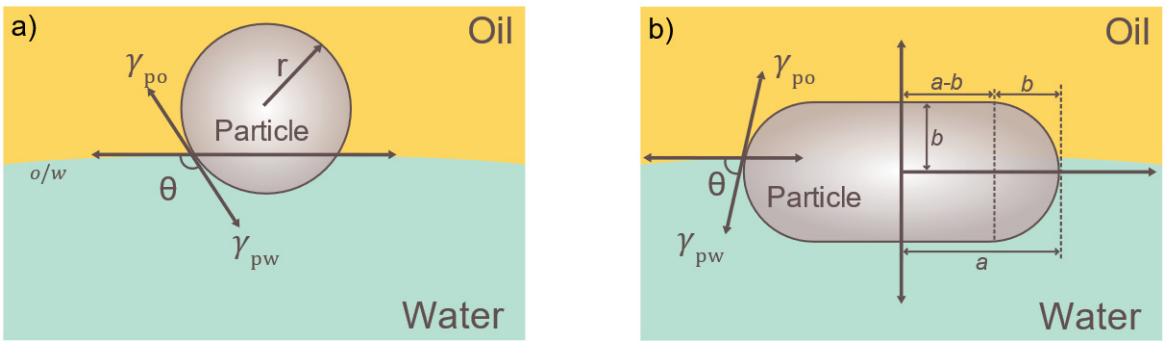

SOURCE: The author (2022) – adapted from Binks; Horozov (2006) and Machado et al. (2019).

The destabilization processes of emulsions occur due to the existence of external forces such as gravitational, centrifugal, electrostatic, or magnetic fields. The droplets **sedimentation** or **creaming** occurs in response to the gravitational or centrifugal force acting on the emulsion; in both processes, a droplet concentration gradient is generated, in which the gravitational or centrifugal force exceeds the Brownian motion, with sedimentation occurring when the droplets are denser than the

continuous medium and creaming when the droplets are less dense than the continuous medium.

Flocculation is related to electrostatic interactions or van der Waals attractive forces, and it occurs when droplets aggregate, maintaining their interface. **Coalescence** and **Ostwald aging** are the result of an attempt to minimize the total surface free energy associated with the interfacial tension existing between the dispersed and continuous phases. These processes tend to happen when there is a high number of non-stabilized droplets, with **coalescence** being the mechanism by which two or more groups of droplets generate a single drop, in a thermodynamically spontaneous process. **Ostwald aging** occurs when the droplets undergo an increase in their volume due to cosolubility or to limited solubility between the two phases, without the coalescence phenomenon. With larger values of droplet radii, there are smaller pressure differences between the dispersed and continuous phases, leading to a minor interfacial free energy, when analysing the product $\Delta A\gamma_{AB}$.

Phase inversion is the complete inversion between the dispersed and continuous phases. The phase inversion depends on specific conditions - such as pH, temperature, concentration, etc. (Cosgrove, 2009; Goodarzi; Zendehboudi, 2019; Kilpatrick, 2012). It is important to emphasize that these processes can occur simultaneously in the same sample, with gravitational or thermodynamic origin – or both! These phase separation mechanisms are illustrated in FIGURE 2.

Figure 2 - SCHEMATIC REPRESENTATION OF INSTABILITY MECHANISMS THAT LEAD TO PHASE SEPARATION IN AN EMULSIFIED SYSTEM.

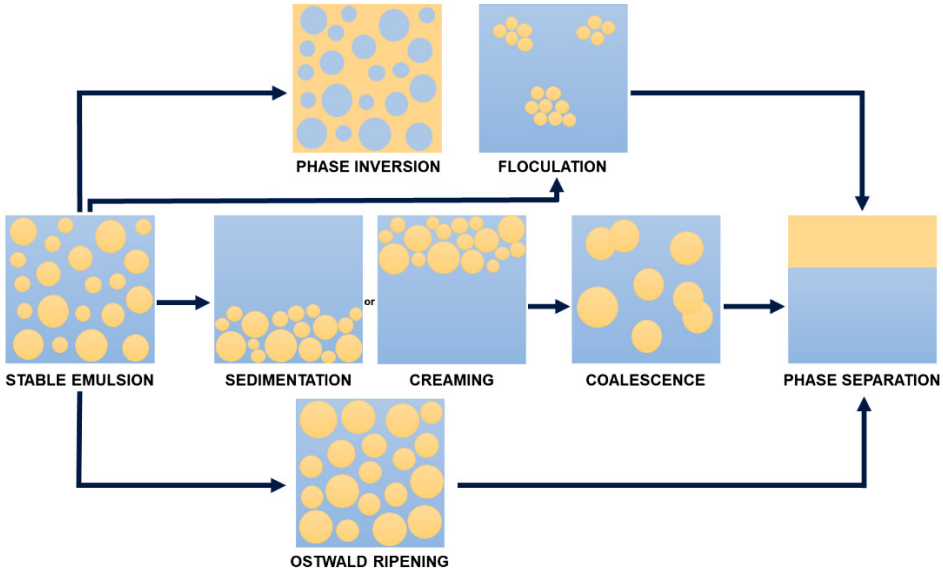

SOURCE: The author (2022) – adapted from Hu et al. (2017).

To avoid creaming or sedimentation, which occur when the gravitational force (given by the product of mass and gravitational acceleration) exceeds Brownian diffusion (given by the product $k_B T$, where k_B is the Boltzmann constant and T is the absolute temperature), one can reduce the size of the disperse phase droplets so that Brownian diffusion is predominant in relation to the gravitational force. Another possibility is to equalize the densities between the dispersed and continuous phase, or to add some thickening agent that generates high viscosities at low shear rates.

Flocculation can be prevented by adding repulsive energy, which can be produced through electrostatic repulsion, or by having high values of continuous phase viscosity (Schramm, 2014).

Ostwald aging can be avoided by either equaling the droplets size distribution or modifying the compressibility of the interfacial thin film in the droplets, increasing their Gibbs elasticity, by adding a small amount of a highly insoluble oil. The oil is responsible for reducing the diffusion coefficient of molecules in the dispersed phase - in the case of emulsions formed by oil and water.

Coalescence can be avoided by obtaining stable films at the dispersed and continuous phase interface, adding polymeric surfactants, for example, or reducing the volume fraction of the dispersed phase, as small droplet sizes lead to a reduction in the frequency of droplet collisions and prevent coalescence (Akbari; Nour, 2018). Phase inversion presents itself as a particular mechanism for each system, which can

be either catastrophic or transient, with no generalized method to prevent this type of destabilization of the emulsion (Tadros, 2009).

2.2 WATER IN WATER EMULSIONS

Water-in-water emulsions are formed by mixing two hydrophilic and immiscible polymers with each other above a critical concentration. Such aqueous two-phase systems have been reported, according to Esquena (2016), in 1896 with the report by Beijerinck who described the phenomenon of phase separation when mixing gelatine and starch. Despite this early report, the real understanding of the physicochemical fundamentals and the behaviour of water-in-water emulsions has been the object of recent studies, both in “model systems”, such as poly(ethylene oxide) (PEO)/dextran (Nguyen et al., 2013, 2015) and in systems with potential application in the most diverse industrial sectors, such as gelatine and starch (Firoozmand et al., 2009), gelatine and maltodextrin (Firoozmand; Rousseau, 2014), starch and locust bean gum (Murray; Phisarnchananan, 2016) or amylopectin and xyloglucan (Freitas et al., 2016).

Biopolymer dispersions that undergo a segregative phase separation process result in droplets of a polymer-A rich phase dispersed in another polymer-B rich phase. Over time, if no stabilizing agent is added, the emulsions lose their micro-heterogeneity characteristic, being destabilized, considering that polymers that have high molar mass are associated with low mixing entropy (Flory, 1953; Hatti-Kaul, 2001). In aqueous two-phase systems (w/w), amphiphilic molecules are not adsorbed at the interface as in o/w systems to reduce the interfacial tension. The adsorption does not happen because the interface between the two aqueous phases is expressed in length scales greater than the correlation length of the macromolecule dispersions, that is, a common surfactant is not able to “see” the interfacial region between two polymers, which has a few nanometers (Tromp et al., 2014). As w/w interfaces are larger and less defined than o/w ones, the interfacial tension values are expected to be smaller, and in fact they are – while for o/w systems the values of γ are in the order of 30 mN m^{-1}, for w/w systems the tensions found are lower than 10^{-2} mN m^{-1} (Esquena, 2016).

Thus, an alternative for the stabilization of water-in-water emulsions is the addition of molecules that are large enough to be adsorbed on the w/w interface, or to covalently bond with the two phases. Some copolymers in the form of diblocks and

triblocks or linear polyelectrolytes were used to stabilize emulsions formed by PEO or PEG and dextran (Buzza et al., 2013; Tea et al., 2019). Another possibility is the addition of colloidal particles that accumulate at the interface, in a similar way to what happens for emulsions formed by oil and water.

In the case of water-in-water emulsions, the interfacial tension is one of the determining parameters to find out whether the interfacial adsorption of particles will occur or not. For these systems, it is possible to modulate such interfacial tensions by varying the polymeric concentrations, without necessarily changing the volumetric ratio between the two phases. FIGURE 3 shows the schematic representation of a ternary phase diagram for water-in-water emulsions, which is often represented as a binary diagram since water is a common solvent in both phases (Atefi et al., 2016). It is known that the interfacial tension is constant in the same tie line, and in the 50:50 (v/v) line (TLL or tie line length), the tension γ_{AB} follows a linear relationship in the form of the power law $\gamma \propto TLL^{\propto}$ (Balakrishnan et al., 2012; Aveyard et al., 2003; Keal et al., 2018). One can deduce that the higher the interfacial tension is, the larger will be the exponent $\propto$. In the phase diagrams of biopolymer mixtures, the binodal line containing the critical point divides the regions where there is macroscopic phase separation, due to the incompatibility of the polymers, from the region where the number of phases is equal to one. Furthermore, there are regions that have the continuous phase of polymers A or B, as shown in FIGURE 3.

Figure 3 – a) TERNARY AND b) BINARY SCHEME REPRESENTATION FOR TWO POLYMERS (A AND B) IN THE SAME SOLVENT, WHICH UNDERGO A SEGREGATIVE PHASE SEPARATION. IN THE DIAGRAM, THERE IS THE BINODAL LINE THAT SEPARATES THE MACROSCOPICALLY SINGLE-PHASE REGION FROM THE TWO-PHASE REGION WITH THE CRITICAL POINT. THE DOTTED LINES ARE THE TIE LINES, WHICH CONNECT ONE COMPOSITION TO THE OTHER, PASSING THROUGH THE 50: 50 LINE (V/V).

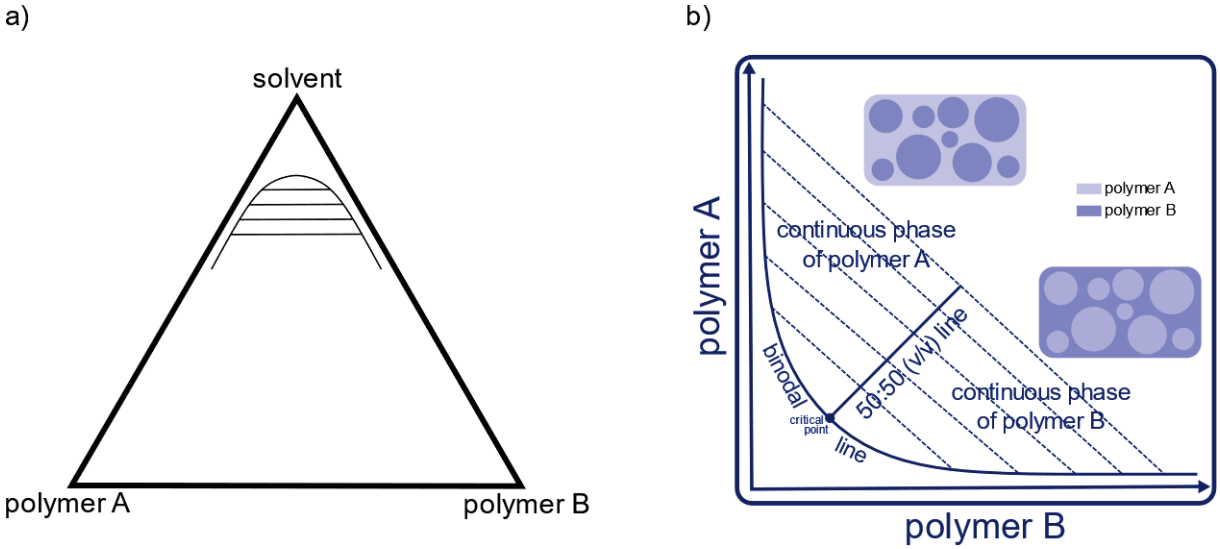

SOURCE: The author (2022) - adapted from Hazt et al. (2020).

Due to the fact that much lower interfacial tensions are associated with w/w emulsions, a discussion arises about how significant is the effect of reducing the free energy (ΔG) when the particle enters the interface. Firoozmand et al. (2009) suggested that the origin of the Pickering effect in water-in-water emulsions could be associated with the depletion force of flocculated particles leaving polymer-rich solutions and accumulating at the solvent-rich interface, where the particles would still be under Brownian motion. However, using simulations considering theoretical polymers without specific interactions between them and the self-consistent field method (SCF), even with low values calculated for $(\gamma_{PA} - \gamma_{PB})$ ($\sim 1\,\mu N\,m^{-1}$ for polymers A and B with different molar masses and architectures), the values of ΔG tend to be larger than the kT kinetic energy term for w/w systems. This happens when considering particles a few nanometers long and far from the critical point of the phase diagram, leading the particle to migrate to the interface associated with the lowest free energy (Ettelaie et al., 2019).

Thus, there is an increase in the value of ΔG because of the increase in the variation of the interfacial area when considering the desorption of the particle from the water/water interface. From equations (2) and (3) already described, it is assumed that gravitational forces are excluded and the angle that the particle makes with the

interface is defined by the difference in the interfacial tension of the particles with phase A or phase B (γ_{PA} e γ_{PB} , respectively), according to the classical Young equation for a particle at an interface between phases A and B (FIGURE 4), as shown in sequence - equation (6). The change in free energy (ΔG) is negative always that $|\gamma_{PA} - \gamma_{PB}| < \gamma_{AB}$ (Dickinson, 2019).

Figure 4 – TENSION VECTORS AND THE THREE-PHASE CONTACT ANGLE θ FOR A SOLID PARTICLE ADSORBED AT AN INTERFACE BETWEEN TWO IMMISCIBLE PHASES A AND B.

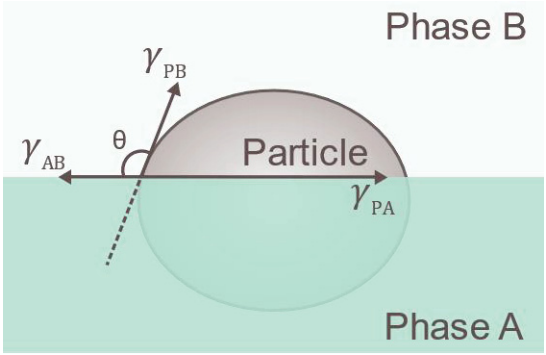

Source: The author (2022).

$$\gamma_{AB} \cos(\theta) = (\gamma_{PA} - \gamma_{PB})$$
$$\cos(\theta) = (\gamma_{PA} - \gamma_{PB})/\gamma_{AB} \quad (6)$$

The w/w emulsions can also go through the gelling process without temperature effect, by cold-gelation. In water-in-water emulsions of PEO and dextran stabilized by particles prepared from a bovine whey protein (β-lactoglobulin), this process occurs induced by the addition of salt or by reducing the net charge density of the protein particles, through changes in the pH in towards the isoionic point of the particle (Gonzalez-Jordan et al., 2017). In this way, instead of adsorbing at the w/w interface, the protein particles form a gelled network in the continuous phase creating stable emulsions. In addition to the increase in viscosity that can be macroscopically observed in these systems, some deformed dispersed phase droplets are noticed through microscopic techniques due to the gel formation.

Gonzalez-Jordan et al. (2016) reported that by varying the reaction conditions, particles produced from β-lactoglobulin can present different morphologies and behave distinctly at the interface of PEO/dextran emulsions. Under conditions of low ionic strength and pH between 2 and 3, β-lg forms nanofibrils with a rigid structure, through nucleation followed by oligomerization. Ordered nuclei are formed only after the

latency phase in a concentrated solution, and then the monomer is cooperatively converted to fibril (Rochet; Lansbury Jr, 2000). At pH 5.2, a value closer to the isoelectric point, the particles produced have a spherical shape and are called microgels. At higher protein concentrations and above the isoelectric point, clusters with the presence of branches are formed, also known as fractal aggregates (Nicolai, 2016).

Freitas et al. (2016) demonstrated the spontaneous adsorption of spherical protein particles of β-lg at the droplet interface of amylopectin (AMP) emulsions in a continuous phase of xyloglucan (XG) (extracted from seeds of *Hymenaea courbaril*), stabilizing the emulsions. Bassani (2017) in her master's thesis, discussed the influence of spherical particles in a system composed of AMP and XG polysaccharides, purified from the seed powder of the tamarind endosperm (TKP or Tamarind Kernel Powder), another source of XG. The stabilization of emulsions occurred with spherical particles at pH ≤ 5.

2.2.1 Biopolymers used on the formation of emulsions

The use of particles as stabilizing agents for food-grade emulsions should be considered when the interest is to apply such emulsions in food products (Nicolai; Murray, 2017). Examples of particles that can be used in emulsions with food applications are the ones formed from β-lactoglobulin (β-lg), one of the proteins present in the whey soluble fraction from ruminant species. When this protein is heated, its denaturation occurs and intermolecular interactions (non-covalent and covalent bonds) give rise to aggregates that form irreversibly. Such aggregates, when present at the water-in-water amylopectin/xyloglucan interface, do not completely inhibit phase separation macroscopically, but increase the stability of the system, slowing down the phase separation process (Freitas et al., 2016). In the next two items, the origins and applications of the materials used in the present work will be presented.

2.2.1.1 Milk protein particles

The proteins used as emulsifiers can be either animal proteins or plant proteins, according to their source. The plant-based ones consist majorly of soy protein, pea protein, wheat gluten, oat protein, buckwheat, sesame protein, and canola

protein. The most common animal ones are whey proteins, casein, bovine serum albumin, lysozyme, and ovalbumin (Kan et al., 2021).

The bovine milk has about 3.4 % of protein in its composition (Månsson, 2008), and the main classes of bovine milk proteins are whey proteins (20%) and casein, which is the main one (80%). Whey proteins used to be a waste product of dairy industry, since it is the residual product of cheese production. Nowadays, they can be commercially found as whey protein concentrate (in which the protein content varies from 60 to 85%), whey protein isolate (WPI – that has fewer minerals and lactose, enhancing the protein content for more than 90%), and whey protein in the form of hydrolysates, which improves the absorption of proteins (Jeewanthi et al., 2015).

The main components of whey proteins are a series of globular proteins: β-lactoglobulin (β-lg), α-lactalbumin (α-la), bovine serum albumin (BSA), and immunoglobulins. The β-lactoglobulin represents around 60% of the protein fraction in whey proteins, and the molar mass of each monomer is 18,300 g mol^{-1} (Hambling et al., 1991). The secondary structure of β-lactoglobulin is 43-50% β-sheets, 10-15% α-helices, 17% reverse-turn, and 17% aperiodic structures (Kinsella; Whitehead, 1989). Its conformation is pH and temperature-dependent, which makes this protein particularly modifiable since it is highly heat-labile. β-lg consists of 162 amino acids in a single peptide chain, owning five cysteine residues, two linking residues disulfide bonds, and one free thiol (SH) group, which interacts to form new thiol-disulphide interchanges leading to the formation of new structures (Wit; Klarenbeek, 1984; Fuente et al., 2002).

The second most-abundant protein fraction in whey proteins is the α-lactalbumin. It has a molar mass of about 14,000 g mol^{-1}, four disulphide bridges that lead to a high degree of renaturation after it denatures, making this protein the most heat-resistant whey protein (Wit; Klarenbeek, 1984). The BSA is a large globular protein, since it has a molar mass of 66,000 g mol^{-1}, containing about 580 amino acids and 17 intrachain disulphide bridges, with one free thiol group. The main types of immunoglobulins are IgG, IgA, and IgM and they consist of basic units composed of four polypeptide chains linked covalently by disulphide bridges (Kinsella; Whitehead, 1989).

When the whey protein isolate (WPI) is heated in controlled conditions of concentration, pH, temperature, and salt concentration, the aggregation of β-lg governs the formation of protein particles. With the denaturation of the whey proteins,

the proteins unfold and have their hydrophobic groups exposed. This structural change is followed by the formation of new disulphide bonding and electrostatic bridges between the proteins, leading to the formation of aggregates that form irreversibly due to these intermolecular interactions (non-covalent and covalent bonds) (Raikos, 2010; Guralnick et al., 2021).

When the pH is set around 2.0, Bolder et al. (2007) demonstrated that the β-lg is the only protein involved in the formation of fibrils, since heating β-lactoglobulin or WPI solutions led to fibril formation whilst heating α-la and BSA solutions did not form fibrils. Concerning the gel formation at moderate pH values, i.e., near the isoelectric point region, the presence of the α-la seems to interfere in the formation of aggregates through a thiol-disulphide interchange reaction during the gel formation, as demonstrated by Matsudomi et al. (1992). Although the contribution from α-la to aggregation is significant when heated together with β-lactoglobulin (due to its participation in the formation of non-covalent bonding), the β-lg dominates the aggregation process under heating (Fuente et al., 2002). To obtain single α-la nanoparticles the increase in hydrophobic interactions is significantly important, as demonstrated by Arroyo-Maya et al. (2012) who prepared α-la nanoparticles by the addition of different desolvation agents.

As well as physical properties, the isoelectric point (IP) of each whey protein also varies. While α-lactoalbumin and bovine serum albumin have IPs in the range of 4.8-5.1, the most common value for the IP of β-lg is around 5.2 (Bryant; Julian McClements, 1998). In order to obtain nanoparticles formed only by β-lg without considering other interactions, it is quite common to find procedures for the isolation of this protein. These procedures consist of anion-exchange chromatography (Fuciños et al., 2019), for example, or selective precipitation using trichloroacetic acid followed by dialysis (Bello-Pérez et al., 1998), which seems to be a simpler method but less adaptable to industrial scale.

2.2.1.2 Amylopectin and xyloglucan polysaccharides

One of the polysaccharides used to form the water-in-water emulsions in this thesis report was amylopectin, which can be found in starch. The starch is a reserve polysaccharide (a form by which plants storage energy) commonly found in higher

plants, in the form of granules with diverse shapes, sizes and compositions (Bergthaller; Hollmann, 2014). The water-insoluble starch granules are commonly found in corn/maize, potato, wheat, cassava, and rice. The granules are built of two distinct glucan polymers – amylopectin and amylose, and the ratio between them can vary according to the origin of the starch (Tester et al., 2004).

The major polymer in the starch granules is amylopectin, and it has a highly branched chain consisting of α-D-glucose units with (1→4) and (1→6) glycosidic bonds interconnected to the main chain (Ryan et al., 2006). The chain has from 20 to 30 monomers, and the chains can be divided in three different categories: A, B or C. A-chains are not substituted and are linked to the macromolecule by their reducing group. B-chains are similarly linked, but they carry A-chains and can be subdivided, depending on other structural details. C-chains terminate in the reducing group of the molecule (Manners, 1989). FIGURE 5a shows the structure of amylopectin.

The other starch component is amylose, which is a hydrophilic polymer lightly branched but not enough to affect its physical properties. This is the main reason why some reviews say that it consists on a linear α-D-glucose chain linked at (1→4), with a molar mass ranging from 10^4 to 10^5 g mol^{-1} (Manners, 1989; Bergthaller; Hollmann, 2014).

The gelatinization process consists on heating the starch granules in the presence of water excess. Since the granular structures present birefringence, when the polarization cross starts to disappear means that the granules have begun to swell irreversibly and their molecular orders have disrupted, with the breaking of hydrogen bonds. Together with the birefringence loss comes the granular swelling with water, starch solubilization, and a viscous behaviour (Manners, 1989; Bello Perez; Agama-Acevedo, 2017). This disruption of the ordered structures is usually a requirement to use the starch. Alter the gelatinization process happens, the starch is applied in a broad range of industrial products. Together with amylose, the amylopectin composes a homopolysaccharide with great nutritional and industrial importance.

After gelatinization, the separation of amylose from amylopectin usually requires harsher conditions – like the Schoch's method, which uses n-butanol to form a complex with amylose that precipitates and can be isolated (Schoch, 1945). Bello-Pérez et al. (1998) proposed a sort of starch purification method, which consists on the dissolution of starch using dimethylsulphoxide and precipitation with ethanol.

The other polysaccharide used to form the w/w emulsions in this thesis report was xyloglucan, which can be found either in plant cell walls or as a storage polysaccharide, in some seeds of trees. In the case of growing cell walls, xyloglucan is an abundant hemicellulosic polysaccharide in most dicot vascular plants. Xyloglucan is the generic name for a shortly branched polysaccharide composed by β-D-glucoses linked at (1 → 4). A part of the glucose units has α-D-xylose branches linked at (1→6), and xylose has some substituents at O-2 by β-D-galactose units. The last D-galactosyl residues can be linked with fucose residue linked at α-(1,2), depending whether the xyloglucan is obtained from plant cell walls (Park; Cosgrove, 2015). The structure of XG is represented in FIGURE 5b.

When in aqueous solutions, the xyloglucan behaves almost as a flexible random-coil polymer, due to the high degree of polymerization, but it is formally a worm like molecule, with some degree of self-association that leads to a higher viscosity. The gelation of the xyloglucan can be achieved through some diversified methods, like by the addition of alcohol, sugar, iodide solution, Congo red, polyphenols, or by enzymatic degalactosylation which removes galactose residues (Yuguchi et al., 2004; Nishinari et al., 2007; and Sakakibara et al., 2017).

The xyloglucan from tamarind seeds (*Tamarindus indica*) is highly water-soluble and it is used in the food industry as a thickener, as it forms viscous aqueous solutions (Nishinari et al., 2007). An overview published by Piqué et al. (2018) suggests that xyloglucan has a “mucin-like” structure, with a high swelling capacity, acting as an anti-invasion agent, preventing bacterial adherence. Among other interesting features, it also has some film-forming properties and the capacity to preserve tight junctions, at intestinal level and at the respiratory mucosa (Piqué et al., 2018).

In a recent review, Dickinson (2019) pointed out that the development of novel w/w microstructures from proteins and polysaccharides is the path to obtaining high-quality water-continuous food products. Since XG is a natural ingredient that behaves as a water-soluble fibre which is not digested, it is a suitable candidate for application in dietary foods and should be considered in the fabrication of these functional foods.

Figure 5 - SCHEMATIC REPRESENTATIONS OF THE CHEMICAL STRUCTURES OF (a) AMYLOPECTIN WITH α-D-GLUCOSE UNITS LINKED AT (1→4) AND (1→6) (IN BLACK) AND (b) XYLOGLUCAN, IN WHICH THE MAIN CHAIN IS COMPOSED OF β-D-GLUCOSES LINKED AT (1 → 4) (IN BLACK), α-D-XYLOSE BRANCHES LINKED AT (1→6) (IN BLUE), AND TWO β-D-GALACTOSE UNITS AS XYLOSE SUBSTITUENTS LINKED AT O-2 (IN RED).

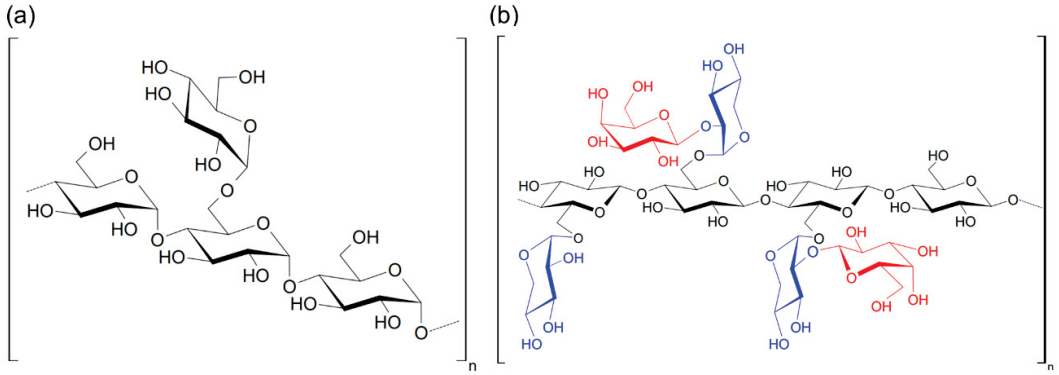

SOURCE: The author (2022) – adapted from Park; Cosgrove (2015) and Tester et al. (2004).

3 MATERIAL AND METHODS

3.1 POLYSACCHARIDE PURIFICATION

3.1.1 Xyloglucan purification

Three different sources of the endosperm of tamarind seeds (*Tamarindus indica L.*) were used to obtain xyloglucan (XG). The first XG was obtained from a commercial powder of the endosperm of tamarind seeds (TKP – Tamarind Kernel Powder) donated by the company Balasanka Mills and will be called **XG1**. The second sample was manually extracted from the powder of the fruit endosperm purchased in the Curitiba City Market, and will be called **XG2**. The third sample is a commercial XG donated by the company Dsp Gokyo Food & Chemicals (Lot 18.08.27-1) and will be called **XG3**.

For sample **XG1**, TKP was dispersed at 40 g L^{-1} in purified water with sodium azide (NaN_3) as preservative at 200 ppm for 12h. The extract was centrifuged at 10^4 g for 30 minutes at 25 °C. The supernatant was separated and filtered through Millipore™ membrane filters (diameter of 25 mm; pore size of 3 and 0.45 µm, composed by mixed cellulose esters). The polysaccharide was precipitated with 2 volumes of 99% ethanol. The precipitant was centrifuged at 10^4 g for 10 minutes and washed several times with ethanol and acetone.

To obtain the **XG2** sample from the seeds of *Tamarindus indica*, the methodology adopted was the one described by Freitas et al. (2003), who performed the extraction of xyloglucan from Jatobá (*Hymenaea courbaril*) seeds. The fruits of *Tamarindus Indica* purchased at the Curitiba City Market were manually peeled and the endosperms were obtained by boiling the seeds in distilled water for approximately 30 minutes, so that enzymatic inactivation occurred. The cotyledons were dried in an oven at 30 ºC and grinded, and from this step a “homemade” TKP (Tamarind Kernel Powder) was obtained. This TKP was subjected to delipidification in a Soxhlet extractor using hexane as solvent (AOCS method - Ac 3.11, 1983), for 48 hours, before following with the xyloglucan extraction procedure from TKP, described in the previous paragraph for XG1 sample.

The **XG3** (commercial) sample underwent a centrifugation test, where the material was dispersed at 2.0, 1.3 and 0.6% (m/m) (these concentration values were

chosen as they are the ones used later for the preparation of emulsions) in purified water with NaN_3 at 200 ppm and centrifuged at 14.1 x 10^3 *g* for 100 minutes, and the sedimentation of the material was observed. Thus, even being a commercial material, it went through the extraction process described for sample XG1 and also performed for sample XG2.

Figure 6 - SCHEME OF THE XYLOGLUCAN EXTRACTION AND PURIFICATION. AS DESCRIBED IN THE SCHEME, XG1 AND XG3 WERE PURIFIED AND XG2 WAS BOTH EXTRACTED AND PURIFIED.

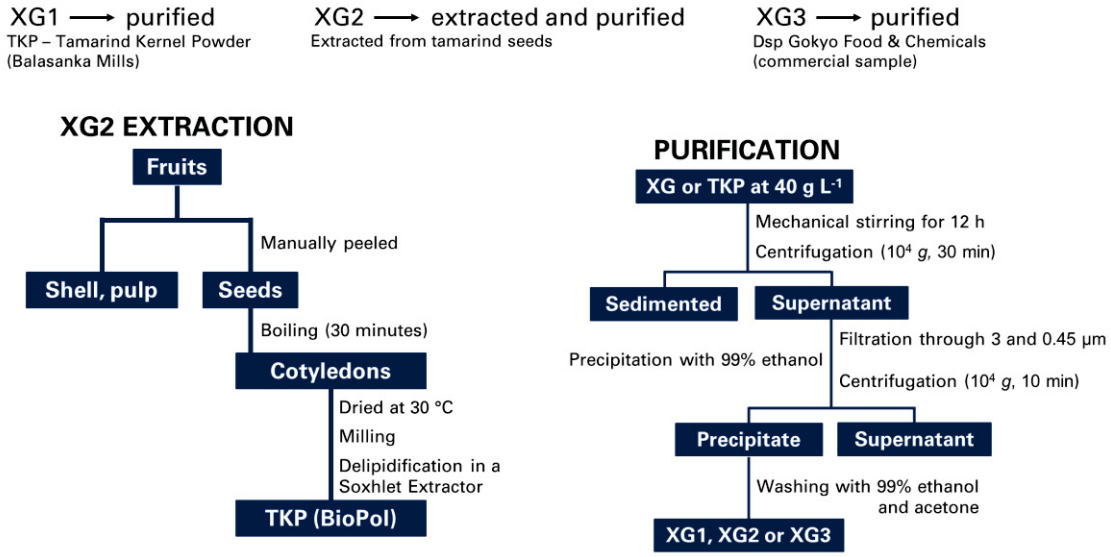

SOURCE: The author (2022).

3.1.2 Amylopectin purification

Amylopectin (AMP) was purchased from Sigma-Aldrich® (lot: BCBV5057). The AMP was dispersed at a concentration of 50 g L^{-1} in a mixture of dimethylsulfoxide and water at 95:5 (v/v), under magnetic stirring for 48 hours. After centrifugation at 10^4 g for 30 min and 20 °C, the polysaccharide was precipitated in the supernatant by adding 3 volumes of 99% ethanol. The purified AMP was then filtered, washed with ethanol, acetone and diethyl ether and then dried in a vacuum oven at 30 °C.

Figure 7 - SCHEME OF THE PROCESS USED IN AMYLOPECTIN PURIFICATION

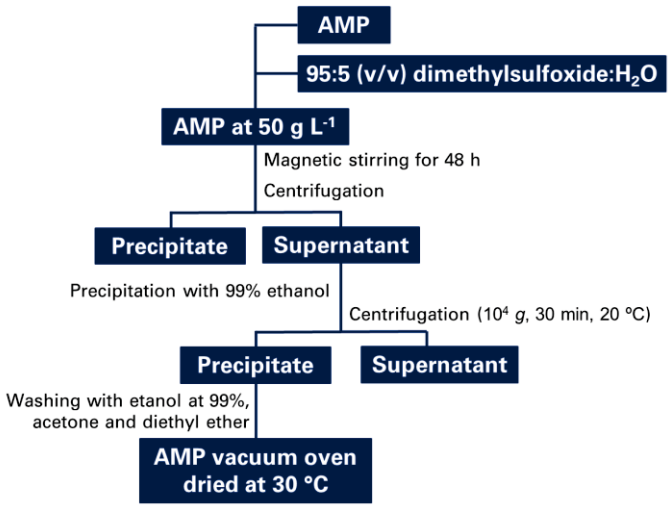

SOURCE: The author (2022).

3.2 WPI PURIFICATION AND NANOPARTICLE PREPARATION

β-lactoglobulin was obtained from the purification of bovine milk whey protein isolate – WPI (Sigma-Aldrich®, lot SLBM4081V). The material was dispersed in purified water (Milli-Q system) at 100 g L^{-1} in the presence of 200 ppm of sodium azide (NaN_3), under constant magnetic stirring for 24 hours. After changing the pH to 4.2 by adding glacial acetic acid, the dispersion was centrifuged at 5000 g for 10 minutes at 25 °C. The supernatant was removed and dialyzed against ultrapure water containing 200 ppm of NaN_3 for three days, with two water changes per day, in 12.4 kg mol^{-1} cut-off dialysis membranes (Sigma-Aldrich®, lot 3110). The water used in the first exchange had its pH adjusted to pH = 4.2 with the addition of glacial acetic acid. The material removed from the membranes was then frozen, for subsequent lyophilization and grinding.

After the purification, to obtain the protein particles, the WPI was slowly added to purified water (Milli-Q system) at a concentration of 100 g L^{-1}, containing 200 ppm of NaN_3 under constant agitation. After 12 hours of stirring, the solubilized material was centrifuged at 8000 g for 15 minutes at 25 °C. The β-lactoglobulin concentration was determined in the supernatant using a spectrophotometer at a wavelength (λ) of 278 nm, using the extinction coefficient of 0.96 L g^{-1} cm^{-1} determined by Townend et al. (1960). From the determined concentration (which was around 75 to 78 g L^{-1},

depending on the purification batch), the material was diluted to a final β-lg concentration of 40 g L^{-1}, for the protein particles preparation.

For the protein particles called **microgels**, the pH of the sample was adjusted to 6.9 with 0.1 mol L^{-1} HCl and the mixture was heated for 12 h at 80 °C in the presence of 5.3 mmol L^{-1} of $CaCl_2$, following the methodology proposed by Phan-Xuan et al. (2014). For the **fibrils**, the β-lg dispersion at 40 g L^{-1} was heated to 90 °C at pH 2.0 for 5 hours, under magnetic stirring (Bolder et al., 2007). The conversion from protein to protein-particles was determined measuring the free β-lg concentration (using a spectrophotometer at a wavelength (λ) of 278 nm, with the extinction coefficient of 0.96 L g^{-1} cm^{-1} determined by Townend et al. (1960) at the supernatant after centrifugation (4 h, 12.1 x 10^4 g) which made the particles sediment. In order to confirm that all of the particles had sedimented, atomic force microscopy images were obtained from the supernatant and no particles were observed.

3.3 CHARACTERIZATION OF THE PURIFIED POLYSACCHARIDES AND PROTEIN

3.3.1 Size Exclusion Chromatography (SEC) of the protein and polysaccharides, ^1H Nuclear Magnetic Ressonance (NMR) and protein content

The molar mass of XG, AMP and β-lg was determined using size exclusion chromatography (SEC - Viscotek, Malvern, United Kingdom). The system was composed of a VE 75010 GPC Degasser – Viscotek, a flow pump VE 1122 solvent delivery system (Viscotek, VE 5200 GPC Autosampler – Viscotek, United Kingdom), a polymethacrylate column (Shodex OHpak SB-806HQ with exclusion limit of 2 x 10^7 g mol^{-1}). The detectors consisted on a UV-Vis detector (Viscotek - VE 3210 UV/Vis) with λ adjusted to 280 nm, refractive index (IR), viscosimeter (η) and light scattering at 7 and 90° angles (LALS and RALS) detectors. The column temperature was 40 ºC. The mobile phase used was $NaNO_3$ at 0.1 mol L^{-1} in the presence of 0.02% (m/v) of NaN_3, at a flow of 0.4 mL min^{-1}. Each one of the purified polysaccharides and protein was dispersed at a concentration of 1 mg mL^{-1} in the mobile phase itself, centrifuged for 10 minutes at 10^4 g and filtered on Millipore™ membrane filters (diameter of 13 mm; pore size of 0.45 (first) and 0.22 µm (second), composed by mixed cellulose esters). The injection volume was 300 µL with a 100 µL loop. The calibration was performed

using the multi-detector homopolymer method type injecting a PEO standard (M_w = 24 kg mol^{-1}, Đ=1.05, Viscotek PolyCAL^{TM}) and checked with two other standards: PEO with M_w = 236 kg mol^{-1} and 250 kg mol^{-1}, both from Viscotek PolyCAL^{TM}.

The dn/dc values for AMP and XG1, 2 or 3 were determined by injecting samples into the same refractive index (IR) detector used for SEC. A stock solution of each polysaccharide at 1 g L^{-1} was prepared and diluted to five concentrations (0.2; 0.4; 0.6; 0.8; 1.0 g L^{-1}). The samples were injected right at the refractive index detector and the dn/dc value was equivalent to the slope of the refractive index increment caused by the concentration effect. For AMP, the dn/dc value was 0.146 mL g^{-1} and for XG it was 0.108 mL g^{-1}. For the β-lactoglobulin sample the value of dn/dc used was 0.180 mL g^{-1} (Van Dijk; Smit, 2000).

The OmniSEC software (version 5.10.461) was used to obtain the elution profiles as well as the values of VE (elution volume), M_w (weight-average molar mass), M_n (number-average molar mass), Đ (dispersion) and recovery after the chromatographic elution, in percentage.

The polysaccharides XG1, XG2 and XG3 under study were sent for ^{1}H NMR analysis. A Bruker AVANCE III 600 with a magnetic field of 14,095 Tesla (600 MHz) was used for obtaining mono and bidimensional spectra of the XG samples. For ^{1}H NMR spectra, 32 scans were recorded, using an inter-scan delay equal to 1 s. The XG1, 2 or 3 was solubilized at 10 g L^{-1} for ^{1}H NMR spectra using 99% D_2O and acetone as an internal standard (with 2.224 and 30.45 ppm chemical shifts, for ^{1}H and ^{13}C).

Total protein content measurements on the extracted and/or purified XG1, 2 and 3 were performed using the method of Lowry et al. (1951), using the Folin-Ciocalteu reagent and the at a wavelength (λ) of 660 nm and the method of Bradford (1976) dye binding assay at a wavelength (λ) of 595 nm. In both quantifications, the standard used was BSA (bovine serum albumin) and the readings were performed in a spectrophotometer (Belphotonics model SP1105).

3.3.2 Size, Particle morphology and Zeta potential

The morphology of the produced particles was characterized using atomic force microscopy (AFM). Sample preparation consisted on diluting 10 µL of the particle dispersion in 2 mL of purified water (Milli-Q system). Then 100 µL of the diluted sample was deposited on freshly cleaved mica substrates (2 x 2 cm). After 60 seconds, the

sample excess was removed by spin coating at 1000 rpm for 10 s and dried at 40 ºC overnight. Images were obtained on an Agilent Technologies 5500 Scanning Probe Microscope (N9410S) using a NSC15/AIBS cantilever, with a force constant of 40 N m^{-1} and a frequency of 320 kHz, with the tapping mode. Images were obtained using the Picoview 14 software and treated in the Gwyddion 2.51 software (Czech Metrology Institute).

The hydrodynamic radius of the spherical particles was evaluated using dynamic light scattering (DLS) in a NanoDLS (Brookhaven Instruments Corporation®), diode laser λ=632.8 nm, and photodetector at 90 ° and with a Zetasizer Nano Series ZS (ZEN3600 - Malvern Instruments and PANalytical), λ=632.8 nm, and photodetectors at 12.3 ° and 170 °.

The zeta potential (ζ potential) was measured using a Zetasizer Nano Series ZS (ZEN3600 - Malvern Instruments and PANalytical) with a 633 nm laser coupled with an automatic multi-purpose titrator MPT-2 (ZEN1001 - Malvern Instruments and PANalytical) and a Stabino Particle Charge Mapping (PMX 400 – Particle Metrix) with a pH probe (Malvern Instruments MV 114-SC SEN0106). The measurements were made while adding quantities (30 µL) of titrants (standardized HCl or NaOH at 0.082 and 0.080 mol L^{-1}) to the produced protein particles. When using the Stabino equipment, 100 µL of protein particles were dispersed at 20 mL of ultrapure water or at NaCl at 0.01 or 0.1 mol L^{-1}. For the Zetasizer analysis, 50 mg of each nanoparticle were dispersed in 10 mL of ultrapure water. The samples were filtered on Millipore™ membrane filters composed by mixed cellulose esters (diameter of 13 mm; pore size 0.22 µm) before each measurement.

3.4 PHASE DIAGRAM CONSTRUCTION

Bassani described the phase diagram for the mixtures of XG1 and AMP in her master's dissertation (Bassani, 2017). In this document the construction of phase diagrams presented will be for the materials XG2 and XG3 with AMP. The construction was performed using also the methodology described from Freitas et al. (2016) for the XG from Jatobá seeds with AMP. From 2 wt.% xyloglucan stock solutions (for tubes 1 to 13) and 5 wt.% (for tubes 14 to 22) containing 200 ppm of sodium azide, mixtures with the concentration values shown in TABLE 1 were prepared.

Table 1 - POLYSACCHARIDE CONCENTRATION VALUES USED IN PHASE DIAGRAM CONSTRUCTION

SAMPLE	XG wt. %	AMP wt. %
1	0.015	0.075
2	0.100	0.500
3	0.175	0.875
4	0.250	1.250
5	0.265	1.325
6	0.280	1.400
7	0.295	1.475
8	0.310	1.550
9	0.325	1.625
10	0.340	1.700
11	0.355	1.775
12	0.370	1.850
13	0.385	1.925
14	0.400	2.000
15	0.475	2.375
16	0.550	2.750
17	0.625	3.125
18	0.700	3.500
19	0.775	3.875
20	0.850	4.250
21	0.925	4.625
22	1.000	5.000

SOURCE: The author (2022).

Each of the mixtures was stirred for 1 minute in a vortex tube shaker (Phoenix^{TM} AT56) and the tubes were placed side by side so that the phase separation could be monitored macroscopically. After phase separation was complete, both upper and lower phases were separately collected to determine the concentration of XG and AMP. The concentration was determined through measurements of the volume fraction of each phase and confirmed through SEC quantification (using the option of calculating the concentration from detectors), which also showed if each phase was pure - as described in item 3.3.1. The calculated concentration after phase separation was plotted in separate phase diagrams for XG2 and XG3.

3.5 EMULSION PREPARATION AND EMULSION STABILITY EVALUATION

The evaluated emulsions were prepared at different points of the phase diagram proposed by Bassani (2017), as well as in new phase diagrams built for XG2 and XG3. In order to prevent microbial growth, 200 ppm of NaN_3 was added to the emulsions. For the macroscopic evaluation of the stability of the emulsions, photos

were taken over time; the microscopic evaluation was performed using confocal laser scanning microscopy (CLSM).

The emulsions were prepared mostly in the proportion of 1.023: 1.300 wt.% (AMP: XG). For example, to prepare an emulsion at this concentration, 1.95 g of a 2 wt.% stock solution of XG was weighted together with 0.3069 g of a 10 % AMP stock solution – and 0.7431 g of water. If any amount of particle was added, this amount should be discounted from the water amount, in order to do not dilute the system. The particles used were nanofibrils or microgels in different proportions, but respecting the maximum concentration of 1.0 wt.% of particles in relation to the emulsion total weight. The pH of the emulsions was adjusted using 0.1 mol L^{-1} HCl or NaOH, which did not have any dilution effect on the system. A titration using the same 0.1 mol L^{-1} HCl or NaOH was performed in order to estimate how much HCl or NaOH should be added to the emulsion to change the pH within the desired units. The pH value of each emulsion was checked using a pH probe calibrated with a three-point calibration. Before either macroscopic evaluation or confocal analyses, the mixtures vortexed (Phoenix^{TM} AT56) for 60 seconds.

For microscopic evaluation, the nanoparticles were labeled with rhodamine at 5 ppm (of the particle's mass – for example – if 10 g of the particle would be labelled, then 0.005 g of rhodamine B at 1 wt.% should be added to the particle). This labelling was performed so that the migration of particles to the interface could be monitored and different stabilization mechanisms for different particles could be differentiated. After preparation, 200 µL of the mixtures of amylopectin, xyloglucan and fluorophore labelled nanoparticles were transferred to a Greiner Bio-one glass bottom cell culture dish for CLSM. In order to avoid sample evaporation, the emulsions analysed at 24 h or more were freshly transferred to the dish for CLSM – as for some emulsions, the top and the bottom had different structures as time went by.

Confocal laser scanning microscopy (CLSM) images were obtained on a Nikon Ti microscope with excitation wavelengths of 488 nm and 561 nm and emission filters of 525/50 nm, 595/50 nm for fluorescein isothiocyanate and rhodamine, respectively. Images were taken at 20x or 60x (with water immersion) magnification, in NIS-Elements Analysis 4.20 software and processed using Fiji (ImageJ) software.

4 RESULTS PRESENTATION

4.1 CHARACTERIZATION OF THE PURIFIED PROTEIN AND POLYSACCHARIDES

4.1.1 Xyloglucan characterization

The first xyloglucan sample XG1 extracted from the commercial powder of the tamarind seeds endosperm (TKP – Tamarind Kernel Powder) donated by Balasanka Mills, was characterized by Bassani (2017) in her master's thesis. The macromolecular information of this material is gathered in TABLE 2.

The second xyloglucan (XG2) was extracted from a TKP produced from the cotyledons of fruits purchased in the Curitiba City Market. FIGURE 8 shows some steps of the TKP production. The final yield of XG2 in relation to the TKP was 20.6%, and the final appearance of the material obtained is that of an opaque and white fibrous material (see FIGURE 8d). The size exclusion chromatography elution profile of the extracted xyloglucan can be seen in FIGURE 9b and the macromolecular parameters in TABLE 2.

Figure 8 - a) TAMARIND FRUITS (TAMARINDUS INDICA) PURCHASED IN THE CURITIBA CITY MARKET. b) TAMARIND SEEDS. c) TKP PRODUCED AFTER MILLING THE COTYLEDONS IN A BLENDER AND PERFORMING SOXHLET EXTRACTION. d) FINAL APPEARANCE OF EXTRACTED XYLOGLUCAN XG2. e) XG3, DONATED BY DSP GOKYO FOOD & CHEMICALS.

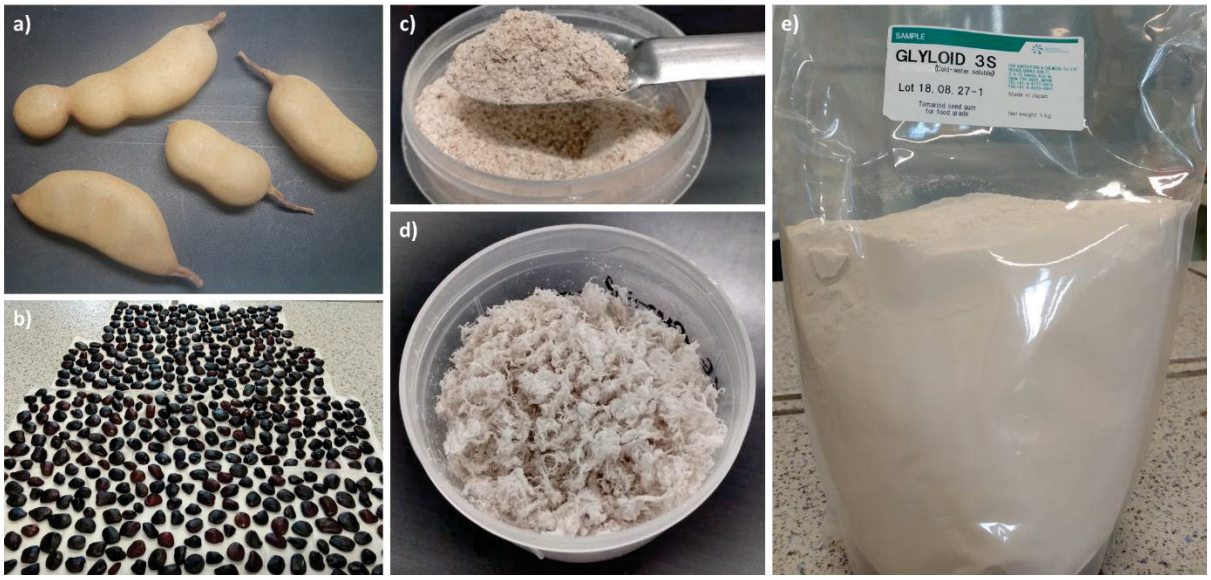

SOURCE: The author (2022).

The third sample of xyloglucan, donated by the company Dsp Gokyo Food & Chemicals (Lot 18.08.27-1), consisted on a fine beige powder (FIGURE 8e). The sample was characterized by size exclusion chromatography (SEC) and after elution, the recovery of the sample was 54.2 wt.%, which indicates that from the 0.1 mg injected (100 µL at a concentration of 1 mg mL^{-1}) only 0.0542 mg matched the polysaccharide itself. In addition to this, a non-symmetrical mass distribution could be seen at the elution profile, indicating the presence of lower molar mass fractions in the sample, which could be associated to proteins or even lower molar mass polysaccharides, which are considered here as sample impurities.

The protein content in the samples were checked using two methods, Lowry et al. (1951) and the Bradford (1976) dye binding assay, and no protein content was detected in the extracted and purified xyloglucans. Also, no signals were observed above 5.2 ppm in the 1D ^{1}H-NMR spectrum of XG1, 2, and 3 samples pointing out to the fact that no aromatic amino acids as contaminant proteins were observed, in the region between δ 6.0 - 7.0 ppm, confirming protein free samples. The integration of the signals on the anomeric region of the 1D ^{1}H NMR spectra gave the information about the molar ratio of galactose: xylose: glucose, which was found to be 1:3:4 for XG1, XG2 and XG3 samples (See Appedix 1). Since the primary structure of these materials is similar, comparing them in terms of macromolecular behaviour in solution is more feasible, than if they presented some structural difference.

After a quick centrifugation test described in section 3.1.1, insoluble material showed up at the bottom of the microtube. Thus, this material (XG3) was subjected to the same purification process described in section 3.1.1 for sample XG1 and XG2. The elution profile of the XG1, XG2 and XG3 samples after purification can be seen in FIGURE 9 and the macromolecular parameters after the purification are gathered in TABLE 2.

Figure 9 - SIZE EXLUSION CHROMATOGRAPHY (SEC) ELUTION PROFILES FOR XYLOGLUCAN a) XG1; b) XG2; AND c) XG3, USING AS MOBILE PHASE $NaNO_3$ 0.1 MOL L^{-1} AND NaN_3 AT 200 PPM AT A FLOW RATE OF 0.4 mL MIN^{-1}.

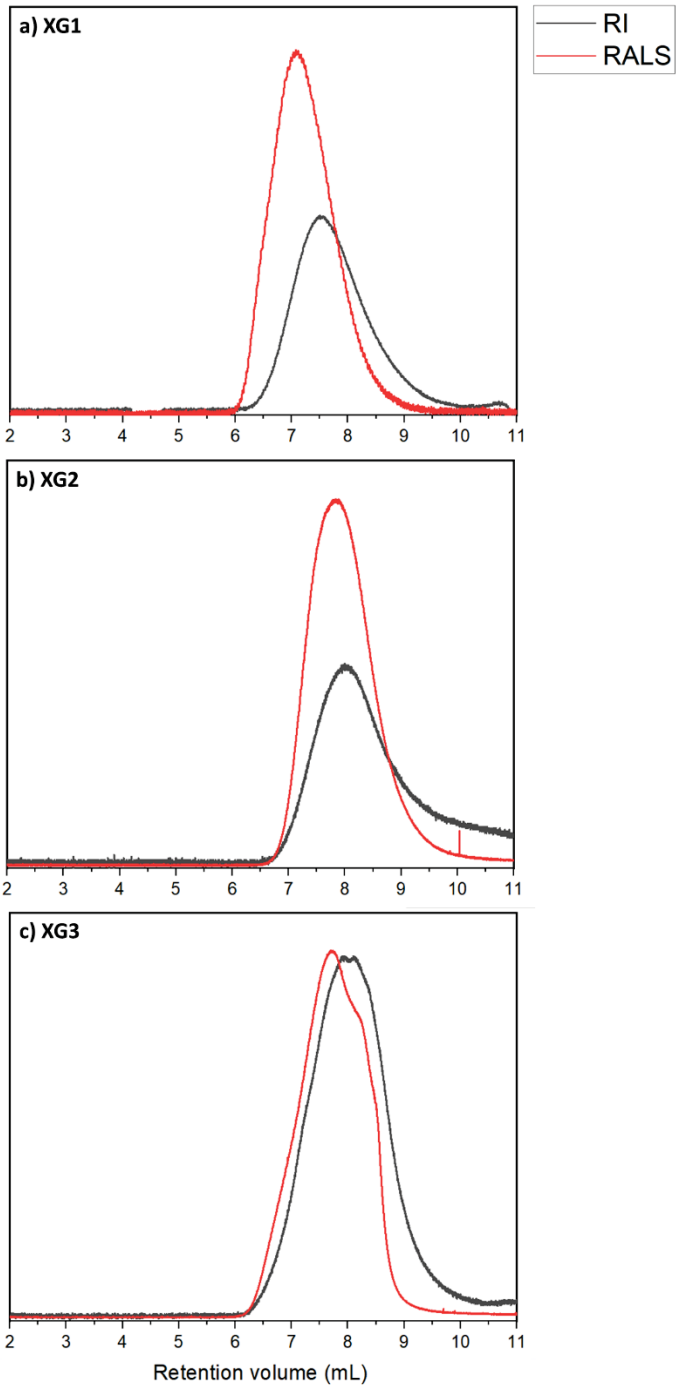

SOURCE: The author (2022).

Samples XG1 and XG2 have unimodal elution profiles, while sample XG3 exhibits a small shoulder peak in the light scattering detector. This does not mean a multimodal mass distribution, but could be associated with either fractions of smaller masses or different radius of gyration on the sample, even though a high recovery

value was observed for XG3 after elution. TABLE 2 presents the macromolecular parameters for the three extracted xyloglucan samples, determined by SEC.

Table 2 - MACROMOLECULAR INFORMATIONS OF THE EXTRACTED AND PURIFIED XYLOGLUCANS

Parameter	XG1	XG2	XG3
M_n /g mol^{-1}	3.4 x 10^4	4.5 x 10^5	1.1 x 10^6
M_w /g mol^{-1}	8.3 x 10^4	1.3 x 10^6	2.2 x 10^6
Đ (M_w/M_n)	2.4	2.8	2.0
Recovery	-	76.4%	92.2%

SOURCE: XG1 – Bassani (2017); XG2 e XG3 – The author (2022).

The dispersion values Đ (M_w/M_n) for the evaluated samples (XG1, XG2 and XG3) are characteristic of polydisperse polysaccharides, as the value for a monodisperse macromolecule is near 1. It is noticed that the M_w of XG2 is approximately 15 times greater than that of XG1, although the value of M_w/M_n does not change significantly. Villares et al. (2017) obtained M_w values for a tamarind-seed XG of 1.4 x 10^5 and 1.03 x 10^6 g mol^{-1}. For a different XG, extracted from the TKP, Souza et al. (2013) found a M_w of 2.1 x 10^5 g mol^{-1}. When comparing the values obtained with those cited from the literature, one can infer that the M_w values obtained for the xyloglucans XG1, XG2 and XG3 are within the range of molar mass normally found for this class of macromolecules.

4.1.2 Characterization of amylopectin

When dispersing the amylopectin acquired from Sigma-Aldrich® in purified water some insoluble granules were observed, which could be attributed to the presence of starch in the sample. This means waxy corn starch was received instead of gelatinized amylopectin. When comparing the solubility of amylopectin with the one from amylose, one can see that amylopectin has a greater solubility due to its highly branched structure, even with amylose having lower molar masses (Guo et al., 2017).

The insoluble granules present in the sample of amylopectin could possibly confuse the interpretation of future data in this project – mainly because the starch granules adsorb the same fluorophore (Rhodamine B) as the protein particles and the granules are also similar in size to emulsion droplets. FIGURE 10 shows a confocal laser scanning microscopy image of a starch sample.

Figure 10 - CONFOCAL LASER SCANNING MICROSCOPY IMAGE OF A STARCH SAMPLE STAINED WITH 5 PPM RHODAMINE.

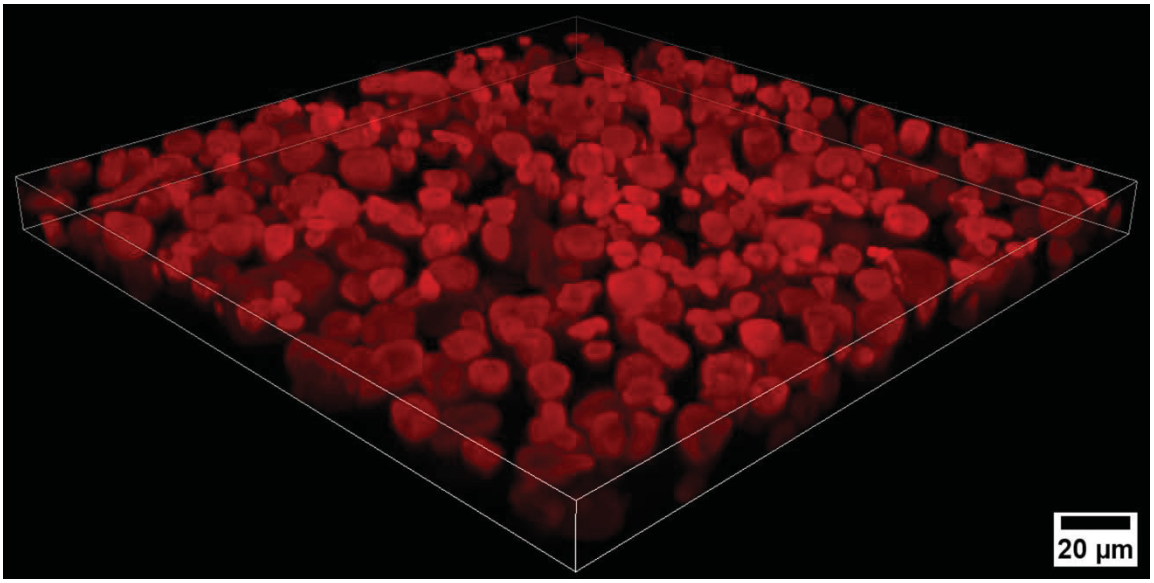

SOURCE: The author (2022).

In order to avoid putting a wrong interpretation on future data, the isolation and purification step of amylopectin, described in item 3.1.2, was performed. FIGURE 11b shows the size exclusion chromatographic profile obtained for the purified sample. In addition to the increase in the recovery after the elution in SEC (see Table 3), it was observed that the purified AMP sample no longer had the insoluble granules that were present in the original sample.

Before the purification process, the elution profile of amylopectin suggests the presence of other polymer populations, as the peak is not symmetrical - it presents a shoulder peak observed in both RI and RALS detectors. The recovery on the injected polysaccharide increased from 24.8% to 74.1% after the purification process, as seen in TABLE 3, which shows some macromolecular parameters extracted from the size exclusion chromatograms. Considering the increased recovery and peak symmetry in the elution profile of purified amylopectin, one can conclude that the purification process used was efficient in removing other molar mass fractions that was present in the sample. Wei et al. (2021) obtained M_w values for corn starch AMP of 1.65×10^8 g mol^{-1}, while Peng; Yao (2020) of 4.54×10^7 g mol^{-1}. Since it is a polysaccharide extracted from corn starch, it is likely that differences in cultivation and even method of extraction could lead to differences in the M_w values.

Figure 11 – SIZE EXCLUSION CHROMATOGRAPHY ELUTION PROFILES FOR SAMPLES (a) AMYLOPECTIN – SIGMA AND (b) PURIFIED AMYLOPECTIN, USING AS MOBILE PHASE $NaNO_3$ 0.1 MOL L^{-1} IN NaN_3 AT 200 PPM AT A FLOW RATE OF 0.4 mL MIN^{-1}.

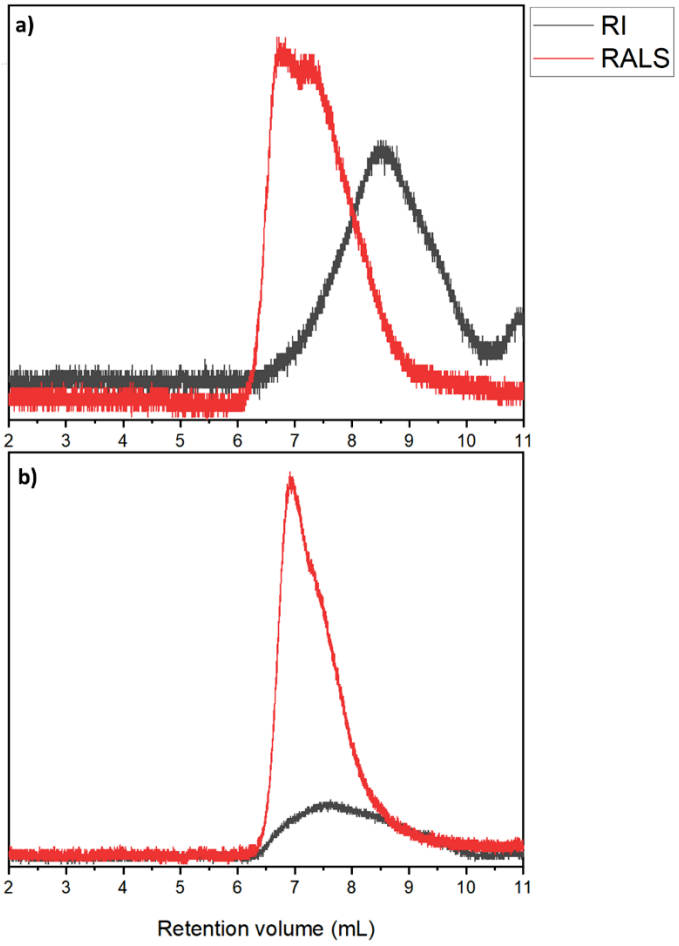

SOURCE: The author (2022).

Table 3 - MACROMOLECULAR INFORMATION OF PURIFIED AND NON-PURIFIED AMYLOPECTIN

Parameter	AMP – SIGMA	AMP – PURIFIED
M_n /g mol^{-1}	1.5 x 10^5	3.96 x 10^6
M_w /g mol^{-1}	4.3 x 10^5	7.65 x 10^6
Đ (M_w/M_n)	2.8	1.9
Recovery	24.8%	74.1%

SOURCE: The author (2022).

4.1.3 Whey Protein Isolate (WPI)

After the purification described in item 3.2, the concentration of isolated bovine whey protein - Whey Protein Isolate (WPI) determined in a spectrophotometer in the UV region was around 75 to 78 g L^{-1}, depending on the purification batch. This material was solubilized in mobile phase for size exclusion chromatography (SEC)

characterization, as described in item 3.3.1, and the elution profile of the purified WPI sample obtained is shown in FIGURE 12.

Figure 12 – SIZE EXLUSION CHROMATOGRAPHY (SEC) ELUTION PROFILE OF THE PURIFIED WPI SAMPLE, NAMED FROM NOW ON β-LACTOGLOBULIN, USING AS MOBILE PHASE NaNO3 0.1 MOL L^{-1} IN NaN_3 AT 200 PPM AT A FLOW OF 0.4 ML MIN^{-1}.

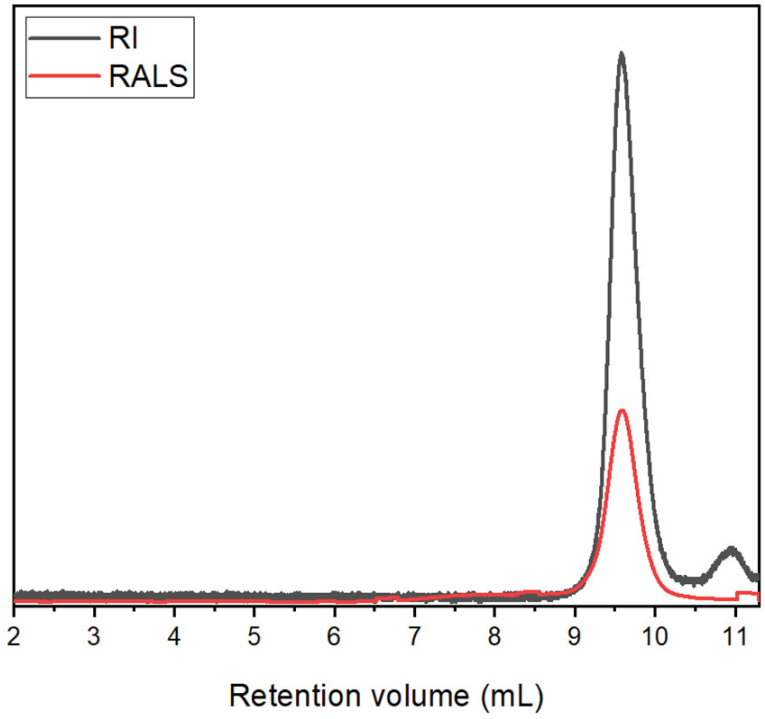

SOURCE: The author (2022).

It is observed that the purified WPI sample has a population of 95% of β-lactoglobulin (β-lg) and 5% of α-lactalbumin (α-la), which will henceforward be called β-lactoglobulin. The 5% of α-la should not affect the w/w behaviour, since the formation of α-lactalbumin nanoparticles requires conditions like desolvation with low polarity solvents or enzymatic/chemical total or partial hydrolysis (Zhang et al., 2021; Balandrán-Quintana et al., 2013), while for β-lactoglobulin simpler conditions like temperature, pH or salt bring forth nanoparticles.

Although the molar mass of β-lactoglobulin is 1.83 x 10^4 g mol^{-1} (Hambling et al., 1991), the M_w value determined by SEC was 2.8 x 10^4 g mol^{-1}. This value obtained for M_w represents the balance between the protein in its monomeric form and in its dimeric form, as proposed by Schokker et al. (1999).

4.1.4 CHARACTERIZATION OF THE PRODUCED PARTICLES

4.1.4.1 Particle morphology

The particles microgels and nanofibrils were produced and some characterizations were made in a period prior to the Masters. For microgels, the radius found by scanning electron microscopy (SEM) was 91 ± 16 nm (n=45). By dynamic light scattering, the hydrodynamic radius of the microgels was 184 ± 7 nm (this value was obtained through the analysis of hydrodynamic radius obtained at low light scattering vectors). The difference between the observed sizes, through the different techniques used, is associated with the sample drying to carry out the SEM experiments.

The appearance of the microgels dispersion was beige, opaque and macroscopically homogeneous. Even after storage, the dispersion did not change, indicating that a stable suspension was obtained. The protein conversion to microgels was 84%. The value is within the expected, as for microgels with a radius of gyration of 140 and 370 nm, Kharlamova et al. (2018) found an 85% conversion of proteins to microgels.

Donato et al. (2009) proposed a mechanism for the formation of microgels only by heat treatment at pH 5.7 - 5.9, where one main pathway is suggested, starting with β-lactoglobulin in its native form. While heating goes ahead, denatured monomers are favoured instead of previously existing dimers and monomers, and this leads to the formation of intermediate aggregates and oligomers of β-lg, then to microgels. The modification of the protein in its native state is characterized by an activated state, from which β-lg interacts with each other via electrostatic, hydrophobic and intermolecular thiol or disulfide bonds (Donato, 2009; Fuente et al. (2002). For the formation of microgels in the same pH and concentration range considered in the present work, Phan-Xuan et al. (2011) found an apparent activation energy of 300 kJ mol^{-1} indicating that protein denaturation is the limiting step in the aggregation process. In this type of synthesis, the steady state is reached when there is no more protein in its native form.

For nanofibrils the conversion was 46%, and this value was considered when calculating the concentration of particles that would be added to the emulsions. Although the conversion values from proteins to nanofibrils are quite varied in the literature, Veerman et al. (2002) found conversions ranging from 43 to 70% for

β-lactoglobulin dispersions at concentrations from 0.5 to 4 wt.%. After the synthesis, the dispersion of fibrous particles had a beige colour, transparent, macroscopically homogeneous and fluid. After being stored in the refrigerator for more than 12 h, the sample showed the behaviour of a strong gel – which was dissolved when left at room temperature (25 ºC), a gel-liquid transition.

The formation of nanofibrils at pH 2 and low ionic strengths follows a complex scheme, yet it is known that the aggregation process sticks to multiple steps, and the aggregation occurs irreversibly after prolonged heating times (Arnaudov et al., 2003). Bolder and Sagis et al. (2007) also showed that the termination step of fibril formation happens after prolonged heating, as the first steps are the rate determining steps because they are relatively slow. In the initial stages of nanofibrils formation Gosal et al. (2002) observed populations of oligomers formed with heights of 2 to 8 nm, measured in atomic force microscopy images. The study of these authors also suggests that the initial aggregation process of β-lactoglobulin nanofibrils is reversible, and the fibrils are only formed after the transition to the fibril maturation phase. At pH 2, the β-lactoglobulin is positively charged and due to the thiol groups stability, they probably are not involved in the fibril formation.

Bolder and Sagis et al. (2007) discussed the effect of producing fibrils from the heat treatment of β-lg solutions at rest or while being constantly stirred at about 200 rpm and proposed different steps on the mechanism of formation in these two cases – since the effect of stirring causes the immature fibrils to break up, producing more active fibrils. The stirring effect also increases the probability of particles to meet each other, increasing the number of formed fibrils. A likely mechanism is presented in FIGURE 13, where fibril formation occurs through an activation and nucleation process followed by the growth and maturation of the elongated structures, which is the termination step. The aggregation of proteins in fibrillar structures is a conformational change, governed by the β-sheet folding. The ending of fibril formation could be attributed either to hydrolysis - which ends with all the reactive monomers; or to inactivation of the fibril ends - due to hydrolysis or intermolecular β-sheets formation (irreversible aggregation) (Bolder, 2007).

Figure 13 - SCHEMATIC MODEL FOR THE MECHANISM OF FIBRIL FORMATION WHILE STIRRING DURING THE HEATING PROCESS AT pH 2.0. THE GREEN CIRCLES REPRESENT THE PROTEIN MONOMERS, WHICH ARE FOLLOWED BY THE ACTIVATED MONOMERS. LIGHTER BLUE OVALS REPRESENT REVERSIBLE AGGREGATES WHILE DARKER BLUE REPRESENTS THE IRREVERSIBLE ONES. THE RED CIRCLES WITH AN "H" ARE HYDROLYZED MONOMERS.

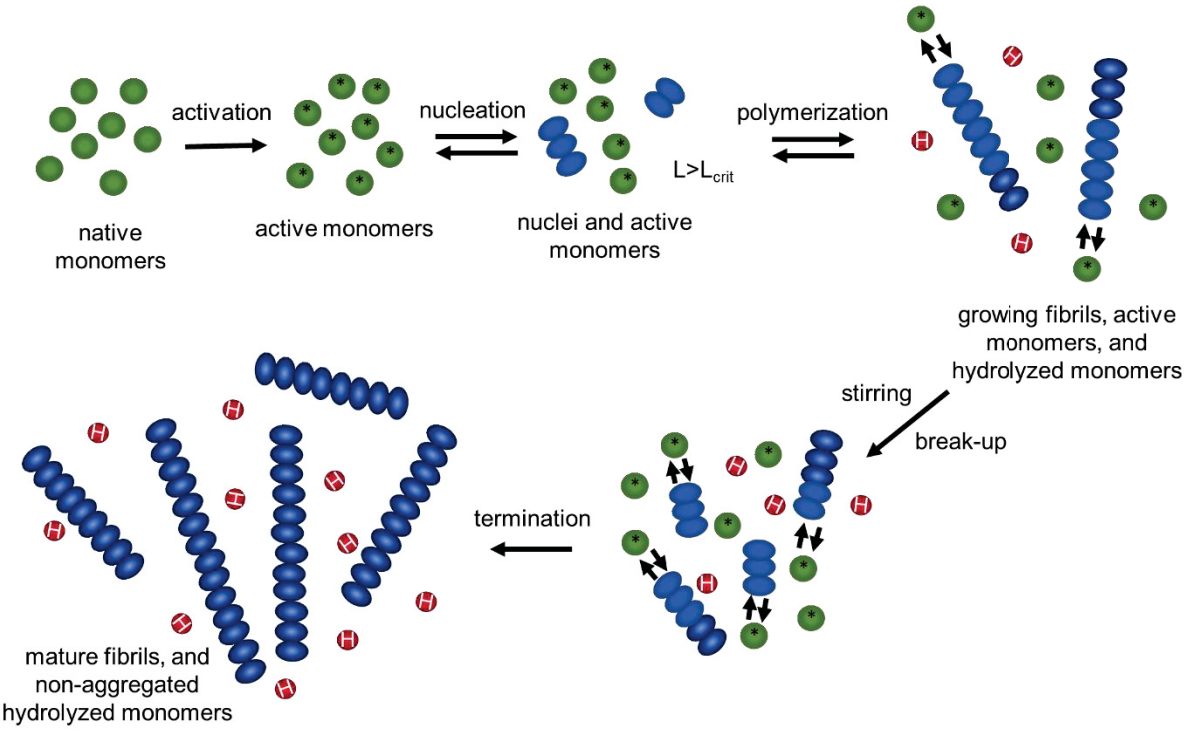

SOURCE: The author (2022) – Adapted from Bolder et al. (2007).

FIGURE 14 shows atomic force microscopy (AFM) images obtained for β-lactoglobulin nanofibrils, right after their synthesis, at pH 2.0. When measuring the diameter of the fibrils by cross-section, values between 40 nm and 50 nm are obtained, however, when measuring the height, values of 5.6 ± 1 nm (n=46) are found (FIGURE 14d). This difference can be explained by the convolution effect of the AFM tip, as the width measurements are close to the size of the tip used in the analysis. Another possibility is the compression of the sample due to interaction with the AFM tip, as discussed by Arnaudov et al. (2003), who also observed the same periodic height fluctuation along the contour of the fibrils, as FIGURE 14c shows. As the nanofibrils were neutralized (to pH = 7.0) before storage, at such pH the formation of disulfide bonds between the residuals proteins can lead to the formation of clusters in the sample, which induce interactions between the nanofibrils and lead to gelation of the sample (Aymard et al., 1999; Bolder et al., 2007).

Figure 14 - ATOMIC FORCE MICROSCOPY IMAGES FOR β-LACTOGLOBULIN NANOFIBRILS AT pH 2.0 OF a) 4 μm² b) 0.6 μm² c) 1.14 μm² d) HEIGHT VERSUS DISTANCE FOR THE LINES 1 AND 2 REPRESENTED IN c). β-LACTOGLOBULIN MICROGELS AT pH 6.9 OF d) 2 μm² e) 0.78 μm²

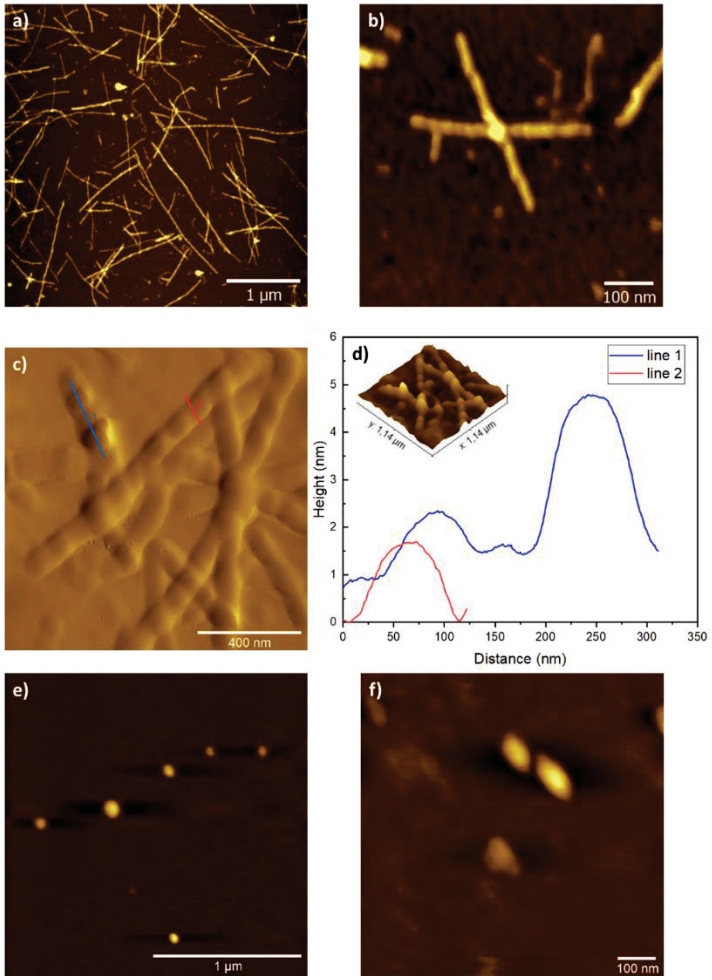

SOURCE: The author (2022).

4.1.4.2 Particle charge

The isoelectric point (IP) of microgels and fractal aggregates was determined by both electrophoretic mobility and streaming potential. The values found for the isoelectric point varied depending on the technique used – although by both techniques it was possible to identify that nanofibrils have an isoelectric point 0.7 pH units above the microgels. For the β-lg nanofibrils (β-lg_{NF}) the value was 5.6 and 5.2, obtained on the Stabino Particle Charge Mapping and on the Zetasizer Nano Series ZS (see section 3.2.2), respectively. For the the β-lg microgels (β-lg_{MG}) the value was 4.9 and 4.5, following the same order as above. Even with the values found being relatively different, they are within the ones found in the literature - since for the protein in its

native form the values vary from 4.8 (Harnsilawat et al., 2006) to 5.1 (Engelhardt et al., 2013) or 5.2 (Zhang et al., 2019), for example.

Figure 15 - TITRATION CURVES OF ζ POTENTIAL IN RELATION TO pH FOR β-LACTOGLOBULIN MICROGELS (β-lg$_{MG}$) AND NANOFIBRILS (β-lg$_{NF}$), CALCULATED FROM a) STREAMING POTENTIAL ON A STABINO PARTICLE CHARGE MAPPING AND b) ELECTROPHORETIC MOBILITY ON A ZETASIZER NANO SERIES ZS.

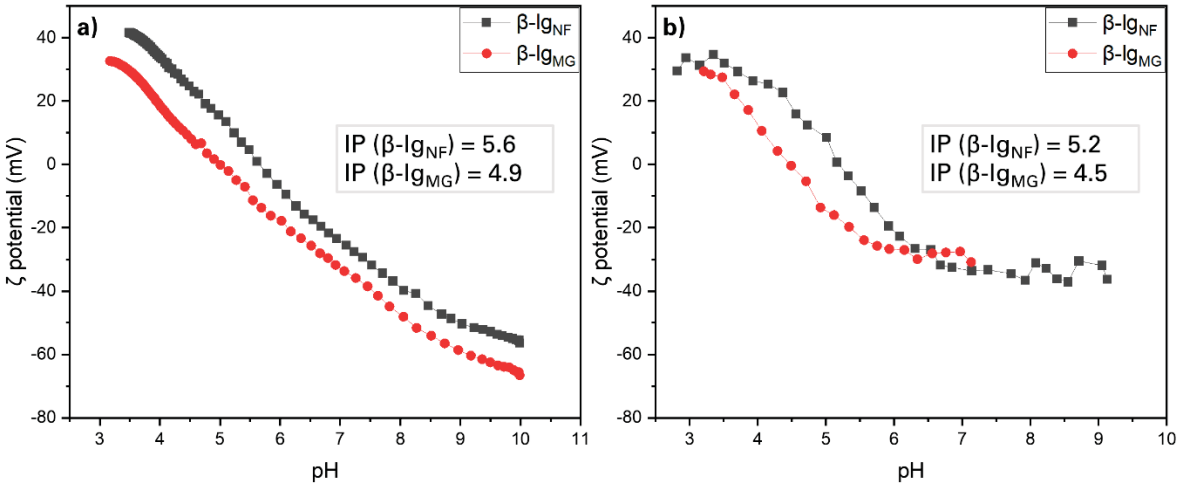

SOURCE: The author (2022).

One can notice that the graph obtained using the Stabino Particle Charge Mapping (Figure 15a) looks cleaner. Using this equipment, it was also easier to set the conditions to achieve results reproducibility – since the automatic titrator has a few more options on editing the standard operating procedure (SOP) file. For this reason, the next titration experiments were performed in this equipment.

In order to investigate the effect of NaCl on the AMP-in-XG emulsions structure, we also performed the titration of the β-lg nanoparticles in 2 different salt concentrations: 0.01 or 0.1 mol L^{-1} of NaCl. Figure 16a shows the graph of nanoparticles at different conditions. Here, the IP did change but not in a significant way among the replicates performed. The average IP found was at pH 5.51 ± 0.46 for nanofibrils and 4.68 ± 0.47 for microgels, in the presence of NaCl. Therefore, in FIGURE 16b only the difference of attractive and repulsive potential windows that the particles have are represented, which decreases as the concentration of NaCl in the medium increases. From this results, one can see that the addition of NaCl screens the electrostatic interactions between the particles.

Figure 16 – a) TITRATION CURVES OF ζ-POTENTIAL IN RELATION TO pH FOR β-LACTOGLOBULIN MICROGELS (B-LG$_{MG}$) AND NANOFIBRILS (β-LG$_{NF}$) IN WATER, NaCl 0.01 MOL L^{-1} OR NaCl 0.1 MOL L^{-1} AND b) REPRESENTATION OF THE POTENTIAL WINDOW ACCESSED AT EACH SOLVENT.

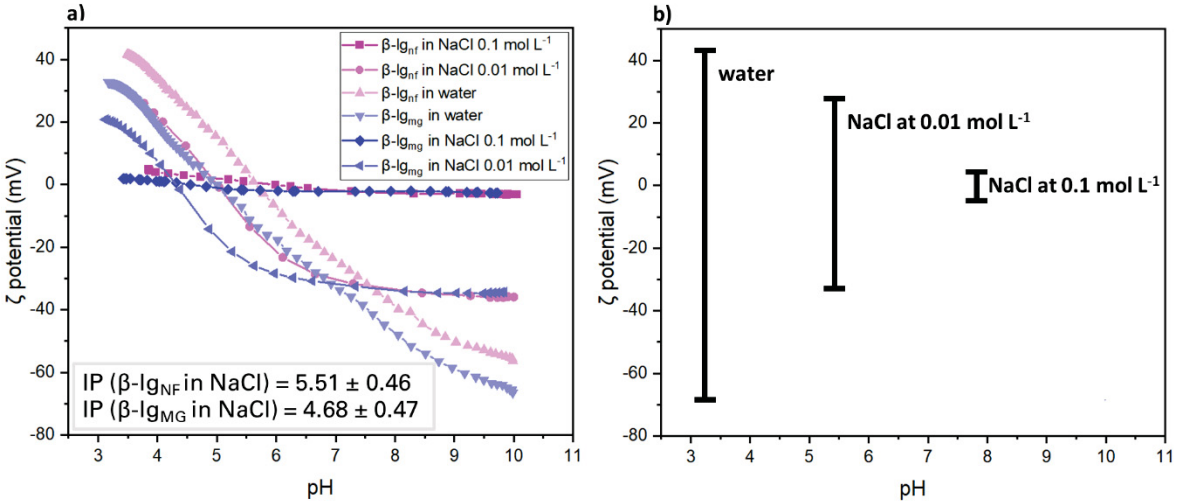

SOURCE: The author (2022).

4.2 PHASE DIAGRAM CONSTRUCTION

The construction of phase diagrams is essential when working with polysaccharides that form water-in-water emulsions. They contain information about where the biphasic regions are, about the tie lines that have constant interfacial tension along its length regardless the assessed concentration. It is also known that phase diagrams formed by macromolecules are not universally established, as variations in the composition of the macromolecules (from different sources or batches) and in their molar masses requires building new phase diagrams for each particular combination of different macromolecules (Capron et al., 2001).

The first emulsions evaluated and presented in this thesis were prepared using the purified materials XG1 and AMP, in polysaccharide concentrations determined from the phase diagram in FIGURE 18a. The red triangles in FIGURE 18 represents the ratio of 1.300: 1.023 wt.% (XG: AMP) and the emulsions presented in item 4.3 of this report were prepared respecting this ratio.

In order to continue the study, since there were not much XG1 material, the XG2 and XG3 were purified and characterized for comparison. After finding out that the last two materials had higher molar masses and distinct macromolecular parameters, the construction of a second and a third phase diagram was also performed. For the phase diagram construction, 22 aqueous mixtures of polymers XG2

(extracted from purchased tamarind fruits) or XG3 (commercial sample) and AMP were prepared, in the concentrations described in TABLE 1 of section 3.4.

The phase separation was complete after 168 h, so it was possible to proceed with the next experimental step, which was the quantification of upper and lower phases, which was done measuring the volume fraction of each phase and the concentration and composition were confirmed through size exclusion chromatography (SEC).

The concentrations by SEC were calculated considering two factors: the recovery value after the elution and the dilution performed before injecting the sample (which was at 0.5 mg mL^{-1}). In this way the quantification of the concentration of the samples in the upper and lower phase was determined, however, even considering the two factors described above, the concentration value provided by the technique was much lower than expected, making it impossible to construct the diagram with the tie lines. However, all values were directly proportional to the concentration values measured through the heights of phase separation in each tube, determined in the Fiji software (ImageJ). In this way, the phase diagrams were constructed considering the height at which the interface was observed, using the elution profiles to confirm the purity of each of the phases and also the concentration calculated from the SEC detectors.

Figure 17 – MACROSCOPIC EVALUATION OF THE MIXTURES PREPARED FOR THE PHASE DIAGRAM CONSTRUCTION FOR XG2 MATERIAL

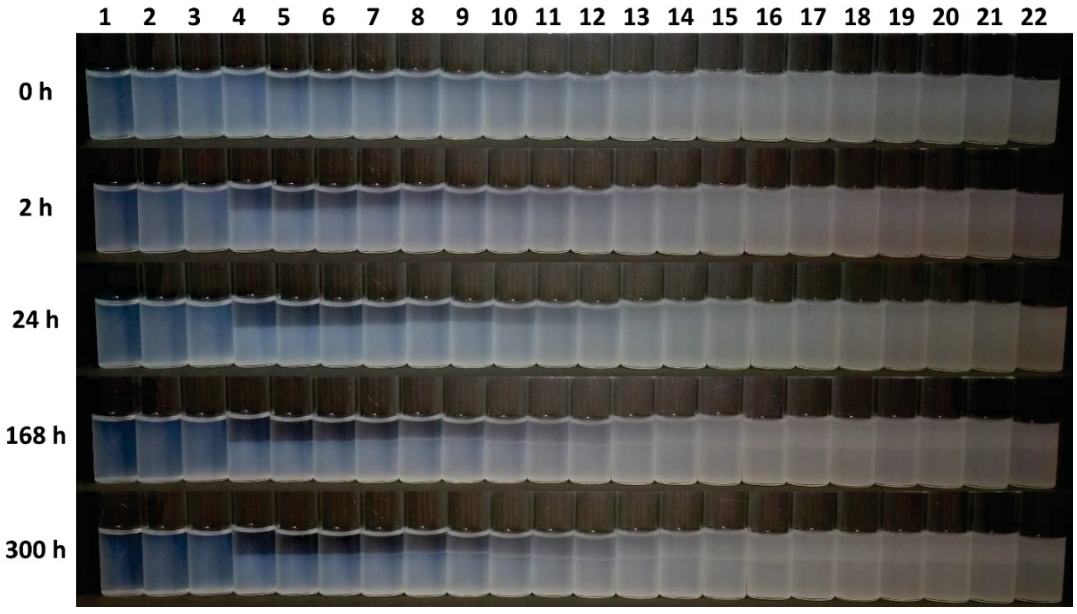

SOURCE: The author (2022).

The phase separation for XG2 can be seen in FIGURE 17. The phase diagrams for XG1, XG2 and XG3 with and AMP are gathered in FIGURE 18.

Figure 18 - PHASE DIAGRAMS FOR AMP AND a) XG1, b) XG2 OR c) XG3, AFTER 162 H (COMPLETE PHASE SEPARATION). THE EMULSIONS WERE PREPARED AT THE CONCENTRATIONS DESCRIBED IN TABLE 1. THE RED AND BLUE TRIANGLES CORRESPONDS TO THE EMULSIONS STUDIED IN THIS REPORT: 1.023: 1.300 AND 5.200: 0.302 AMP: XG wt.%, RESPECTIVELY.

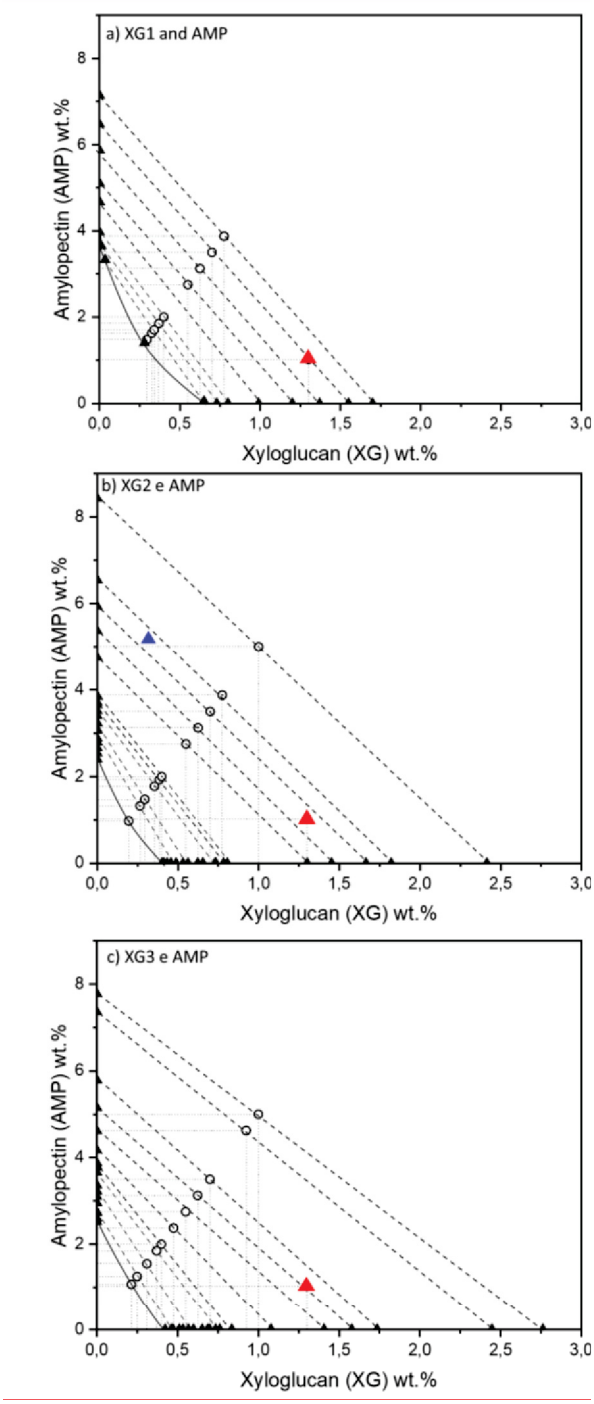

SOURCE: (a) Bassani (2017); (b) and (c) The author (2022).

The constructed phase diagrams present some interesting properties, such as differences in the binodal lines as well as in the critical points, which delimit the macroscopic immiscibility region. Note that in the phase diagram for the material XG2 the critical point is situated at 0.195: 0.975 wt.% XG2: AMP while for XG3 the critical point appears at a slightly higher concentration of both polysaccharides, at 0.214: 1.070 wt.% XG3: AMP, whereas for XG3 the phase separation took a few more hours to start. Phase separation at higher concentrations for XG3 makes sense since a low mixing entropy is expected, considering that it has a higher molar mass than XG2 and XG1.

Regarding the morphology of the emulsions, when in the absence of other agents that promote specific interactions, it is expected that the phase with the highest volume fraction will behave as the continuous phase. In the diagrams, the tie lines are represented in dotted lines, all of which pass through the composition of the phases in equilibrium (the 50: 50 v/v line), which is an expected behaviour for mixtures of two nonionic polymers. The closer one works to the critical point on each phase diagram, the shorter the tie lines are and it is expected to be less likely to obtain pure phases from each polymer (Dickinson, 2019). Furthermore, it is observed that the parallelism between the tie lines exists in the three phase diagrams presented, indicating that the measurement of the concentration was carried when phase separation had reached the equilibrium condition.

4.3 MACRO AND MICROSCOPIC EMULSION STABILITY

4.3.1 Emulsions of XG1 and AMP

In order to determinate the stability of the emulsions using confocal laser scanning microscopy (CLSM) it was necessary to assess whether the presence of the fluorophores used (described in item 2.5 of this document) would influence or not the course of phase separation between AMP and XG. Fluorescein isothiocyanate had been used in previous studies in order to identify which of the phases behaved as a dispersed and continuous phase, and it was used to label amylopectin. Rhodamine was used to label the protein particles at 5 ppm through physical adsorption. FIGURE 19 shows the evaluation of emulsions (1.023: 1.300 wt.% AMP: XG) in the presence of different dyes, which did not lead to differences in the phase separation.

Figure 19 - MACROSCOPIC EVALUATION OF AMP EMULSIONS IN XG1 (1.023: 1.300 wt.%) IN THE (1) ABSENCE OF FLUOROPHORE, AND IN THE PRESENCE OF (2) AMYLOPECTIN LABELED WITH FLUORESCEIN ISOTHIOCYANATE (AMP-FITC) (3) AMYLOPECTIN LABELED WITH ISOTHIOCYANATE AND 5 PPM OF RHODAMINE 4) 5 PPM OF RHODAMINE.

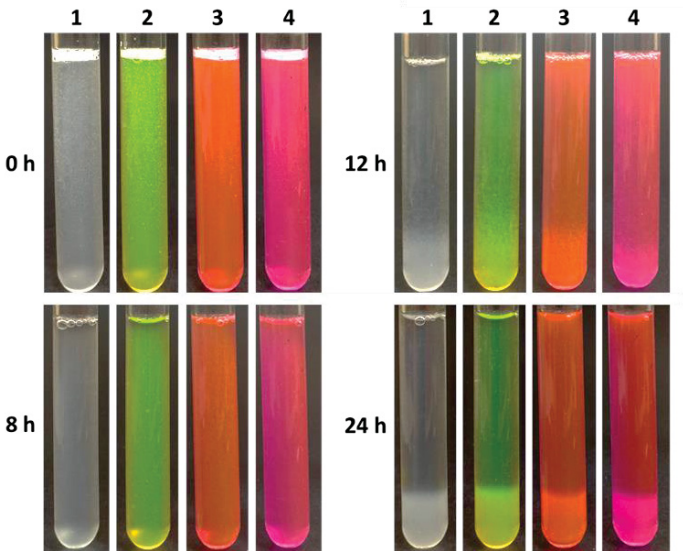

SOURCE: The author (2022).

It is important to emphasize that since the amount of fluorophore is always calculated as a function of the particle's mass, and here in these tubes no particle concentration was added, the labelling agent was added in the polysaccharide mixture, leading to an excess of added fluorophore than in future evaluated emulsions (see, for example, FIGURE 20, which does not look as pink as the fourth tube in FIGURE 19). The presence of fluorophore at 5 ppm has no effect on macroscopic phase separation of XG1, XG2 and XG3 in AMP emulsions either, and this observation was used to infer no influence of fluorophore in the phase separation on macro and microscopical analysis.

Previous results that evaluated AMP emulsions in XG1 (1.023 and 1.300 wt.%) in the presence of β-lg microgels and nanofibrils with concentrations ranging from 0.1 to 1.5 wt.% showed that, for all evaluated pH values, the concentration of particles that adsorb at the interface and lead to stabilization of the emulsions for a longer period was above 1.0 wt.%. Since no additional emulsion stabilization was found for concentrations above 1.0 wt.%, the chosen concentration of β-lg nanoparticles on the emulsions was 1.0 wt.%.

Thus, β-lg microgels and nanofibrils have been added to emulsions at a concentration of 1.0 wt.% in order to compare the effect of particle morphology on the stabilization of AMP in XG emulsions. The pH of the emulsions was adjusted as

described in item 3.5 and, macroscopically, it is observed that while for microgels (β-lg_{MG}) there is sedimentation of some material at higher pH values (at pH 6.0 and 7.0), in the presence of nanofibrils (β-lg_{NF}) the emulsions remain stable in the first 24 h of evaluation (FIGURE 20).

Figure 20 - MACROSCOPIC EVALUATION OF AMP IN XG1 EMULSIONS (1.023: 1.300 wt.%) IN THE PRESENCE OF β-LG MICROGELS AND NANOFIBRILS AT DIFFERENT pH VALUES (4.0; 5.0; 6.0 AND 7.0).

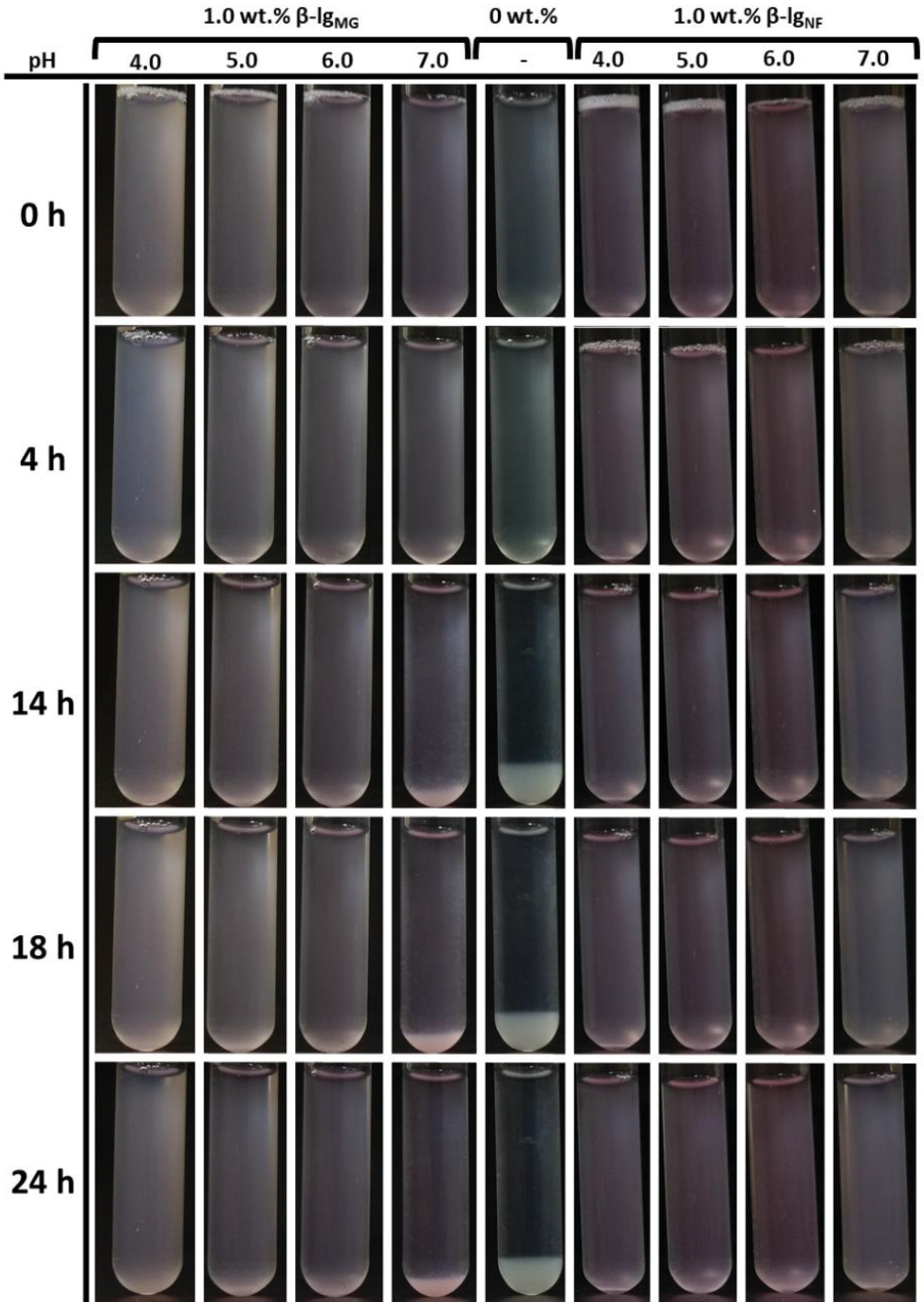

SOURCE: The author (2022).

From the evaluation by confocal laser scanning microscopy (CLSM) of the emulsions in the presence of the microgels shown in FIGURES 21, 22 and 23, one can notice that at pH 4.0 the particles adsorb at the interface between amylopectin and xyloglucan, stabilizing the emulsion for 24 h through the so-called Ramsden-Pickering effect. At pH 5.0 deformed droplets are observed, in addition to the presence of aggregates of protein particles, making the emulsion stable - not through the interfacial adsorption of particles, but through the gelation of one of the phases. Gtari et al. (2016) evaluated the spontaneous interaction between XG and protein microgels at pH < 5.6 leading to the formation of core-shell particles, even in the absence of quantifiable charged groups in the XG structure by titration. Some mechanisms are suggested to explain the observed interactions, such as coordination with positively charged protein amino acids, hydrophobic interactions, hydrogen bonds with side chains or with amino groups. Such core-shell particles accumulated at the interface stabilizing AMP and XG (from Jatobá seeds) emulsions at pH ≤ 5.0 (Freitas et al., 2016).

When performing a test called “tilt-test”, in which the tube is tilted at 45º, it was found that the some of the emulsions had the behaviour of a solid-like emulsion. After inverting all the tubes, it was noticed that for the AMP emulsions in XG1 in the presence of microgels at pH 5.0, 6.0 and 7.0 the gelling of the continuous phase had occurred, since a gel that supported its own weight for a few minutes was formed (FIGURE 21). A strong gel was not formed for the emulsion at pH 4.0, indicating different stabilization mechanisms of AMP emulsions in XG1 in the presence of microgels (predominant Pickering effect at pH 4.0 and phase gelation at pH > 5.0). Even though a strong gel was not formed, one can notice that the volume fraction of AMP droplets in the upper phase of the emulsion at pH 4 on FIGURE 21 is high – this inevitably leads to a slight increase in the sample’s viscosity.

By measuring the area that each droplet fills in relation to the total area of CLSM images, it was possible to determine the emulsified fraction ($\emptyset_{AMP\ in\ XG}$), which was equal to 0.69 for the emulsion with microgels at pH 4 after 24 h of rest. This explains the minor increase in viscosity observed at this pH when performing the tilt test, since the gelled structure was not strong enough to support its own weight. However, in comparison to the emulsion without particles, it had a higher flow resistance. This value is consistent with the volume of amylopectin emulsified in the tube, in the macroscopic evaluation, after 24 hours of rest. Figure 22 shows the 53

CLSM slices overlapped (with 0.5 μm intervals), which was used to determinate the discussed volume fraction.

Figure 21 - MACRO AND MICROSCOPIC EVALUATION (CLSM) OF AMP EMULSIONS IN XG1 (1.023: 1.300 wt.%) IN THE PRESENCE OF 1.0 wt.% β-LG MICROGELS AT DIFFERENT pH VALUES (4, 5, 6 AND 7) AFTER 24 H OF REST.

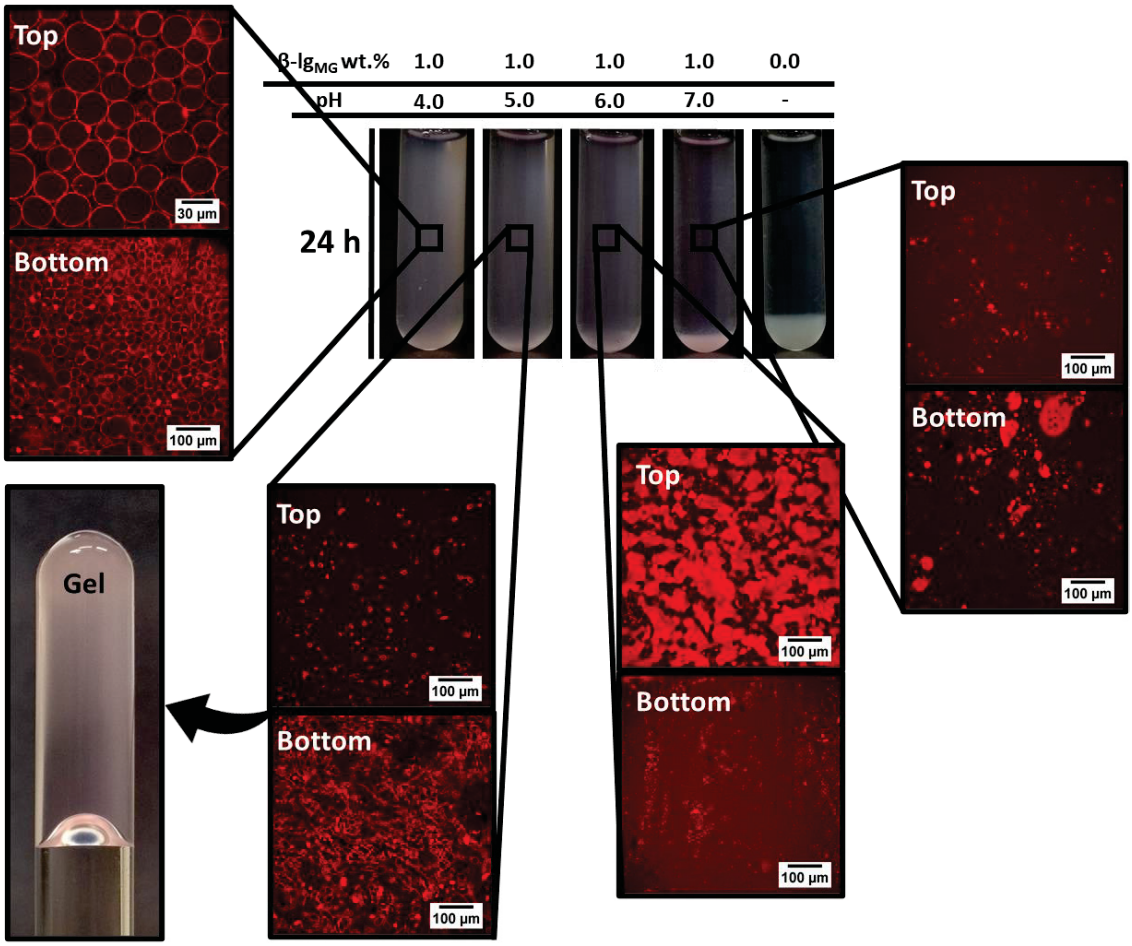

SOURCE: The author (2022).

Figure 22 – CONFOCAL LASER SCANNING MICROSCOPY (CLSM) 3D PROJECTION OF AN AMP IN XG1 (1.023: 1.300 WT.%) EMULSION AT pH 4 AFTER 24 H OF RESTING, IN THE PRESENCE OF 1.0 wt.% β-lg MICROGELS.

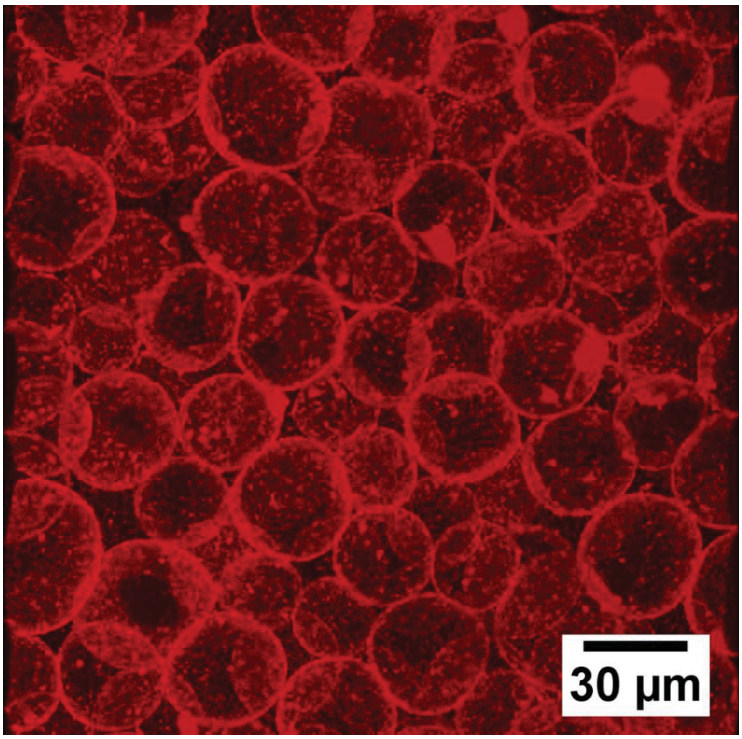

Source: The author (2022).

The pH region in which the behaviour of the microgels at the interface changes is close to the where the isoelectric point of these particles is located, which was determined as 4.9. In this region, the formation of protein aggregates occurs and there is less partition of the particles between the phases, due to the absence of electrical potential in the hydrodynamic shear plane of the particle. As shown in section 4.1.4.2, the addition of salt is associated with the reduction of this effect, even at pH values above the isoelectric point. This topic will be discussed in the next pages.

By analysing the behaviour of β-lactoglobulin nanofibrils (β-lg_{NF}) at the interface considering different pH values, one can notice that they are adsorbed at the interface of AMP emulsions in XG1 for all pH values, unlike microgels, as can be seen in FIGURE 23. By inverting the tube, it was not possible to notice the gelling effect as pronounced as in the presence of microgels, and although the presence of nanofibrils is associated with a slight increase in the viscosity of the continuous phase (XG) of the emulsion, the interfacial adsorption behaviour of these particles is shown to be dominant. The rheological behaviour of microgels and nanofibrils in xyloglucan and amylopectin dispersions is outside the scope of this thesis, although they might be the

next step to go further into the discussion of the protein particles interaction with both amylopectin and xyloglucan.

Figure 23 - MICROSCOPIC EVALUATION (CLSM) OF AMP EMULSIONS IN XG1 (1.023: 1.300 wt.%) WITH 1.0 wt.% β-LG a) MICROGELS (ABOVE) OR b) NANOFIBRILS (BELOW) AT DIFFERENT pH VALUES AFTER 1 H OF REST. EACH IMAGE IS ACCOMPANIED BY A DROPLET ZOOM-IN.

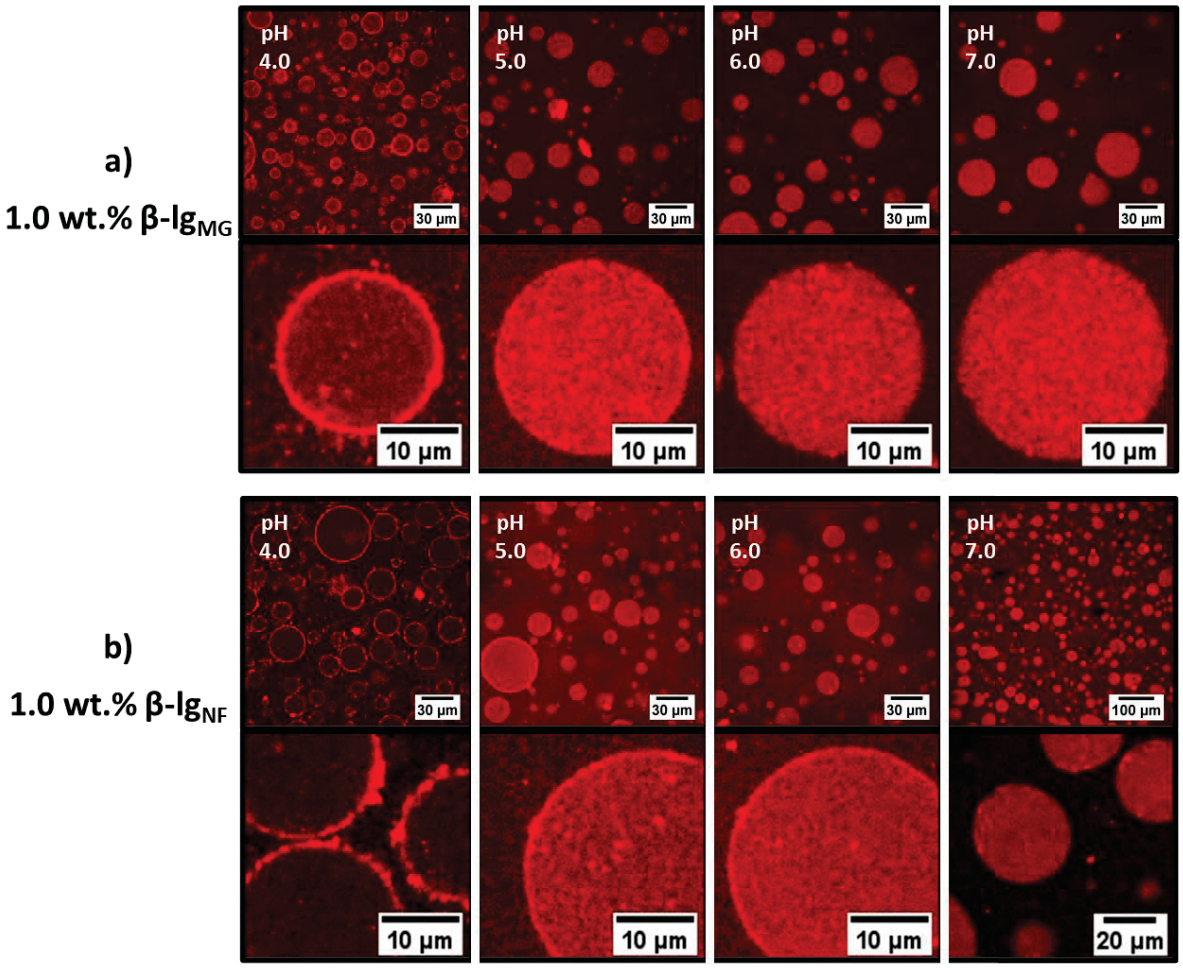

SOURCE: The author (2022).

As gelation results were observed for the emulsions in the presence of microgels, some CLSM images were obtained only by mixing each β-lg nanoparticle (fibrils or microgels) with either amylopectin or xyloglucan (XG1). These experiments were performed in order to evaluate the gelation without the effect of temperature or saline addition (the so-called cold gelation process). For this, each of the two particles produced (microgels and nanofibrils) were labelled with rhodamine and then added in amylopectin, xyloglucan or in water (for the negative control). After 24 h of rest, images

of the aggregation were obtained in order to observe in which pH conditions the presence of aggregates would occur.

Figure 24 – CLSM EVALUATION OF PARTICLE AGGREGATION (MICROGELS – β-lg$_{MG}$ OR NANOFIBRILS – β-lg$_{NF}$ at 1.0 wt.%) ONLY IN AMP OR IN XG1 FROM pH 4.0 TO 7.0, AFTER 24 H OF REST.

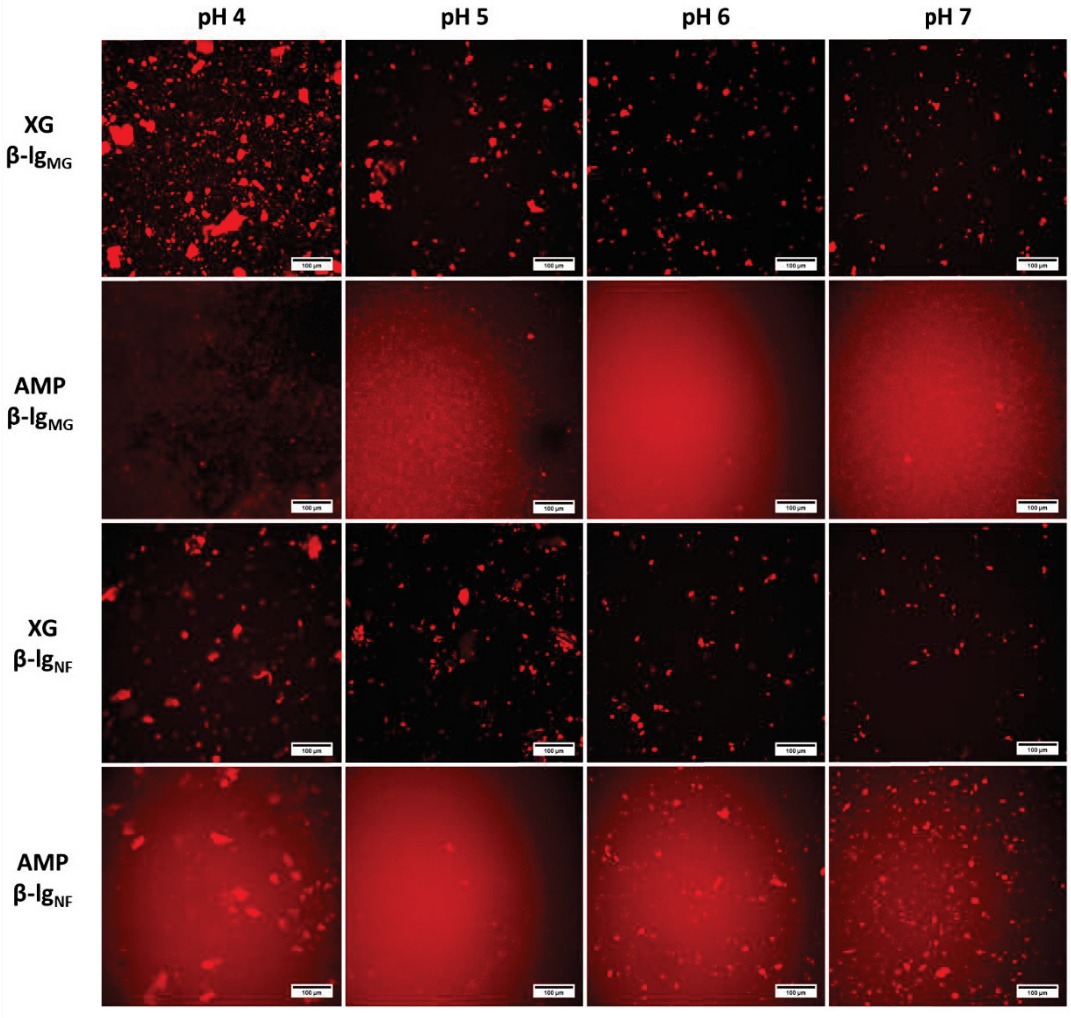

SOURCE: The author (2022).

Note in the images in FIGURE 24 that particles aggregate mostly at pH < 5 for microgels and nanofibrils in xyloglucan. This corroborates the results of Gtari et al. (2016) who demonstrated the formation of core-shell structures between microgels and xyloglucan. When the particles were dispersed in AMP, it is observed that there was no evident aggregation for the microgels, even at a pH below the isoelectric point. On the other hand, the nanofibrils, aggregated at the extremes of pH values. Rheological analyses should help understand the gel formation over time at certain pH values. Such

studies should contribute to the understanding of the cold gelation processes in mixtures of β-lg particles with xyloglucan and amylopectin.

4.3.2 Emulsions with XG2 and AMP

The material XG2 has a molar mass 15x greater than XG1, which may indicate some influence of this parameter on the formation of w/w emulsions. In order to evaluate this effect, a test was carried out with emulsions of AMP in XG2 (1.023: 1.300 wt.% (FIGURE 25) and of XG2 in AMP (0.302: 5.200 wt.% (FIGURE 26) in the presence of 1.0 wt.% of microgels - according to the concentrations represented by the red and blue triangles in FIGURE 18b.

Figure 25 - MACRO AND MICROSCOPIC (CLSM) EVALUATION OF AMP IN XG2 EMULSIONS (1.023: 1.300 wt.%) IN THE PRESENCE OF 1.0 wt.% β-LG MICROGELS. ALL OF THE CLSM IMAGES ARE IN THE PRESENCE OF 1.0 wt.% β-LG_{MG}.

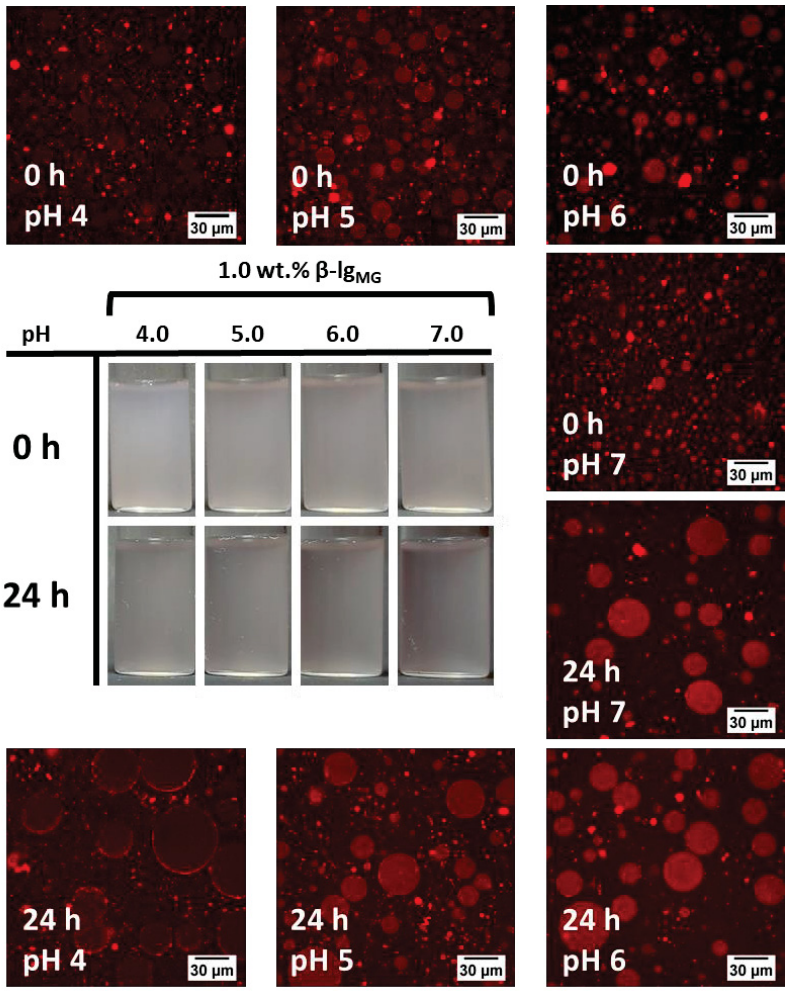

Source: The author (2022).

The CLSM analysis shows that the emulsions at pH 4.0 and 5.0 in the presence of 1.0 wt.% of microgels had AMP droplets coated with a ring of protein particles, while for pH 6.0 and 7.0 the microgels did not adsorb at the interface. It is observed that in the presence of an XG with greater molar mass (XG2), the microgels also induce gelation, although the morphology of deformed droplets (which are a characteristic of a gelled continuous phase) was not seen. However, the increase in emulsion viscosity was notable when removing the emulsion and depositing it in the holder for CLSM analysis at 24 h, as well as in the tilt test.

Whilst for XG1 there seemed to be no difference of microgel particles adsorption at the interface for pH ≤ 5 at 0 and 24 h, one can notice that in FIGURE 25, the coating of AMP droplets by microgels at pH ≤ 5 after 24 h is more evident than at 0 h. This suggests that in this pH condition the kinetics of particle migration to the interface is slower. Thus, the 15 times larger molar mass of XG2 than XG1 causes an increase in viscosity, which provides transient stability, reducing the phase separation kinetics until the interface is stabilized by Pickering particles, and reducing the particle diffusion coefficient.

Even though emulsions with XG2 are not stabilized by the Pickering effect at pH 6.0 and 7.0 as the CLSM images show in FIGURE 25, macroscopically the phase separation is slowed down, since at 48 h the AMP layer at the bottom of the tube is starting to appear, a fact not previously observed for emulsions with XG1 (with lower molar mass) or by Freitas et al. (2016) when working with AMP emulsions (M_w = 1.3 x 10^7 g mol^{-1}) in XG (M_w = 2.9 x 10^6 g mol^{-1}, similar to XG2). Since here the emulsions were stable at pH values higher than the isoelectric point, other parameters of stabilization are suggested in addition to the molar mass, like the particle concentration – as Freitas (2016) used a concentration ten times lower of microgels.

Figure 26 - MACRO AND MICROSCOPIC (CLSM) EVALUATION OF XG2 IN AMP EMULSIONS (0.302: 5.200 wt.%) IN THE PRESENCE OF 1.0 wt.% β-LG MICROGELS, AT pH 4.0; 5.0; 6.0 AND 7.0.

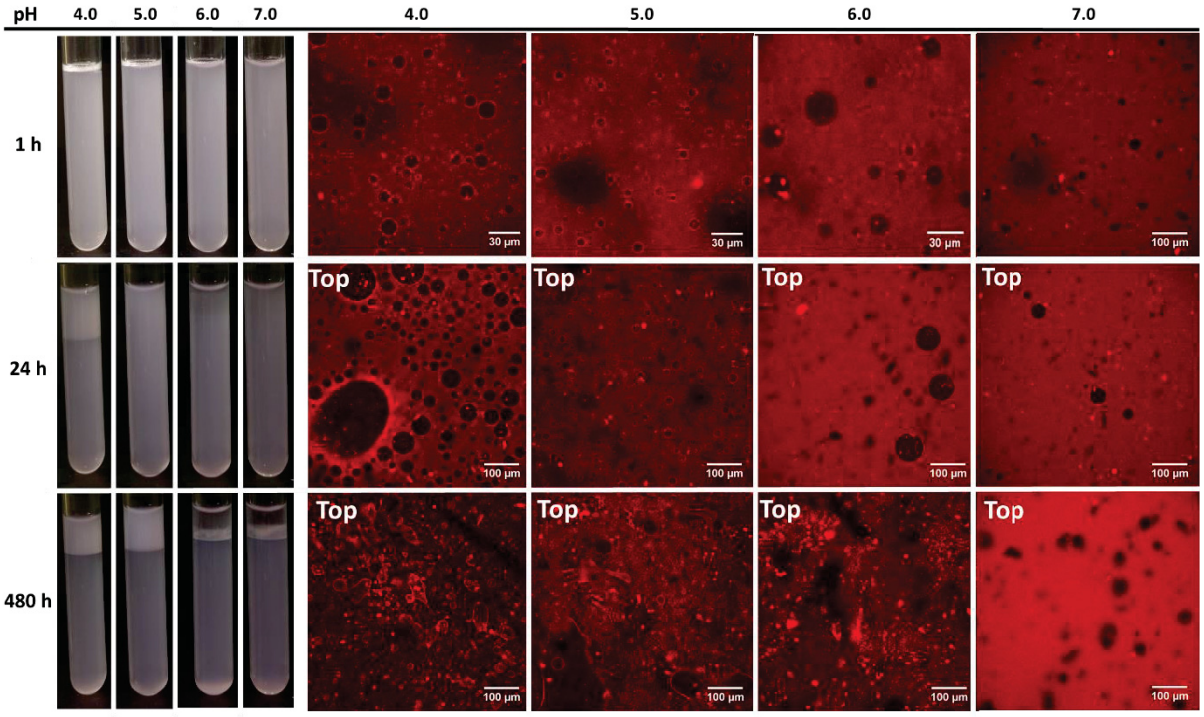

SOURCE: The author (2022).

In FIGURE 26 the emulsions of xyloglucan as dispersed phase and amylopectin as continuous phase are observed (XG2 in AMP emulsions - 0.302: 5.200 wt.%). Here, the addition of the particles also generated an increase in viscosity – indicating gelation of the continuous phase. After 24 h of rest at pH 4.0 and 5.0, on the top of the emulsion there were still AMP droplets in XG, and the lower phase is a continuous XG phase without AMP droplets. After 480 h and at pH 6.0 and 7.0, the presence of an emulsion in the upper phase of the tube is no longer observed, and at pH 4.0 and 5.0 droplets of AMP in XG are observed.

The preferential interaction of β-lg microgels with xyloglucan favours the formation of AMP emulsions in XG. Similar results were observed by Bassani et al. (2017) and Freitas et al. (2016), in which emulsions of XG in AMP were not observed above the isoelectric point of the particle. Below such pH conditions, the migration of the particles from the interface to the amylopectin phase was observed.

When analysing the behaviour of β-lg nanofibrils at the interface of AMP droplets in XG2, it was noticed that the behaviour of interfacial adsorption by the Pickering effect appears in higher pH values than for microgels, since at pH 6.0 and

7.0 β-lg_{NF} particles were observed at the interface (since the same effect will be discussed for XG3, these images are not shown).

4.3.3 Emulsions with XG3 and AMP

Previously, with the XG1, the distinguished behaviour of fibrils and microgels in the interface was noticed, since the nanofibrils were capable of stabilizing emulsions at a higher range of pH. This notably distinguished behaviour of microgels and nanofibrils at the interface was reproducible for XG2 and now will be last-checked and presented for XG3. Since XG3 was a commercial sample kindly donated by the company Dsp Gokyo Food & Chemicals (Lot 18.08.27-1), the next evaluations of emulsion behaviour were prepared using this material.

The macroscopic evaluation of AMP-in-XG3 (1.023:1.300 wt.%) emulsions is shown in FIGURE 27. Macroscopically it is not possible to differentiate distinct mechanisms for emulsions in the presence of microgels or nanofibrils [both at 1.0 wt.%], however, the increase in viscosity for emulsions in the presence of both particles is noticeably high when performing the tilt test, in which the tube is tilted to a specific angle and it is observed how much does the emulsion flow. When comparing the stabilized emulsions with the one that has no particles (represented in FIGURE 27 by the tube of 0 wt.%), one can notice that the macroscopic phase separation occurs more slowly for XG3 than it ocurred for XG1 (see FIGURE 21, in which the phase separation was complete at 24 h) and for XG2, in the same way as observed in the phase diagrams.

Figure 27 - EMULSIONS IN THE PRESENCE OF 1.0 wt.% OF MICROGELS (β-lg$_{MG}$) OR NANOFIBRILS (β-lg$_{NF}$) AT CONCENTRATIONS OF 1.300: 1.023 XG3: AMP wt.%.

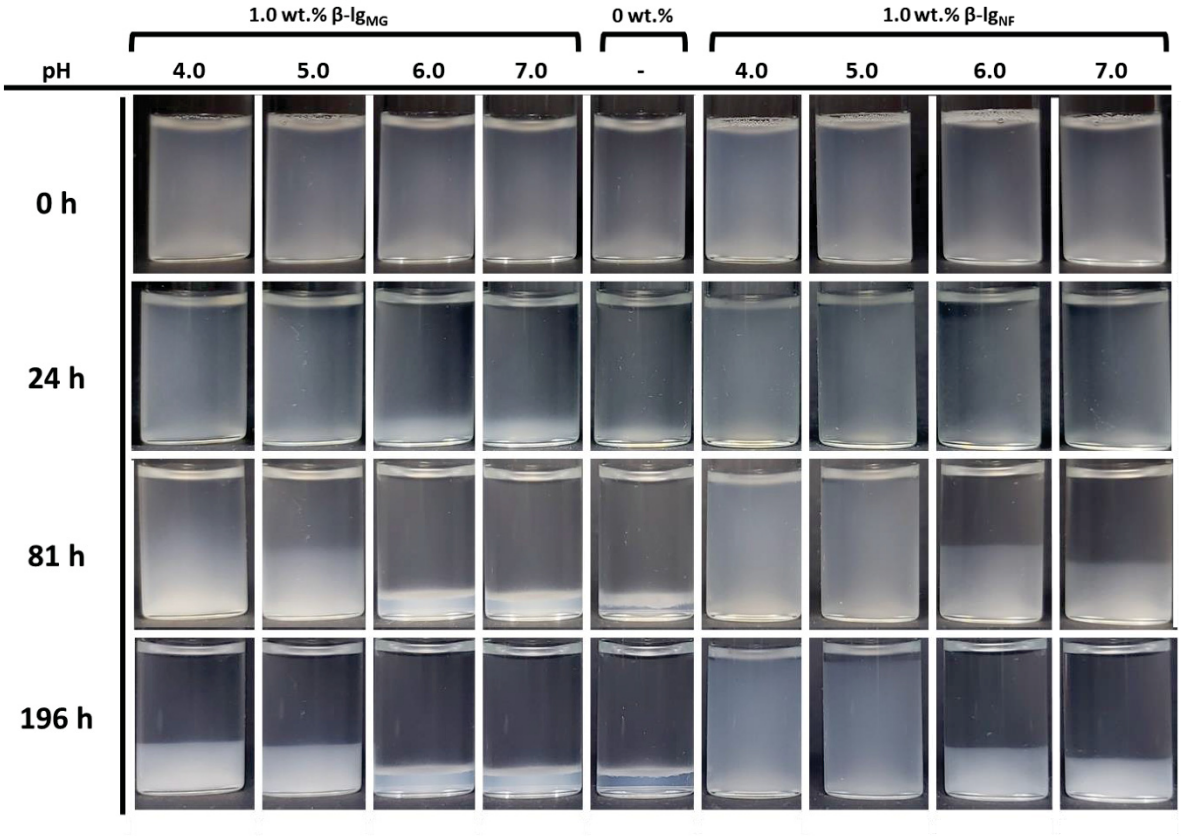

SOURCE: The author (2022).

The microscopic images of the emulsions displayed in FIGURE 27 are shown in FIGURE 28. The CLSM images only are represented for top and bottom in cases when distinct microstructures were observed in the upper and lower emulsion regions. Previously, with the XG1, the distinguished behaviour of fibrils and microgels in the interface was noticed, since the nanofibrils were capable of stabilizing emulsions at a higher range of pH. Apparently, this was reproducible in this xyloglucan (XG3) with greater molar mass – as the zoom of the droplets show in FIGURE 29.

Figure 28 - CONFOCAL LASER SCANNING MICROSCOPY (CLSM) IMAGES OF AMP-IN-XG3 EMULSIONS AT 1.023:1.300 wt.% AT 1H AND 24 H AT DIFFERENT pH VALUES.

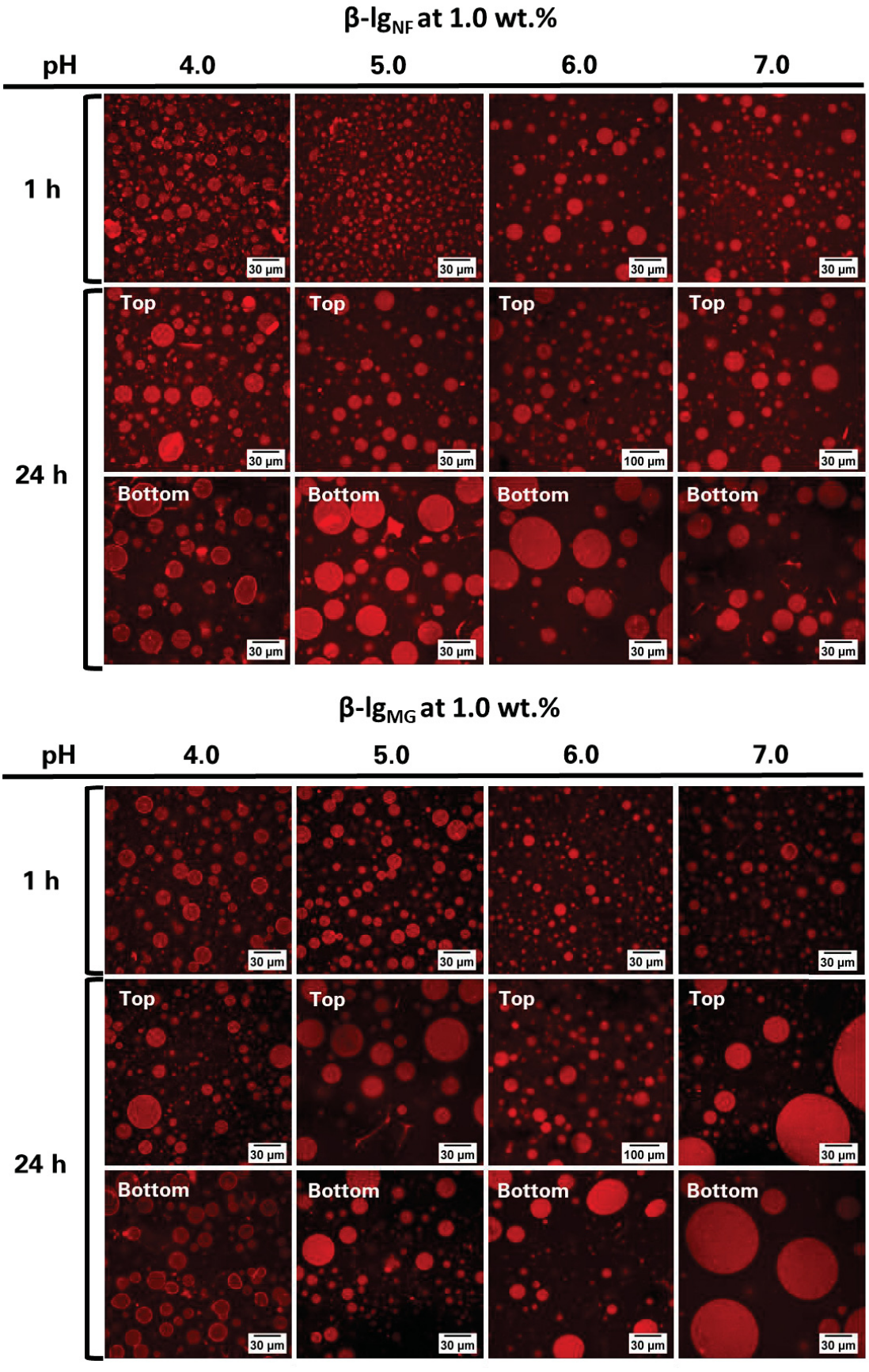

SOURCE: The author (2022).

Figure 29 – COMPARISON BETWEEN THE BEHAVIOUR OF β-LG_{MG} AND β-LG_{NF} AT THE INTERFACE OF AMP IN XG3 (1.023:1.300) EMULSIONS AT DIFFERENT pH VALUES.THE NANOFIBRILS ADSORB AT THE INTERFACE WITHIN A HIGHER RANGE OF pH.

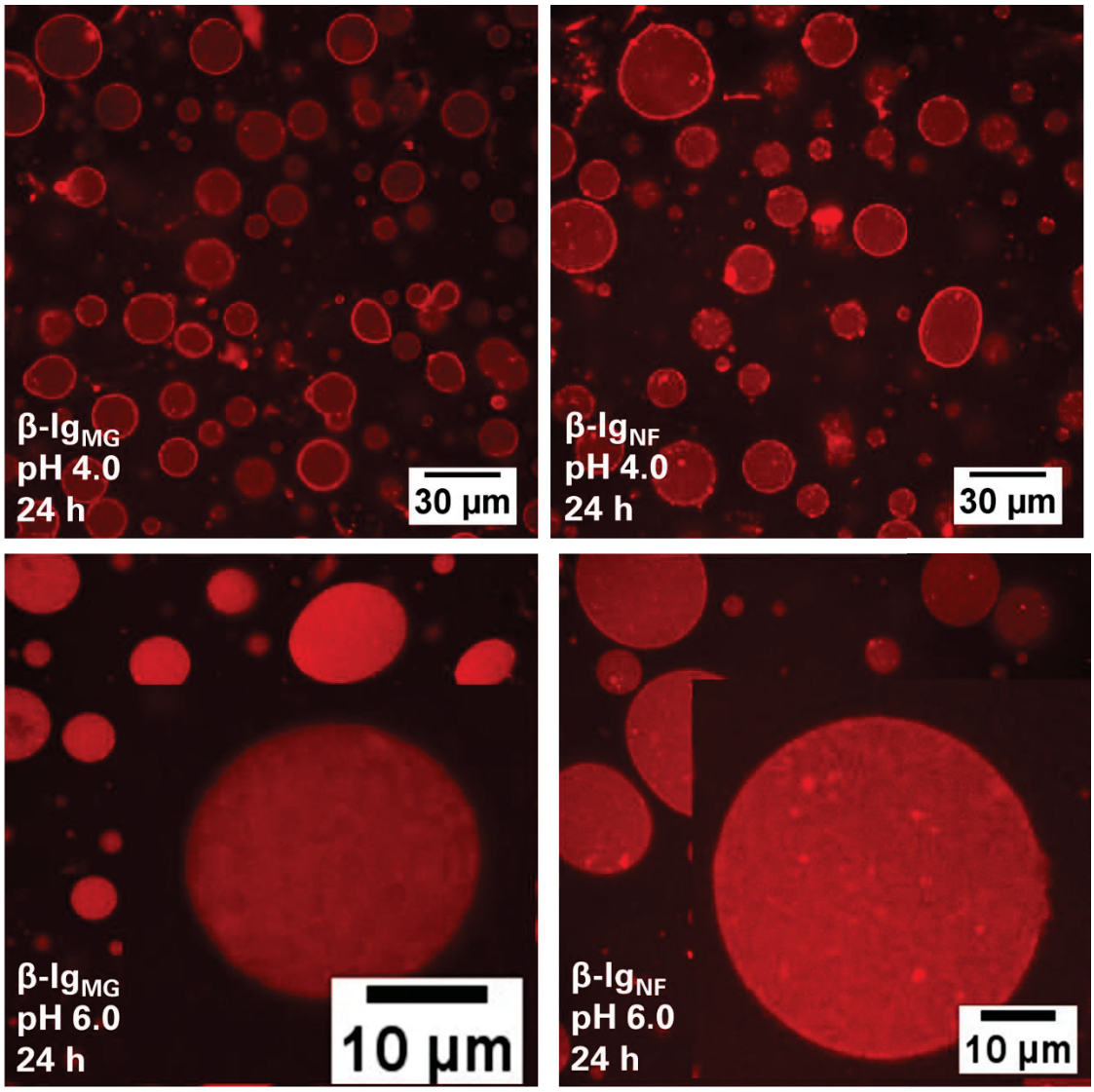

SOURCE: The author (2022).

Knowing that nanofibrils adsorb at the interface of the AMP in XG emulsion droplets at pH 6 and 7 while microgels at lower pH values, the idea of using mixtures of these particles came up, aiming to verify which of the two nanoparticles would present a predominant behaviour in the emulsion. The emulsions composed by XG3 and AMP were chosen to the next experiments over XG2 and AMP, since XG3 was a commercial sample. FIGURE 30 shows that the behaviour of microgels and nanoparticles at 1.0 wt.% in AMP-in-XG3 emulsions (1.023: 1.300 wt.%) is exactly a mixture of what was previously found for each individual particle. Microgels migrate to the amylopectin phase at pH > 5.0, while nanofibrils remain at the interface. Note that

this combined effect stabilizes emulsions macroscopically for longer than the condition in which particles were added alone (as shown in FIGURE 30, these emulsions were stable for at least 196 h).

The emulsions were also prepared using XG3 and AMP (1.300: 1.023 wt.%) in the presence of either 0.01 mol L^{-1} or 0.1 mol L^{-1} NaCl. This concentration values were chosen in order to evaluate the effect of decreasing the attractive and repulsive ζ-potentials that particles contain in normal situations, as described in section 4.1.4.2.

It was possible to notice that the macroscopic evaluation (FIGURE 31) did not exhibit considerable changes when comparing to the emulsions without salt – except by nanofibrils at pH 4.0 and 5.0, which in the absence of any salt concentration had complete colloidal stability in 196 h, while for the concentration of NaCl of 0.01 mol L^{-1} the phase separation is discrete, and at 0.1 mol L^{-1} of NaCl the phase separation is evident. Another difference was that the emulsions with microgels at pH > 5.0 and for nanofibrils at pH > 6.0 had a slightly delayed sedimentation of AMP compared to the salt-free condition.

In the confocal laser scanning microscopy (CLSM) analysis of the emulsions from the FIGURE 31, one can notice that when raising the ionic strength and consequently decreasing the range of repulsive potentials of the particles, the effects previously observed for each particle in each pH condition become much more pronounced: while the nanofibrils had a slight ability to adsorb at the interface of the AMP droplets at pH 6.0 and 7.0, now, in the presence of salt, the adsorption is more evident and a gelled layer, associated to deformed droplets observed, can be seen at the droplet interface mainly at the time of 24 h. Apparently, the particles have had enough time to migrate to the interface. At pH 6.0 and 7.0 for microgels, the effect of particle migration to the amylopectin phase, previously observed, is even more pronounced in the presence of saline concentrations (see FIGURE 32).

Figure 30 – MACROSCOPIC AND MICROSCOPIC (CLSM) EVALUATION OF AMP-IN-XG3 EMULSIONS (1.023: 1.300 wt.%) IN THE PRESENCE OF AN EQUAL MIXTURE OF NANOFIBRILS AND MICROGELS, EACH ONE AT 1.0 wt.%.

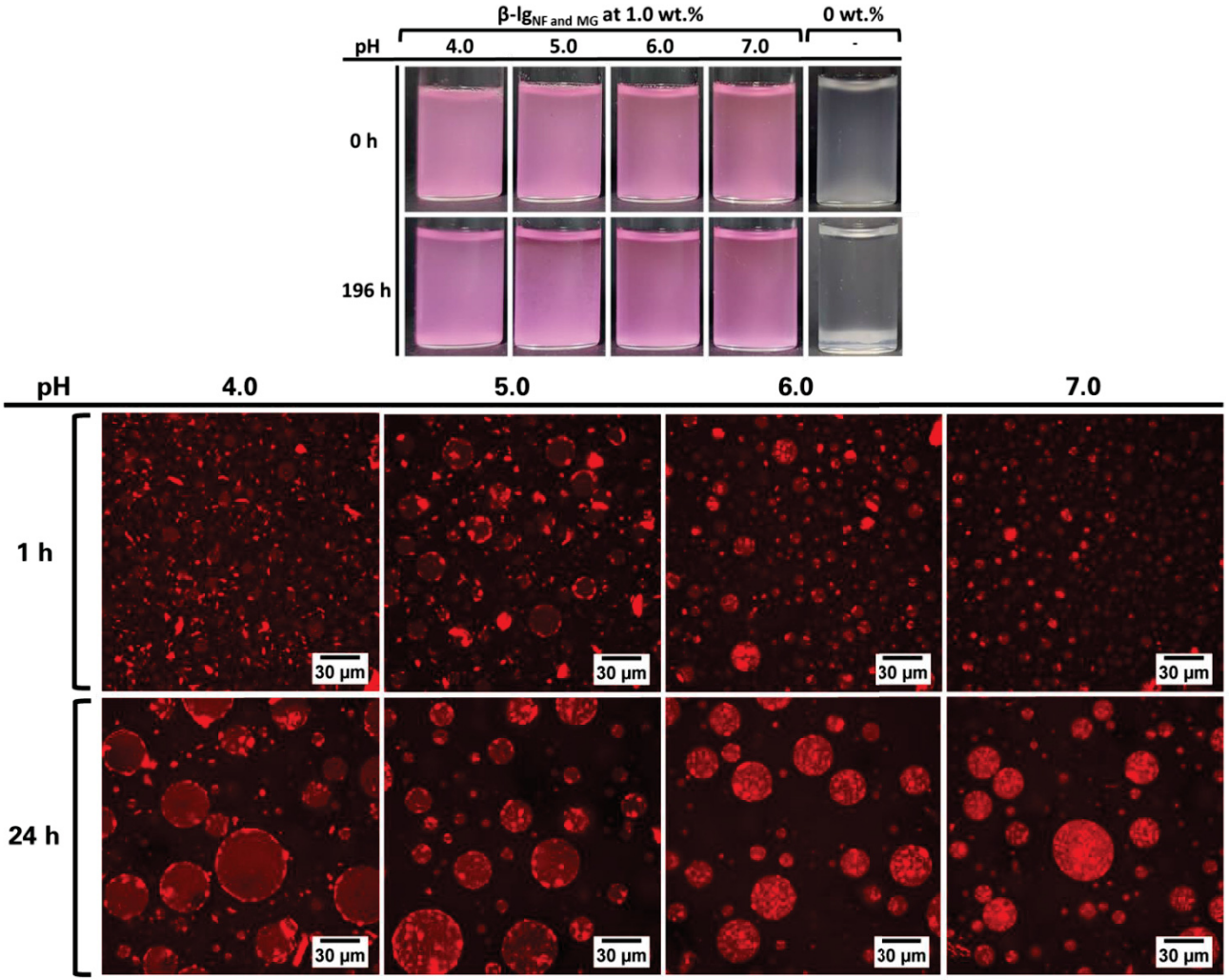

SOURCE: The author (2022).

Figure 31 – MACROSCOPIC EVALUATION OF AMP IN XG3 EMULSIONS (1.023: 1.300 wt.%) WITH β-LG MICROGELS OR FIBRILS AT a) 0.01 MOL L^{-1} NaCl AND b) 0.1 MOL L^{-1} NaCl.

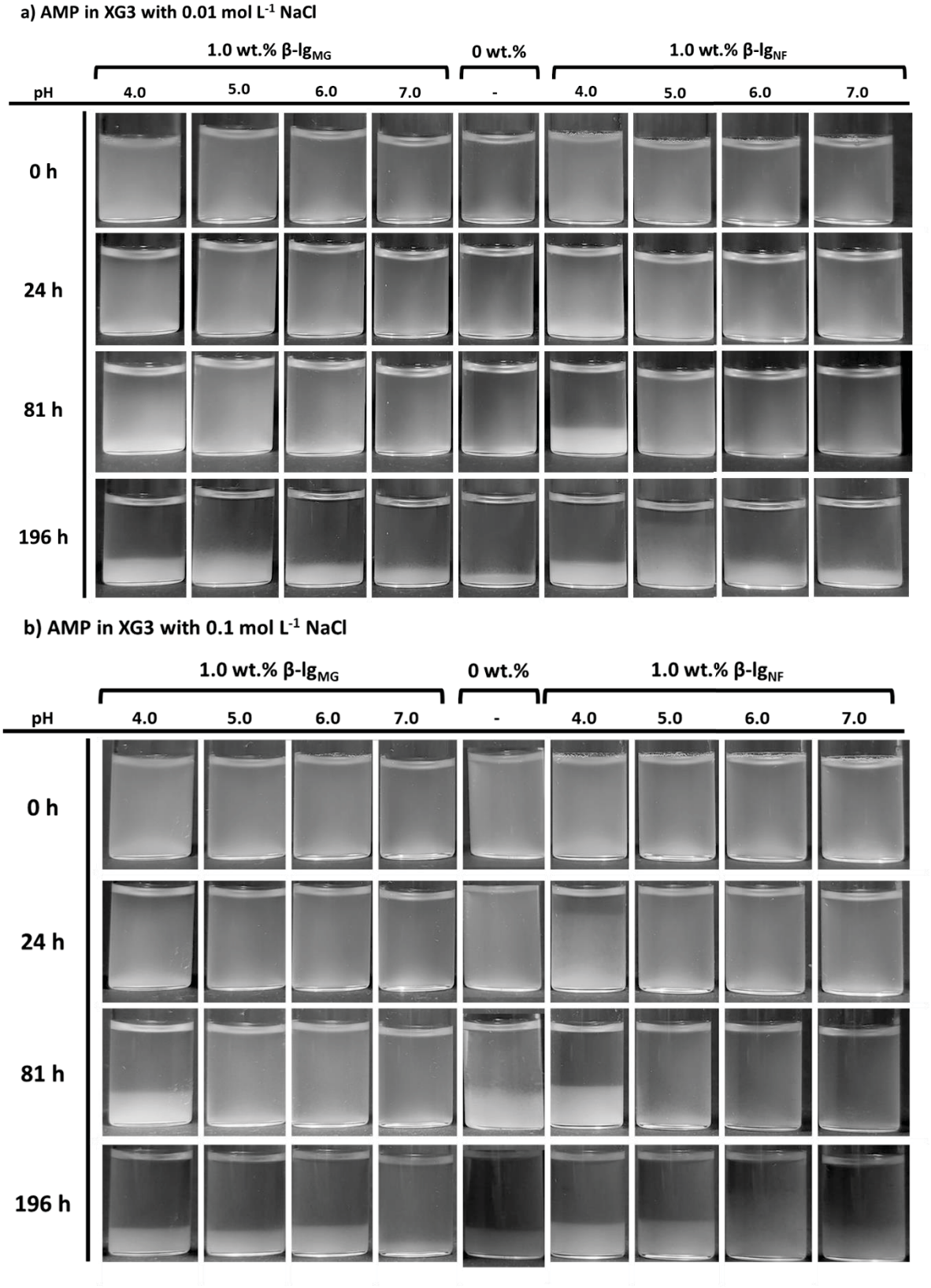

SOURCE: The author (2022).

Figure 32 - MICROSCOPIC EVALUATION OF AMP IN XG3 EMULSIONS (1.023: 1.300 wt.%) WITH β-LG MICROGELS OR FIBRILS AT BOTH 0.01 MOL L^{-1} NaCl OR 0.1 MOL L^{-1} NaCl.

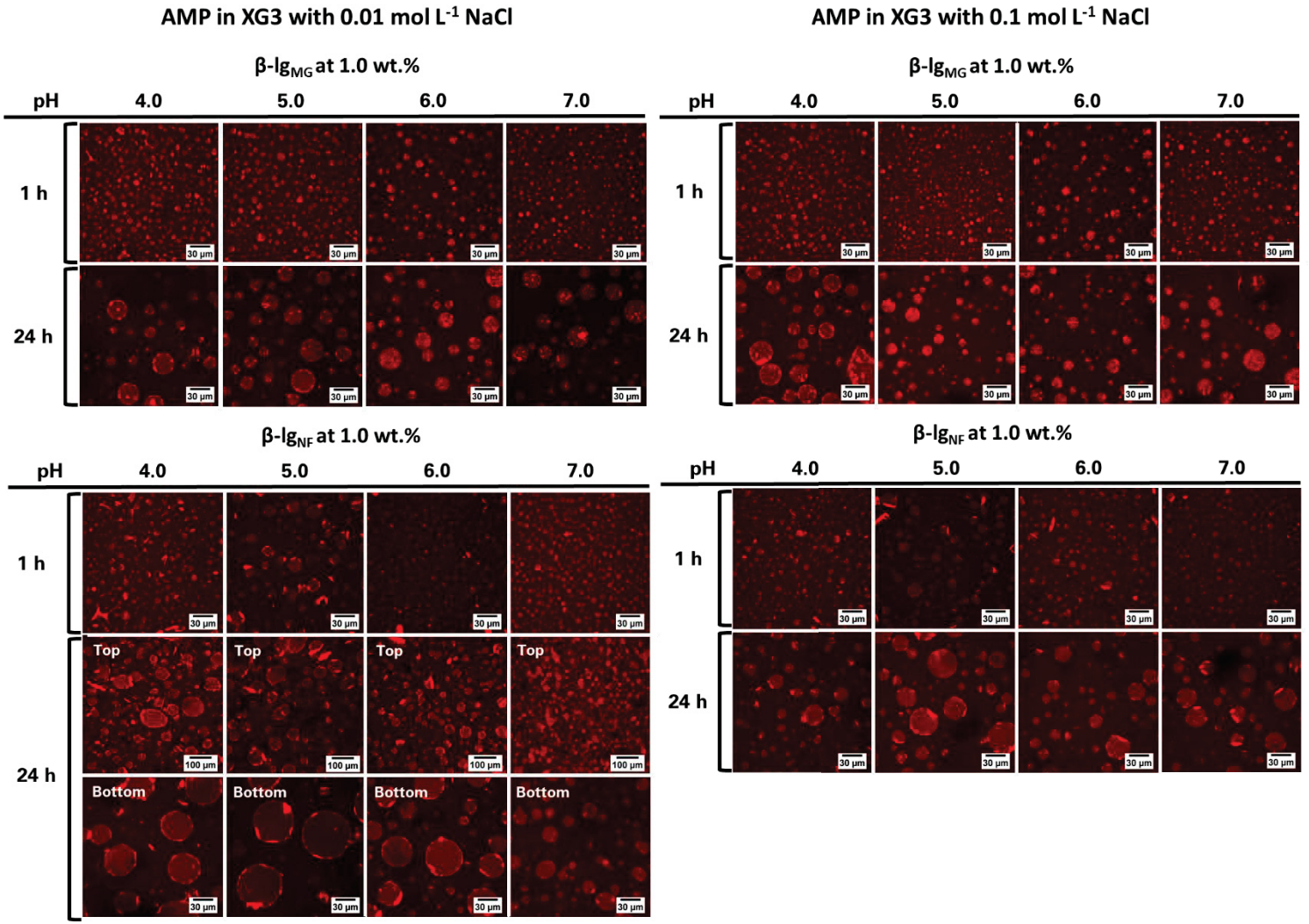

SOURCE: The author (2022).

So far, regarding emulsions stabilized by the Pickering effect, some hypotheses have been investigated:

- That fibrils and microgels adsorb distinctly at the AMP/XG interface regardless of the molar mass of the XG;
- That mixing both nanofibrils and microgels is an interesting approach since they cover emulsions stabilization in a large range of pH for longer periods of time;
- That screening the ionic strength proved the influence of the particle's charge on the behaviour of AMP in XG emulsions.

What we presented here is that the protein particles entered the interface always that the pH was not much higher than the isoelectric point of the nanoparticle, since the nanofibrils with higher isoelectric point than the microgels were able to stabilize the emulsions through Pickering effect in a wider pH range. Even though xyloglucan is a neutral polysaccharide, the results in this thesis comply with the possibility of specific binding between the protein particles and xyloglucan, observed by Gtari et al. (2016). The authors discussed that one possible mechanism of xyloglucan-protein particles binding is through coordination contacts with positively charged amino acids in the protein (Gtari et. al, 2016). This could reasonably explain how the interaction with the xyloglucan phase made the particles migrate from amylopectin to xyloglucan, especially in the case of protein particles with higher isoelectric points (and consequent positive charges at higher pH values) that migrate to the interface.

As a last note, the strong gelation of the AMP-in-XG emulsions was only observed when using a xyloglucan with lower molar mass (XG1), whereas using XG2 or XG3 (xyloglucans with higher molar masses) only a slight increase in the viscosity for emulsions with protein particles was observed – without gelling. A similar observation was made by Gtari et. al. (2016), when coating β-lg microgels with xyloglucan, the smaller molar mass XG fractions bound preferentially to the protein microgels.

5 FINAL CONSIDERATIONS

So far, the behaviour of spherical particles (microgels) and particles with a higher aspect ratio (nanofibrils) was evaluated in water-in-water emulsions formed by AMP and XG. The confocal laser scanning microscopy imaging protocol was standardized - from that, it was possible to notice differences in the images acquired at different heights of the sample. This is the reason why “top” and “bottom” images appear at this thesis, and this standardizing was fundamental to understand the mechanisms that act to stabilize (or destabilize) the water-in-water emulsions studied here. It was found that different morphologies act to stabilize the emulsions through the Pickering effect or continuous phase gelling, depending on the XG molar mass, at different pH values. The results obtained for the material XG1 and AMP were published in the Food Hydrocolloids magazine (IF 9.147).

In order to evaluate the effect of molar mass on the stabilization of AMP in XG emulsions, the construction of new phase diagrams was done for two different xyloglucans, XG2 and XG3. For the XG2 and XG3 materials, the emulsions were stabilized by the Pickering effect in the presence of β-lg microgels and nanofibrils at the same pH conditions as XG1, except when the stabilization of AMP in XG emulsions occurred by gelation of the continuous phase, since this effect presented a molar mass-dependency.

From these results, we intend to study the rheological characteristics on the behaviour of AMP and XG emulsions with the same proportion of polysaccharides (with consequent distinct interfacial tensions) in the presence of protein particles. The XG3 has a similar molar mass to XG2, but these materials did not show the same stabilization by the continuous-phase gelation effect as the XG1 did. Nevertheless, despite the higher viscosity associated with XG3 which made particles migrate with a slower rate to the interface, the behaviour of particles at the interface of AMP and XG3 and XG2 was similar to the one observed for XG1 – a macromolecule with lower molar mass. These results point out that if the macromolecular structure does not present great variation, there must similar emulsion stabilization results.

From the new diagrams it was also possible to analyse the emulsions in the presence of mixtures of particles with different morphologies, which was a successful approach since the emulsions maintained their stability for longer periods of time. A step further would be to determine if there is a migration kinetics of the particles

towards the interface when carrying out a minimal change in pH, for example. It is also intended to evaluate the gelled network formed through rheological analysis and light scattering in order to identify what governs the aggregation of particles observed in samples that showed continuous phase gelation.

As well as the rheological investigation, another hypothesis that still needs to be formally investigated is the one concerning the protein particle isoelectric point. Through the addition of a cationic polymer (for example PEI – polyethylenimine), one could change the isoelectric point of the protein particles by producing PEI-coated particles. This could open up some possibilities on how to modulate the isoelectric point of the particles and how does this affect the w/w emulsions behaviour.

REFERENCES

AKBARI, S.; NOUR, A. H. Emulsion types, stability mechanisms and rheology : A review. **International Journal of Innovative Research and Scientific Studies**, v. 1, n. 1, p. 14–21, 2018.

AOCS (AMERICAN OIL CHEMIST'S SOCIETY. **Official methods and recommended practices of the American Oil Chemist's Society**. 3º ed. Champaign, 1983.

ARNAUDOV, L. N.; DE VRIES, R.; IPPEL, H.; VAN MIERLO, C. P. M. Multiple steps during the formation of β-lactoglobulin fibrils. **Biomacromolecules**, v. 4, n. 6, p. 1614–1622, 2003.

ARROYO-MAYA, I. J.; RODILES-LÓPEZ, J. O.; CORNEJO-MAZÓN, M.; et al. Effect of different treatments on the ability of α-lactalbumin to form nanoparticles. **Journal of Dairy Science**, v. 95, n. 11, p. 6204–6214, 2012.

ATEFI, E.; FYFFE, D.; KAYLAN, K. B.; TAVANA, H. Characterization of Aqueous Two-Phase Systems from Volume and Density Measurements. **Journal of chemical & engineering data**, v. 61, p. 1531–1539, 2016.

AVEYARD, R.; BINKS, B. P.; CLINT, J. H. Emulsions stabilised solely by colloidal particles. **Advances in Colloid and Interface Science**, v. 100–102, p. 503–546, 2003.

AYMARD, P.; NICOLAI, T.; DURAND, D.; CLARK, A. Static and Dynamic Scattering of β-Lactoglobulin Aggregates Formed after Heat-Induced Denaturation at pH 2. **Macromolecules**, v. 32, n. 8, p. 2542–2552, 1999.

BALAKRISHNAN, G.; NICOLAI, T.; BENYAHIA, L.; DURAND, D. Particles Trapped at the Droplet Interface in Water-in-Water Emulsions. **Langmuir**, v. 28, p. 5921–5926, 2012.

BALANDRÁN-QUINTANA, R. R.; VALDÉZ-COVARRUBIAS, M. A.; MENDOZA-WILSON, A. M.; SOTELO-MUNDO, R. R. α-Lactalbumin hydrolysate spontaneously produces disk-shaped nanoparticles. **International Dairy Journal**, v. 32, n. 2, p. 133–135, 2013.

BASSANI, H. P. **Desenvolvimento de emulsões água-água baseadas em polissacarídeos e estabilizadas com nanopartículas**, 2017. Universidade Federal do Paraná.

BELLO-PÉREZ, L. A.; ROGER, P.; BAUD, B.; COLONNA, P. Macromolecular Features of Starches Determined by Aqueous High-performance Size Exclusion Chromatography. **Journal of Cereal Science**, v. 27, n. 3, p. 267–278, 1998.

BELLO PEREZ, L. A.; AGAMA-ACEVEDO, E. **Starch**. Elsevier Inc., 2017.

BERGTHALLER, W.; HOLLMANN, J. Starch. **Reference Module in Chemistry, Molecular Sciences and Chemical Engineering**, p. 1–29, 2014.

BINKS, B. P.; HOROZOV, T. S. **Colloidal Particles at Liquid Interfaces**. 1º ed. Cambridge: Cambridge University Press, 2006.

BOLDER, S. G.; SAGIS, L. M. C.; VENEMA, P.; VAN DER LINDEN, E. Effect of stirring and seeding on whey protein fibril formation. **Journal of Agricultural and**

Food Chemistry, v. 55, n. 14, p. 5661–5669, 2007.

BOLDER, S. G.; VASBINDER, A. J.; SAGIS, L. M. C.; VAN DER LINDEN, E. Heat-induced whey protein isolate fibrils: Conversion, hydrolysis, and disulphide bond formation. **International Dairy Journal**, v. 17, n. 7, p. 846–853, 2007.

BRADFORD, M. M. A rapid and sensitive method fot the quantitation of microgram quantities of protein utilizing the principle of protein-dye binding. **Analytical Biochemistry**, v. 72, n. 5, p. 248–254, 1976.

BRYANT, C. M.; JULIAN MCCLEMENTS, D. Molecular basis of protein functionality with special consideration of cold-set gels derived from hat-denatured whey. **Trends in Food Science and Technology**, v. 9, n. 4, p. 143–151, 1998.

BUZZA, D. M. A.; FLETCHER, P. D. I.; GEORGIOU, T. K.; GHASDIAN, N. Water-in-water emulsions based on incompatible polymers and stabilized by triblock copolymers-templated polymersomes. **Langmuir**, v. 29, n. 48, p. 14804–14814, 2013.

CAPRON, I.; COSTEUX, S.; DJABOUROV, M. Water in water emulsions: Phase separation and rheology of biopolymer solutions. **Rheologica Acta**, v. 40, n. 5, p. 441–456, 2001.

COSGROVE, T. **Colloid Science: Principles, Methods and Applications**. 2009.

DICKINSON, E. Particle-based stabilization of water-in-water emulsions containing mixed biopolymers. **Trends in Food Science & Technology**, v. 83, p. 31–40, 2019.

DONATO, L.; SCHMITT, C.; BOVETTO, L.; ROUVET, M. Mechanism of formation of stable heat-induced β-lactoglobulin microgels. **International Dairy Journal**, v. 19, n. 5, p. 295–306, 2009.

ENGELHARDT, K.; LEXIS, M.; GOCHEV, G.; et al. PH effects on the molecular structure of β-lactoglobulin modified air-water interfaces and its impact on foam rheology. **Langmuir**, v. 29, n. 37, p. 11646–11655, 2013.

ESQUENA, J. Water-in-water (W/W) emulsions. **Current Opinion in Colloid and Interface Science**, v. 25, p. 109–119, 2016.

ETTELAIE, R.; MURRAY, B. S.; LIU, S. On the Origin of Seemingly Nonsurface-Active Particles Partitioning between Phase-Separated Solutions of Incompatible Nonadsorbing Polymers and Their Adsorption at the Phase Boundary. **Langmuir**, v. 35, p. 9493–9503, 2019.

FARAUDO, J.; BRESME, F. Stability of particles adsorbed at liquid/fluid interfaces: Shape effects induced by line tension. **Journal of Chemical Physics**, v. 118, n. 14, p. 6518–6528, 2003.

FINKLE, P.; DRAPER, H. D.; HILDEBRAND, J. H. The theory of emulsification. **Journal of the American Chemical Society**, v. 45, n. 12, p. 2780–2788, 1923.

FIROOZMAND, H.; MURRAY, B. S.; DICKINSON, E. Interfacial structuring in a phase-separating mixed biopolymer solution containing colloidal particles. **Langmuir**, v. 25, n. 3, p. 1300–1305, 2009.

FIROOZMAND, H.; ROUSSEAU, D. Tailoring the morphology and rheology of phase-separated biopolymer gels using microbial cells as structure modifiers. **Food Hydrocolloids**, v. 42, p. 204–214, 2014.

FLORY, P. J. **Principles of Polymer Chemistry**. 1º ed. Nova York: Cornell University Presss, 1953.

FREITAS, R. A.; GORIN, P. A. J.; NEVES, J.; SIERAKOWSKI, M. R. A rheological description of mixtures of a galactoxyloglucan with high amylose and waxy corn starches. **Carbohydrate Polymers**, v. 51, n. 1, p. 25–32, 2003.

FREITAS, R. A.; NICOLAI, T.; CHASSENIEUX, C.; BENYAHIA, L. Stabilization of Water-in-Water Emulsions by Polysaccharide-Coated Protein Particles. **Langmuir**, v. 32, n. 5, p. 1227–1232, 2016.

FUCIÑOS, C.; FUCIÑOS, P.; ESTÉVEZ, N.; et al. One-step chromatographic method to purify α-lactalbumin from whey for nanotube synthesis purposes. **Food Chemistry**, v. 275, n. September 2018, p. 480–488, 2019.

FUENTE, M. A.; SINGH, H.; HEMAR, Y. Recent advances in the characterisation of heat-induced aggregates and intermediates of whey proteins. **Trends in Food Science and Technology**, v. 13, n. 8, p. 262–274, 2002.

GONZALEZ-JORDAN, A.; BENYAHIA, L.; NICOLAI, T. Cold gelation of water in water emulsions stabilized by protein particles. **Colloids and Surfaces A**, v. 532, n. April, p. 332–341, 2017.

GONZALEZ-JORDAN, A.; NICOLAI, T.; BENYAHIA, L. Influence of the Protein Particle Morphology and Partitioning on the Behavior of Particle-Stabilized Water-in-Water Emulsions. **Langmuir**, v. 32, n. 28, p. 7189–7197, 2016.

GOODARZI, F.; ZENDEHBOUDI, S. A Comprehensive Review on Emulsions and Emulsion Stability in Chemical and Energy Industries. **The Canadian Journal of Chemical Engineering**, v. 97, n. 97, p. 281–309, 2019.

GOSAL, W. S.; CLARK, A. H.; PUDNEY, P. D. A.; ROSS-MURPHY, S. B. Novel Amyloid Fibrillar Networks Derived from a Globular Protein : -Lactoglobulin †. **Langmuir**, v. 18, n. 3, p. 7174–7181, 2002.

GTARI, W.; ASCHI, A.; NICOLAI, T.; FREITAS, R. A. Core-shell particles formed by a-lactoglobulin microgel coated with xyloglucan. **International Journal of Biological Macromolecules**, v. 92, p. 357–361, 2016.

GUO, M. Q.; HU, X.; WANG, C.; AI, L. **Polysaccharides: Structure and Solubility**. 1º ed. IntechOpen, 2017.

GURALNICK, J. R.; PANTHI, R. R.; BOT, F.; et al. Pilot-scale production and physicochemical characterisation of spray-dried nanoparticulated whey protein powders. **International Journal of Dairy Technology**, v. 74, n. 3, p. 581–591, 2021.

HAMBLING, S. G.; MCALPINE, A. S.; SAWYER, L. β-lactoglobulin, advanced dairy chemistry. **Proteins Structure Function and Bioinformatics**, p. 211–259, 1991.

HARNSILAWAT, T.; PONGSAWATMANIT, R.; MCCLEMENTS, D. J. Characterization of β-lactoglobulin-sodium alginate interactions in aqueous solutions: A calorimetry, light scattering, electrophoretic mobility and solubility study. **Food Hydrocolloids**, v. 20, n. 5, p. 577–585, 2006.

HATTI-KAUL, R. Aqueous two-phase systems: A general overview. **Applied Biochemistry and Biotechnology - Part B - Molecular Biotechnology**, v. 19, n. 3, p. 269–277, 2001.

HAZT, B.; RÉGNIER, B.; GUEDES, P. H.; FREITAS, R. A. Emulsões água em água: potencial aplicação alimentícia. In: Silvani Verruck (Org.); **Avanços em Ciência e Tecnologia de Alimentos**. 1º ed, p.508, 2020. Guarujá: Editora Científica Digital.

HU, Y.-T.; TING, Y.; HU, J.-Y.; HSIEH, S.-C. Techniques and methods to study functional characteristics of emulsion systems. **Journal of food and drug analysis**, v. 25, p. 16–26, 2017.

JEEWANTHI, R. K. C.; LEE, N. K.; PAIK, H. D. Improved functional characteristics of whey protein hydrolysates in food industry. **Korean Journal for Food Science of Animal Resources**, v. 35, n. 3, p. 350–359, 2015.

KAN, X.; CHEN, G.; ZHOU, W.; ZENG, X. Application of protein-polysaccharide Maillard conjugates as emulsifiers: Source, preparation and functional properties. **Food Research International**, v. 150, p. 110740, 2021.

KEAL, L.; COLOSQUI, C. E.; TROMP, R. H.; MONTEUX, C. Colloidal Particle Adsorption at Water-Water Interfaces with Ultralow Interfacial Tension. **Physical Review Letters**, v. 120, n. 208003, p. 1–6, 2018.

KHARLAMOVA, A.; NICOLAI, T.; CHASSENIEUX, C. Calcium-induced gelation of whey protein aggregates: Kinetics, structure and rheological properties. **Food Hydrocolloids**, v. 79, p. 145–157, 2018.

KILPATRICK, P. K. Water-in-crude oil emulsion stabilization: Review and unanswered questions. **Energy and Fuels**, v. 26, n. 7, p. 4017–4026, 2012.

KINSELLA, J. E.; WHITEHEAD, D. M. PROTEINS IN WHEY: CHEMICAL, PHYSICAL, AND FUNCTIONAL PROPERTIES. **ADVANCES IN FOOD AND NUTRITION RESEARCH**, v. 33, n. C, p. 1–50, 1989.

LI, S.; LAU, H. C.; TORSÆTER, O.; HENDRANINGRAT, L.; TEMIZEL, C. Nanoparticles for enhanced oil recovery. **Sustainable Materials for Oil and Gas Applications**. p.125–174, 2021. INC.

LOWRY, O. H.; ROSEBROUGH, N. J.; FARR, A. L.; RANDALL, R. J. Protein measurement with the folin phenol reagent. **J. Biol. Chem**, v. 193, n. 265–175, 1951.

MACHADO, J. P. E.; BENYAHIA, L.; NICOLAI, T. Effect of adding a third polysaccharide on the adsorption of protein microgels at the interface of polysaccharide-based water in water emulsions. **Journal of Colloid and Interface Science**, v. 603, p. 633–640, 2021.

MACHADO, J. P. E.; FREITAS, R. A.; WYPYCH, F. Layered clay minerals, synthetic layered double hydroxides and hydroxide salts applied as pickering emulsifiers. **Applied Clay Science**, v. 169, p. 10–20, 2019.

MÅNSSON, LINDMARK H. Fatty acids in bovine milk fat. **Food and Nutrition Research**, v. 52, p. 1–3, 2008.

MANNERS, D. J. Recent developments in our understanding of amylopectin structure. **Carbohydrate Polymers**, v. 11, n. 2, p. 87–112, 1989.

MATSUDOMI, N.; OSHITA, T.; SASAKI, E.; KOBAYASHI, K. Enhanced Heat-induced Gelation of β-Lactoglobulin by α-Lactalbumin. **Bioscience, Biotechnology and Biochemistry**, v. 56, n. 11, p. 1697–1700, 1992.

MCCLEMENTS, D. J. **Food Emulsions**. 3º ed. Boca Raton: CRC Press - Taylor & Francis Group, 2016.

MCNAUGHT, A. D.; WILKINSON, A. **IUPAC. Compendium of Chemical Terminology**. 2º ed. Oxford: Blackwell Scientific Publications, 1997.

MURRAY, B. S. Pickering emulsions for food and drinks. **Current Opinion in Food Science**, v. 27, p. 57–63, 2019.

MURRAY, B. S.; PHISARNCHANANAN, N. Whey protein microgel particles as stabilizers of waxy corn starch + locust bean gum water-in-water emulsions. **Food Hydrocolloids**, v. 56, p. 161–169, 2016.

NGUYEN, B. T.; NICOLAI, T.; BENYAHIA, L. Stabilization of Water-in-Water Emulsions by Addition of Protein Particles. **Langmuir**, v. 29, p. 10658–10664, 2013.

NGUYEN, B. T.; WANG, W.; SAUNDERS, B. R.; BENYAHIA, L.; NICOLAI, T. pH-Responsive Water-in-Water Pickering Emulsions. **Langmuir**, v. 31, p. 3605–3611, 2015.

NICOLAI, T. Formation and functionality of self-assembled whey protein microgels. **Colloids and Surfaces B: Biointerfaces**, v. 137, p. 32–38, 2016.

NICOLAI, T.; MURRAY, B. Particle stabilized water in water emulsions. **Food Hydrocolloids**, v. 68, p. 157–163, 2017.

NISHINARI, K.; TAKEMASA, M.; ZHANG, H.; TAKAHASHI, R. Storage Plant Polysaccharides: Xyloglucans, Galactomannans, Glucomannans. p.613–652, 2007. Comprehensive Glycoscience.

PARK, Y. B.; COSGROVE, D. J. Xyloglucan and its interactions with other components of the growing cell wall. **Plant and Cell Physiology**, v. 56, n. 2, p. 180–194, 2015.

PENG, X.; YAO, Y. Molecular rotor as a structural probe of glucan polymers: Amylopectin, phytoglycogen, and their β-limit dextrins as models. **Carbohydrate Polymers**, v. 250, n. 17, p. 116859, 2020.

PHAN-XUAN, T.; DURAND, D.; NICOLAI, T.; et al. On the crucial importance of the pH for the formation and self-stabilization of protein microgels and strands. **Langmuir**, v. 27, n. 24, p. 15092–15101, 2011.

PHAN-XUAN, T.; DURAND, D.; NICOLAI, T.; et al. Heat induced formation of beta-lactoglobulin microgels driven by addition of calcium ions. **Food Hydrocolloids**, v. 34, p. 227–235, 2014.

PICKERING, S. U. Emulsions. **J. Chem. Soc., Trans.**, v. 91, p. 293–306, 1907.

PIQUÉ, N.; GÓMEZ-GUILLÉN, M. DEL C.; MONTERO, M. P. Xyloglucan, a plant polymer with barrier protective properties over the mucous membranes: An overview. **International Journal of Molecular Sciences**, v. 19, n. 3, 2018.

RAIKOS, V. Effect of heat treatment on milk protein functionality at emulsion interfaces. A review. **Food Hydrocolloids**, v. 24, n. 4, p. 259–265, 2010.

RAMSDEN, W. Separation of solids in the surface-layers of solutions and suspensions. **Royal Society**, v. 72, n. 477–486, 1904.

ROCHET, J.; LANSBURY JR, P. T. Amyloid fibrillogenesis: themes and variations. **Structural Biology**, v. 10, p. 60–68, 2000.

RYAN, S. M.; FITZGERALD, G. F.; VAN SINDEREN, D. Screening for and identification of starch, amylopectin, and pullulan-degrading activities in bifidobacterial strains. **Applied and Environmental Microbiology**, v. 72, n. 8, p. 5289–5296, 2006.

SAKAKIBARA, C. N.; SIERAKOWSKI, M. R.; CHASSENIEUX, C.; NICOLAI, T.; DE FREITAS, R. A. Xyloglucan gelation induced by enzymatic degalactosylation; kinetics and the effect of the molar mass. **Carbohydrate Polymers**, v. 174, p. 517–523, 2017.

SCHOCH, T. J. The Fractionation of Starch. **Advances in Carbohydrate Chemistry**, v. 1, n. C, p. 247–277, 1945.

SCHOKKER, E. P.; SINGH, H.; PINDER, D. N.; NORRIS, G. E.; CREAMER, L. K. Characterization of intermediates formed during heat-induced aggregation of β-lactoglobulin AB at neutral pH. **International Dairy Journal**, v. 9, n. 11, p. 791–800, 1999.

SCHRAMM, L. L. **Emulsions, Foams, Suspensions and Aerosols - Microscience and Applications**. 2º ed. Weinheim, Germany: Wiley - VCH - Verlag GmbH & Co. KGaA, 2014.

SHAW, D. J. **Introduction to colloid and surface chemistry**. 4º ed. 1992.

SONG, Y.; SHIMANOVICH, U.; MICHAELS, T. C. T.; et al. Fabrication of fibrillosomes from droplets stabilized by protein nanofibrils at all-aqueous interfaces. **Nature Communications**, v. 7, p. 1–8, 2016. Nature Publishing Group.

SOUZA, C. F.; LUCYSZYN, N.; WOEHL, M. A.; et al. Property evaluations of dry-cast reconstituted bacterial cellulose/tamarind xyloglucan biocomposites. **Carbohydrate Polymers**, v. 93, n. 1, p. 144–153, 2013.

TEA, L.; NICOLAI, T.; RENOU, F. Stabilization of Water-In-Water Emulsions by Linear Homo-Polyelectrolytes. **Langmuir**, v. 35, p. 9029–9036, 2019.

TESTER, R. F.; KARKALAS, J.; QI, X. Starch - Composition, fine structure and architecture. **Journal of Cereal Science**, v. 39, n. 2, p. 151–165, 2004.

TADROS, THARWAT F. **Emulsion Science and Technology**. 1º ed. Weinheim, Germany: Wiley-VCH Verlag GmbH & Co. KGaA, 2009.

TOWNEND, R.; WINTERBOTTOM, R. J.; TIMASHEFF, S. N. Molecular Interactions in β-Lactoglobulin. II. Ultracentrifugal and Electrophoretic Studies of the Association of β-Lactoglobulin below its Isoelectric Point. **Journal of the American Chemical Society**, v. 82, n. 12, p. 3161–3168, 1960.

TROMP, R.; VIS, M.; ERNÉ, B. H.; BLOKHUIS, E. M. Composition, concentration and charge profiles of water-water interfaces. **Journal of Physics Condensed Matter**, v. 26, n. 46, 2014.

VAN DIJK, J. A. P. P.; SMIT, J. A. M. Size-exclusion chromatography-multiangle laser light scattering analysis of β-lactoglobulin and bovine serum albumin in aqueous solution with added salt. **Journal of Chromatography A**, v. 867, n. 1–2, p. 105–112, 2000.

VEERMAN, C.; RUIS, H.; SAGIS, L. M. C.; VAN DER LINDEN, E. Effect of electrostatic interactions on the percolation concentration of fibrillar β-lactoglobulin gels. **Biomacromolecules**, v. 3, n. 4, p. 869–873, 2002.

VILLARES, A.; BIZOT, H.; MOREAU, C.; ROLLAND-SABATÉ, A.; CATHALA, B. Effect of xyloglucan molar mass on its assembly onto the cellulose surface and its enzymatic susceptibility. **Carbohydrate Polymers**, v. 157, p. 1105–1112, 2017.

WEI, B.; QI, H.; ZOU, J.; et al. Degradation mechanism of amylopectin under ultrasonic irradiation. **Food Hydrocolloids**, v. 111, p. 106371, 2021.

WIT, J. N.; KLARENBEEK, G. Effects of Various Heat Treatments on Structure and Solubility of Whey Proteins. **Journal of Dairy Science**, v. 67, n. 11, p. 2701–2710, 1984.

YUGUCHI, Y.; KUMAGAI, T.; WU, M.; HIROTSU, T.; HOSOKAWA, J. Gelation of xyloglucan in water/alcohol systems. **Cellulose**, v. 11, n. 2, p. 203–208, 2004.

ZHANG, T.; XU, J.; CHEN, J.; et al. Protein nanoparticles for Pickering emulsions: A comprehensive review on their shapes, preparation methods, and modification methods. **Trends in Food Science and Technology**, v. 113, n. January, p. 26–41, 2021.

ZHANG, X.; HEMAR, Y.; LV, L.; et al. Molecular characterization of the β-lactoglobulin conjugated with fluorescein isothiocyanate: Binding sites and structure changes as function of pH. **International Journal of Biological Macromolecules**, v. 140, p. 377–383, 2019.

APPENDIX 1 – ^{1}H NMR SPECTRA OF XG1, 2 AND 3

Anomeric signals of the ^{1}H NMR spectra for XG1, XG2 and XG3

Solvent: D_2O

Temperature: 70 ºC

Internal standard: acetone [2.224 ppm]

Signal at 5.17 ppm refers to the substituted α-xylose units

Signal at 4.98 ppm refers to the terminal non-reducing α-xylose

Signals at 4.58 ppm refers to the overlaped β-glucose and β-galactose

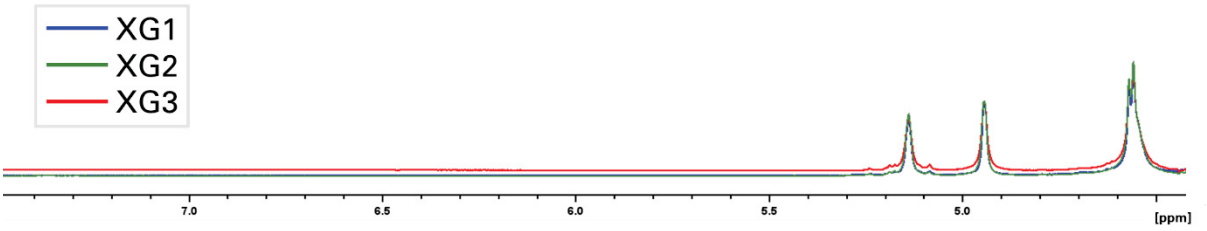

Source: The author (2022)

ANNEX 1 – ACADEMIC INFORMATION

I. SUBJECTS AND GRADES

Subject	Total hours/credits	Concept*
Seminars M1	15/1	A
Seminars M2	15/1	A
Chemical Riscology And Good Laboratory Practices	30/2	A
Teaching Practice in Chemistry	15/1	A
Colloids and Surface Chemistry	60/4	A
Quantum Chemistry and Spectroscopy	60/4	A
Physico-Chemical Methods of Macromolecular Characterization and Colloids	60/4	A
Advanced Physical Chemistry	60/4	A

Resolution no. 32/17 - CEPE Score: A = Excellent (9.0 to 10.0) B = Very Good (8.0 to 8.9) C = Good (7.0 to 7.9) D = Insufficient (0.0 to 6.9)

II. CONGRESSES AND EVENTS

- E-poster at LatinXChem 2021: A comparison between protein nanofibrils and microgels as water-in-water emulsions stabilizers; in September of 2021;

- Lecture at Future Scientists program (Center of Strategic Technologies for Northeastern Brazil - CETENE); in July of 2021;

- Participation in the university extension course: 7th summer school on colloids and surfaces University of São Paulo – USP); January of 2020;

- Lecture at XXIV Chemistry Academic Week – UFPR: Shall we play puzzles? From colloid chemistry to nanobiotechnology; in October of 2019;

- Lecture at 1st Graduate Program in Chemistry week at Regional University of Blumenau: Stabilization of water-in-water emulsions based on polysaccharides through the addition of nanoparticles; in August of 2019;

III. PUBLICATIONS

HAZT, BIANCA; BASSANI, HELEN P.; ELIAS-MACHADO, JOÃO P.; ALDINUCCI BUZZO, JOÃO LUIZ; SILVEIRA, JOANA L.M.; FREITAS, RILTON A.: Effect of pH and protein particle shape on the stability of amylopectin-xyloglucan water-in-water emulsions. FOOD HYDROCOLLOIDS, v. 104, p. 105769, 2020.

HAZT, BIANCA; RÉGNIER, BERNARDO MAUAD; GUEDES, PEDRO HENRIQUE; FREITAS, RILTON ALVES: EMULSÕES ÁGUA EM ÁGUA: POTENCIAL APLICAÇÃO ALIMENTÍCIA. In: Silvani Verruck. (Org.). Avanços em Ciência e Tecnologia de Alimentos. 1ed.: Editora Científica, 2020, v. 2, p. 233-258.

IV. PRIZES

1st place in the #LXChemPhys category at the LatinXChem Twitter Conference 2021; in September of 2021;